Optimal Vibration Control in Structures using Level set Technique

by

Masoud Ansari

A thesis
presented to the University of Waterloo
in fulfillment of the
thesis requirement for the degree of
Doctor of Philosophy
in
Mechanical Engineering

Waterloo, Ontario, Canada, 2013

AUTHOR'S DECLARATION

I hereby declare that I am the sole author of this thesis. This is a true copy of the thesis, including any required final revisions, as accepted by my examiners.

I understand that my thesis may be made electronically available to the public.

Masoud Ansari

Abstract

Vibration control is inevitable in many fields, including mechanical and civil engineering. This matter becomes more crucial for lightweight systems, like those made of magnesium. One of the most commonly practiced methods in vibration control is to apply constrained layer damping (CLD) patches to the surface of a structure. In order to consider the weight efficiency of the structure, the best shape and locations of the patches should be determined to achieve the optimum vibration suppression with the lowest amount of damping patch. In most research work done so far, the shape of patches are assumed to be known and only their optimum locations are found. However, the shape of the patches plays an important role in vibration suppression that should be included in the overall optimization procedure.

In this research, a novel topology optimization approach is proposed. This approach is capable of finding the optimum shape and locations of the patches simultaneously for a given surface area. In other words, the damping optimization will be formulated in the context of the level set technique, which is a numerical method used to track shapes and locations concurrently.

Although level set technique offers several key benefits, its application especially in time-varying problems is somewhat cumbersome. To overcome this issue, a unique programming technique is suggested that utilizes MATLAB© and COMSOL© simultaneously.

Different 2D structures will be considered and CLD patches will be optimally located on them to achieve the highest modal loss factor. Optimization will be performed while having different amount of damping patches to check the effectiveness of the technique. In all cases, certain constraints are imposed in order to make sure that the amount of damping material remains

constant and equal to the starting value. Furthermore, different natural frequencies will be targeted in the damping optimization, and their effects will also be explained.

The level set optimization technique will then be expanded to 3D structures, and a novel approach will be presented for defining an efficient 4D level set function to initialize the optimization process. Vibrations of a satellite dish will be optimally suppressed using CLD patches. Dependency of the optimum shape and location of patches to different parameters of the models such as natural frequencies and initial starting point will be examined. In another practical example, excessive vibrations of an automotive dash panel will be minimized by adding damping materials and their optimal distribution will be found.

Finally, the accuracy of the proposed method will be experimentally confirmed through lab tests on a rectangular plate with nonsymmetrical boundary conditions. Different damping configurations, including the optimum one, will be tested. It will be shown that the optimum damping configuration found via level set technique possesses the highest loss factor and reveals the best vibration attenuation.

The proposed level set topology optimization method shows high capability of determining the optimum damping set in structures. The effective coding method presented in this research will make it possible to easily extend this method to other physical problems such as image processing, heat transfer, magnetic fields, etc. Being interconnected, the physical part will be modeled in a finite element package like COMSOL and the optimization advances by means of Hamilton-Jacobi partial differential equation. Thus, the application of the proposed method is not confined to damping optimization and can be expanded to many engineering problems.

In summary, this research:

- offers general solution to 2D and 3D CLD applications and simultaneously finds the best shape and location of the patches for a given surface area (damping material);
- extends the level set technique to concurrent shape and location optimization;
- proposes a new numerical implementation to handle level set optimization problems in any complicated structure;
- makes it possible to perform level set optimization in time dependent problems;
- extends level set approach to higher order problems.

Acknowledgements

First, I would like to thank God for all that he has given me. Please give me the strength to continue to conquer life and continue to walk in your will.

I would like to express my deep gratitude to my supervisors, Prof. Amir Khajepour and Prof. Ebrahim Esmailzadeh for all their guidance, support, kindness, patience and constant encouragement during my research. Working with you has been a true privilege.

To my thesis readers, Prof. Noureddine Atalla, Prof. Fathy Ismail, Prof. Steven Waslander, Prof. Marianna Polak, I thank you greatly for your valuable input and experience. Your critiques have helped to improve the quality of my thesis.

I thank my friends, Babak Ebrahimi, Alireza Kasaiezadeh, Adrian Wong, Mohammad Pournazeri, Neda Darivandi, and Soroosh Hassanpour for their all their support and care during my course of studies at the University of Waterloo.

I am grateful to my parents, Jamshid and Shahnaz, for supporting me spiritually throughout my life.

Finally, I am deeply indebted to my darling wife, Tahereh, for all her love and endless supply of encouragement and support.

Dedication

To Tahereh

Table of Contents

List of Figures

List of Tables

Chapter 1
Introduction

Although vibrations are desirable in cases such as loudspeakers or the reed in woodwind instruments, they are often undesirable because of their propensity to waste energy and create unwanted noise. An example of an undesirable vibration is the oscillatory motions in automotive engines or the vehicle body during operation. These unwanted vibrations can cause irritating rattles and metal fatigue, which can cause parts to break, resulting in potentially lethal consequences. Due to these undesired consequences of unwanted vibrations, the control of vibration is important in many fields, including mechanical engineering.

Active [1,2], passive [3] and semi-active or hybrid [4] control methods can be used for vibration suppression. In an active system, a force is applied in an equal and opposite direction to the forces imposed by the external excitations, while in a passive control system, the energy of vibration is dissipated by a damping element without any feedback capability. Hybrid methods make use of both approaches and combine features of active and passive control systems. It is often desirable to lower the control effort as much as possible to achieve the optimal control law. While this may seem strange regarding passive vibration control (since no input force is involved in the control process), minimizing the number of dissipative elements and finding their best locations in the system will be targeted by the optimal control strategy. This fact becomes more critical in energy efficient systems such as lightweight structures. In lightweight structures, the energy consumption is reduced by lowering the weight of the system. An example of such systems is the BMW Z4, which uses magnesium-aluminum alloy in its crankcase to lower its weight by 24 percent [5].

Noise vibration and harshness analysis is essential for such lightweight structures, as the vibrational properties of the structure changes and the lower mass makes it more prone to vibration.

Passive vibration control via constrained layer damping (CLD) has demonstrated suitable efficiency in the vibration control of lightweight structures, and has been used in airplanes and some cars. Although CLD patches are used in lightweight structures, a comprehensive method to achieve optimal (and desired) control effort with minimum usage of CLD patches is needed. How much damping patches should be used? Where in the system should they be applied? What is the best shape of the patches? All these questions should be answered to achieve the optimal solution. Despite the fact that several researchers have worked on the optimal vibration suppression in dynamical systems, simultaneous optimization of shape and location of added damping material has not yet been addressed comprehensively.

This research proposes a novel method that concurrently answers all the above questions. It can simultaneously optimize the shape and locations of CLD patches, while their area remains constant. In fact, a structural topology optimization approach is introduced to optimize damping materials applied to a structure.

Level set technique offers several advantages, however its application is somewhat challenging, especially in time varying systems. The reason is that in level set approach the optimization advances according to a partial differential equation (PDE) which possesses a pseudo time. If the system condition is not static, the system time can mix up with the PDE time and can lead to wrong solutions. In order to perform level set optimization without this issue, a versatile computer code is developed in MATLAB© and COMSOL©. This new approach will

avoid time mix-up and will make it possible to perform structural optimization in time and/or frequency domain. The other key feature for this computer code is that the optimization technique will not be limited to damping optimization. Optimization problems with any form of objective functions (image processing, magnetic systems, thermal systems, etc.) can be solved with this code because it is supported by a powerful finite element package that is only responsible for evaluating the objective function and is not mixed with optimization portion.

Chapter 2 will perform a thorough literature review on the problem of optimal vibration control, with a special focus on vibration control via constrained layer damping. Different configurations of surface treatment will be discussed, and their application will be explained. Furthermore, the problem of optimal control in systems with surface treatment will be explained in full detail. This chapter will also examine and discuss key theories and methods such as the modal strain energy method, which are used in modeling constrained layer dampers.

Chapter 3 addresses the new level set method, which is a numerical technique to track shapes and interfaces. Following the explanation of this method and pointing out its advantages, the application of this method to different areas, especially in the field of topology optimization, will be studied. A structural topology optimization (compliance minimization) will be formulated in the context of the level set method with all the necessary details.

Chapter 4 the level set technique is reformulated and applied to the damping optimization problem. The new formulations and objective function will be discussed and developed. This novel approach will address both the shape and location optimization simultaneously. In most research work available in literature, in order to reduce the complexities of dynamic systems, especially in level set context, they are modeled as static-equivalent. In contrast, to perform level

set topology optimization in frequency domain (without any need to consider a static-equivalent model), in this research an interactive computer code is developed in MATLAB© and COMSOL©. Objective function is evaluated using finite element technique and the optimization progresses according to Hamilton-Jacobi equations.

A 2D structure with structural damping, undergoing flexural vibrations, will be considered. The best shape for damping patches as well as their optimum location of the structure will be determined to minimize the modal energy of the different vibrational modes of the system, and the highest energy dissipation will be eventually achieved. During optimization process, certain constraints are imposed to keep the total area of the patches constant. Another numerical example will include a nonsymmetrical plate. The damping configuration will be optimized in the system, and results will be compared with the literature.

Chapter 5 expands the level set damping optimization technique to 3D structures. A novel method will be presented to generate initial 4D level set function. This approach will also make it possible to model higher order systems and is not limited to 3D. Since satellite dishes are so sensitive to vibrations, in the first 3D numerical example, CLD patches will be optimally shaped and located on a satellite dish. Different natural frequencies and different amounts of damping will be considered to examine the effectiveness of the method. In the second example, the vibration of an automotive dash panel will be optimally suppressed via CLD patches.

Chapter 6 explains experimental tests, and considers a rectangular plate with non-symmetric boundary conditions. Optimal damping configurations will initially be found for the system, and then four different damping configurations, including those found via the level set technique, will be tested and their vibrational performance compared. It will be experimentally shown that the

CLD shape and location, found via the level set technique, delivers the largest vibration suppression.

Finally, conclusions and suggestions for future work will be discussed in Chapter 7.

Chapter 2

Literature Review and Background

Although different methods can be utilized in vibration control, choosing the right approach largely depends on the level of vibrations. One of the best and most efficient methods of vibration control in structures with low to mid-range vibration amplitude and frequency is the application of viscoelastic materials.

In practice, viscoelastic materials, which are mostly polymers, cannot be used to build a structure because they are not strong enough to tolerate loads. However, they can be efficiently added on top of a structure. This vibration control approach (damping treatment) tries to add viscoelastic materials to a structural system in such a way that maximum possible energy is dissipated to achieve the highest vibration suppression. To do so, one needs to know the dynamic behavior of the structure, as well as that of the viscoelastic materials [6].

As shown in Figure 2-1, viscoelastic materials can be added to a structure in different configurations. Among these, the use of free layer viscoelastic materials is the simplest form of treatment. However, in order to achieve a desired level of dampening characteristics, the viscoelastic layer should have high levels of thickness, modulus, and loss factor.

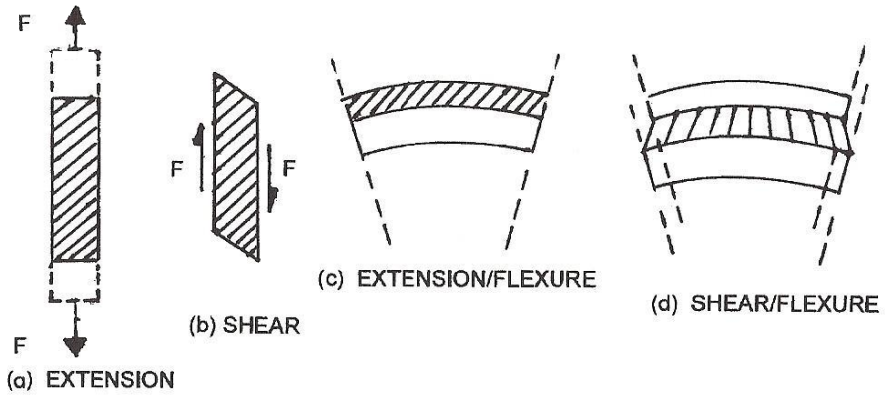

Figure 2-1: Deformation of viscoelastic elements in different configurations [6]

Although manufacturing costs and material price for this type of treatment are the lowest among all available types, it is not weight efficient, so it is not applicable for vibration control in lightweight structures. In order to attain higher dampening behaviour with lower viscoelastic material (lighter weight), a more complicated treatment is commonly utilized. This treatment is known as shear or constrained-layer damping (CLD) treatment. CLD comprises of a viscoelastic layer that is capped by another metal layer, as shown in Figure 2-2.

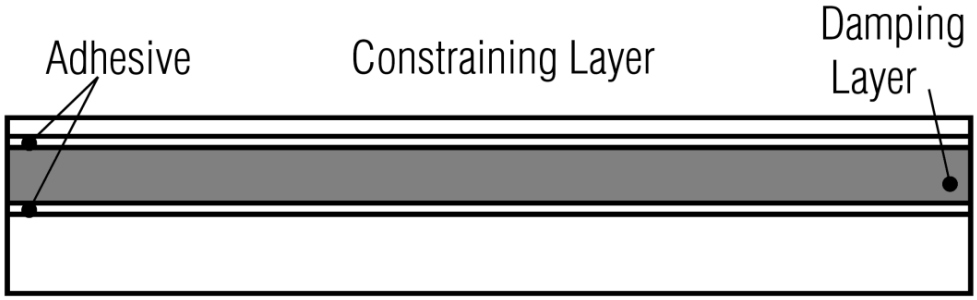

Figure 2-2: Constrained Layer Damping (CLD) configuration [7]

When the structure vibrates, the CLD undergoes shear deformation as shown in Figure 2-3, resulting in energy dissipation through damping properties of the CLD layers.

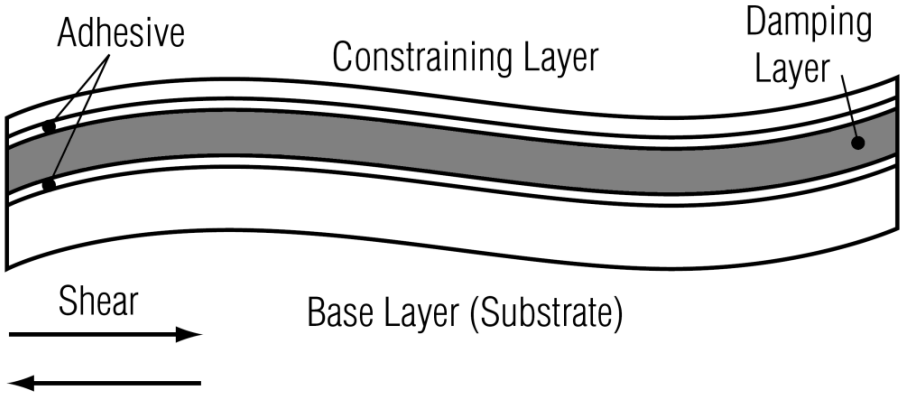

Figure 2-3: Damping layer under shear while system vibrates [7]

CLD layers have been utilized in several mechanical systems, including component vibration isolation, acoustical damping of planar surfaces, aircraft fuselage panels, dash panel vibration control [8].

Misiurek and Sniady [9] worked on the dynamic response of a finite, simply supported sandwich beam subjected to a moving force with a constant velocity. Their system included a classic sandwich beam with a rectangular cross-section consisting of two thin, stiff, elastic sheets and a thick core layer. They showed that from the two infinite series, whose sum reveals the classical solution for transverse displacement and the rotation of the cross-section, the one representing aperiodic vibrations of the beam could be presented in a closed form. Xin and Lu [10] theoretically formulated the wave propagation in an infinite sandwich panel reinforced by orthogonal rib-stiffeners during harmonic point force excitation. They determined the response of the sandwich using the Fourier transform and the periodical nature of the structure. Challamel et al. [11] worked on theoretical and numerical modeling of out-of-plane vibrations of composite beams with interlayer slip or three-layer sandwich beams. Hamilton's principle was utilized to derive the governing differential equations. For the out-of-plane vibrations problems, they noticed a phenomenon of cut-on frequency associated with a change of the shape of the natural modes with respect to a critical frequency.

Won et al. [12] used the virtual work principle to derive a 2-node damped beam element for three-layered symmetric straight damped sandwich structures. In the forced vibration, they add three pairs of boundary conditions to the three-constrained-layer damped beam, so the rotation of the mid-surface was added for the damped beam element to have three degrees of freedom per node. They also considered the frequency dependence of the viscoelastic material properties. Their proposed damped beam element showed more rapid convergences in resonance

frequencies. Chalak et al. [13] studied vibration of laminated sandwich beams with soft core. They developed a C_0 finite element beam model to obtain the free vibration response of the laminated sandwich beams having a soft core. In their developed model the in-plane displacement variation was considered to be cubic for both the face sheets and the core. Their proposed model would satisfy the condition of transverse shear stress continuity at the layer interfaces and the zero transverse shear stress condition at the top and bottom of the beam. In the same line, Sudhakar et al. [14] developed a super convergent finite element for analysis of sandwich beams with soft core. Their element was a two-nodded, six degrees of freedom per node. They assumed that all the axial and flexural loads were taken by face sheets, while the core takes only the shear loads, however they considered exact representation of beam stiffness in the formulation. They validated the performance of the developed element under static loadings and for free vibration of the sandwich beams with metallic as well as composite face sheets.

Grewal et al. [15] worked on the vibration analysis and design optimization of sandwich beams with constrained viscoelastic core layer. They used finite element method to analyze the dynamic properties of sandwich beam-type structures. A comparison was made between their results for linear and nonlinear models with those available in the literature. They showed that the natural frequency and loss factor at the first mode of clamped-free sandwich beam did not show considerable difference in linear and nonlinear models. The difference was more significant for the clamp-clamp boundary condition. Eventually, they performed systematic parametric studies to verify the effects of the location and length of both treated and untreated patches on both natural frequency and the modal loss factor of the sandwich structure. Lopatin and Morozov [16] modeled and analyzed symmetrical vibrations of composite sandwich panels. They solved the vibration problem for a sandwich plate with identical composite facings and orthotropic core.

They used Hamilton's variational principle to derive differential equation of symmetric vibrations. They assumed that the tangential displacements of the core material were negligible and the normal displacements of the core material were nonlinearly varying from the value of the facing deflection to zero. With these assumptions, they also defined the effective modulus of elasticity of the core material in transverse direction. They finally compared the computational results with those obtained from the finite element analysis. Arikoglu and Ozkol [17] analyzed vibration and damping of a three-layered sandwich plate with composite face layers and a viscoelastic core. They used the principle of virtual work to derive the governing equations and related boundary conditions. They also took into account the frequency dependency of the core layer. The eigenvalue problem was solved using the generalized differential quadrature method to determine both the natural frequencies and loss factors. A comparison was made between their results and those reported in the literature. They found that the core material providing the highest damping would depend on the geometrical properties of the plate. Alijani and Amabili [18] investigated the geometrically nonlinear vibrations of completely free laminated and sandwich rectangular plates. They obtained the governing equations using multi-modal energy approach based on Lagrange equations. Their numerical analysis was based on the nonlinear classical and higher-order shear deformation theories. They found the solution based on highly accurate natural modes calculated by linear analysis.

Hamidzadeh [19] investigated the effect of viscoelastic core thickness on the modal loss factors of a thick three-layer cylinder. He accomplished the constrained-layer damping by sandwiching a linear viscoelastic material between two isotropic elastic cylinders having the same properties. The governing equations were derived using Newton's second law of motion, and employing the complex elastic moduli for the sandwiched layer. Then the natural frequencies

and modal loss factors for different circumferential wave numbers were determined. It was concluded that most frequency factors changed linearly when the middle-layer thickness varied, i.e. frequency factors were linear functions of the middle-layer thickness, and for circumferential wave number n = 0, all six modes of the modal loss factors increased linearly when the core thickness increased. Wu et al. [20] studied the initial decay rate of vibrating plates in relation to estimates of loss factor. They worked experimentally on the initial decay rate of the energy decay curves on single, coupled, undamped, and damped rectangular plates. They confirmed that the loss factors obtained when using the decay rate and the power input methods agree with each other for undamped, lightly damped, highly damped (up to a specific frequency) and coupled plates. Clarkson and Pope [21] carried out a study on experimental determination of modal densities and loss factors of flat plates and cylinders. In their experiments several accelerometers were required to determine the spatial average. The tests should be repeated several times with different driving positions to obtain the average force position. Mead and Markus [22] studied forced transverse vibration of a three-layer sandwich beam with a viscoelastic core. They derived differential equations of motion for the system for different boundary conditions, and discussed the orthogonality of the corresponding complex modes. Johnson and Kienholz [23] offered an efficient method to predict damping in a structure with constrained viscoelastic layers. They estimated the modal damping ratio from undamped normal modes via the modal strain energy method (MSE). Maheri and Adams [24] used finite elements method based on laminated plate theories to predict modal properties of a free-free Fibre Reinforced Polymer (FRP) plate and validated their work with experimental results. More recently, Hambic et al. suggested a new approach to infer viscoelastomer dynamic moduli with better accuracy [25]. Torvik and Runyon [26] modified the method of modal strain energy to improve loss factor estimations for damped

structures. It was found that the traditional application of MSE method would be appropriate for the damping element with a very low stiffness. However, they observed that the error, resulting from the use of MSE, would increase significantly for systems with higher damping element stiffness, unless the material loss factor of the damping element is small (i.e., << 1). Instead of analytical Ross-Kerwin-Ungar equations [27], they used the finite element model of CLD-treated beams in their proposed inference method. They also performed experimental studies on beams with CLD treatments.

After choosing the amount of CLD to be used to control unwanted vibrations, one of the most important aspects to be aware of is the locations of the damping patches. A great deal of research has been done on the optimal location of damping elements on a structure.

Gurgoze and Muller investigated the optimal positioning of one viscous damper in a linear mechanical system with no structural damping [28]. They concluded that the positioning on the basis of an "energy" criterion is more reasonable than other criteria. Although they analytically formulated the positioning problem for one damper, for more general cases with two or more dampers, the calculations have to be performed numerically. Optimal placement of viscous elements on a structure, and the selection of their physical properties were addressed in [29] via optimization techniques. The authors investigated and solved both continuous and discrete optimization problems. Kincaid emphasised local search methods in solving the damper placement problem in flexible space truss structures [30]. It was found that the coupling of linear programming and Taboo search [31] would provide the highest quality solutions in the shortest amount of computing time.

Takewaki in [32-36] studied the location optimization of a passive damper location via minimum transfer function. The sum of amplitudes of the transfer functions for the undamped fundamental natural frequency of a structural system is minimized, subject to a constraint on the sum of damping coefficients of the added dampers. The advantage of this method is that the results are not affected by the characteristics of input motions because of the application of a general dynamical property (amplitude of a transfer function), independent of system inputs.

Amini and Karagah addressed the optimal semi-active damper placement problem using the pole assignment method [37]. They studied the effects of the locations of the controllers on the control force and control performance, and concluded that the number of controllers can be reduced by means of optimization. In other words, an optimum system with lesser numbers of controllers will work more effectively than a non-optimum system with more semi-active dampers. Joshi [38] used the H_∞-norm optimization to find the damper location for space-borne interferometers. He introduced a general methodology that included optical-structural modeling, damper modeling, H_∞ cost functional formulation and combinatorial optimization. Since in space, interferometers offer several distinct disturbance sources, such as a reaction wheel, can act at once and two separate optical performance metrics are of interest, he defined a cost criterion based on a system H∞-norm that allows consideration of multiple dissimilar disturbance sources and multiple dissimilar performance metrics. He considered a discrete combinatorial optimization problem of a finite number of dampers and finite number of possible damper locations. Since the number of possible combinations grows $N!/[(N!)(N-\kappa)!]$, where N is the number of possible damper locations and κ is the number of dampers to be placed, some heuristic optimization techniques needed to be applied. He investigated both Genetic Algorithm and Simulated Annealing methods, and observed more efficiency from Simulated Annealing.

Agrawal and Yang worked on combinatorial optimization of the location of passive dampers on seismic and wind-excited buildings [39]. They used three intelligent search algorithms, namely, sequential, Worst-Out-Best-In (WOBI) and Exhaustive Single Point Substitution (ESPS), to determine the best locations of dampers. They concluded that WOBI and ESPS could be implemented to effectively improve the optimal locations of the dampers, determined by a sequential search method. The optimal position of energy absorbing devices in high-rise buildings to suppress wind-induced vibrations were also studied in [40] by means of the Genetic algorithm. Other than the vibration control effect, both economic effects and damper performance were considered in the optimization. In this line, Mahendra [41], Guo [42], Bishop [43], Movaffaghi [44] and Roy [45] worked on the optimal vibration control of structures using Genetic algorithm.

Park [46] addressed different approaches related to the mathematical modeling of viscoelastic dampers and compared their theoretical basis. He found that the standard mechanical model (SMM), which comprises of linear springs and dampers, accurately described the broadband rheological behaviour of common viscoelastic dampers. SMM was shown to be more advantageous than other models such as the fractional derivative model and the modified power law. Lam et al. discussed active and passive control by means of CLD treatment and piezoelectric actuating [47]. The Golla-Hughes-McTavish (GHM) method was utilized to model the damping of viscoelastic material. They also investigated the treatment of a beam with separate active and passive CLD elements, and introduced two new hybrid configurations, as shown in Figure 2-4. It was shown that the hybrid treatment, which is comprised of both the CLD layers and piezoelectric elements, was capable of lowering the control effort with more inherent damping.

Therefore, hybrid treatment is a better approach to suppress vibration than active treatment, which only consists of a piezoelectric element.

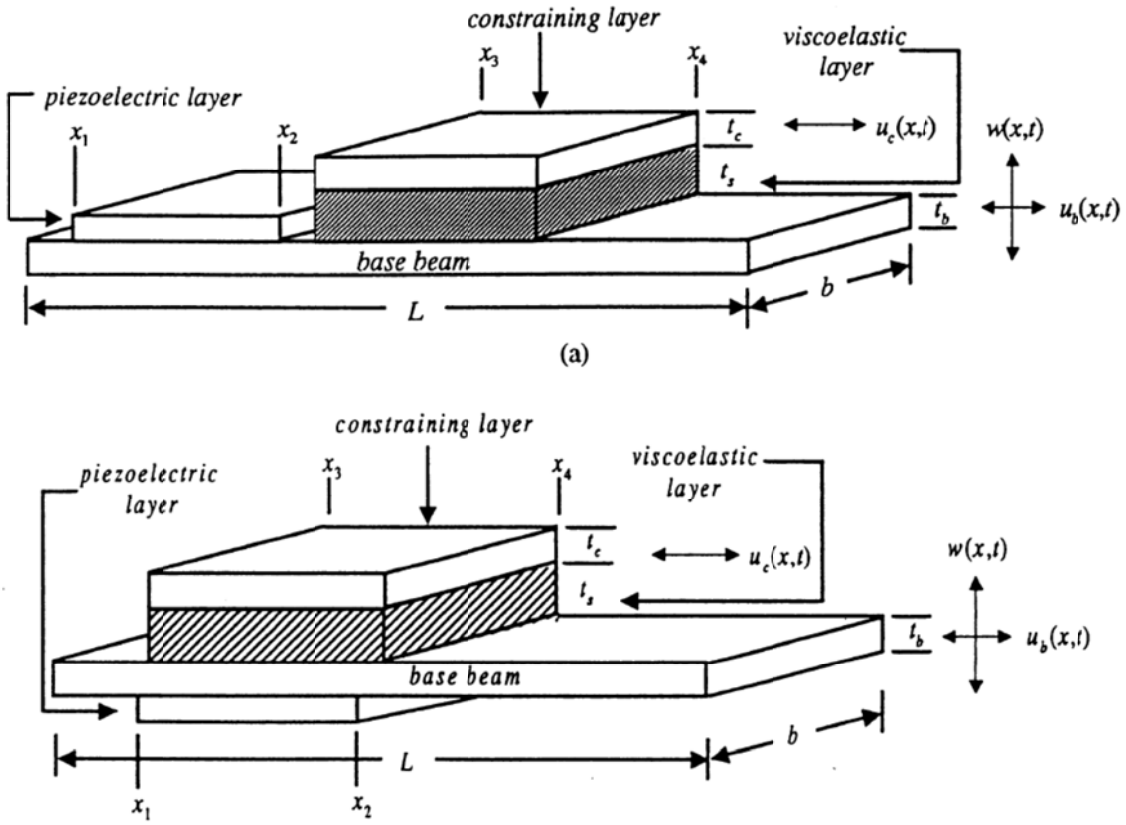

Figure 2-4: Two hybrid treatment configurations: (a) PZT and passive CLD on same side, (b) PZT and passive CLD on opposite sides [47]

Avelid developed a design method for the optimal positioning of CLD layers [48]. The objective was to minimize the frequency averaged transverse vibration levels of a plate with a harmonic excitation. He implemented a modified gradient method using finite-elements method to successively add pieces of CLD layers at the elemental positions, showing the steepest gradient of the cost function as a result of the treatment. It was found that the optimal covering of less than one third of a square plate with CLD layers, which requires a few iterations, can reduce the average vibration level up to 18 dB.

Zheng and Tan applied a Genetic Algorithm-based penalty function method to optimize partial CLD treated beams [49]. The main goal was to minimize the vibrational energy of vibrating beams with passive CLD treatment. They further performed a parameter sensitivity analysis to determine the dominant parameters on the vibration response of the damped beam. It was shown that the vibration response of the CLD treated beam showed more sensitivity to the location/length of the covered passive CLD patches and the shear modulus of the viscoelastic layer than other parameters such as the thickness of the viscoelastic layer, and the constraining layer (CL) with its elastic modulus fixed.

Many researchers have devised a modal strain energy (MSE) method to optimally locate CLD layers on the structures. This method makes use of finite elements to accurately predict the damping levels in structures comprising of layers with elastic and viscoelastic elements. Damping levels are found as modal loss factors or modal damping ratios.

Moreira et al. used this method to optimally locate passive constrained viscoelastic damping layers on structures [50]. They also verified their work by comparing the results with experimental tests. In order to improve the MSE method, Kodian and Molnar introduced a new method to account for viscoelastic material property variation with changes in frequency [51]. This method was based on using the gradients of the strain energy ratio in the hybrid Taylor series linearization with respect to the frequencies. Similarly, Ro and Baz [52] used the MSE method to optimize the location of the active constrained layer damping (ACLD) patches on flexible structures. They used a finite element approach to determine the modal strain energies of plates treated with ACLD. Furthermore, their work aimed to minimize the total weight of ACLD treatments subjected to achieving a certain level of modal damping ratio.

The MSE method will also be used in the present research; as such, it is appropriate to explain it in more detail here. Johnson [53] suggested the MSE method and Chang et al. [54] proved its accuracy (for low to moderate damping) by means of experimental tests.

Consider a finite element model of a structure with an added viscoelastic layer. The equation of motion for free vibrations of such a system can be written as

$$M\ddot{x} + Kx = 0 \tag{2.1}$$

where M is the mass matrix and K being the stiffness matrix, which is complex. Considering $K=K_1+jK_2$, Equation (2.1) can be rewritten in the frequency domain as

$$M\ddot{X}(j\omega) + (K_1 + jK_2)X(j\omega) = 0 \tag{2.2}$$

where X is the displacement vector in the frequency domain, $j = \sqrt{-1}$, $K_1 = K_{VR} + K_P$ and $K_2 = \eta_v K_{VR}$ are the respective elastic and loss stiffness (damping) matrices of the system. K_{VR} is the storage stiffness of the CLD layer, η_v is the CLD loss factor, and K_P is the elastic stiffness of the primary system. It should be noted that K_2 is the damping achieved from the added CLD layers alone, and K_1 is the combined stiffness composed of the storage stiffness of the CLD layers and the elastic stiffness of the primary system (structure without CLD layer).

Equation (2.2) shows an eigenvalue problem, which can be expressed as

$$\left[\left(K_{VR} + K_P\right) + j\eta_v K_{VR}\right]\psi_i^* = \lambda_i^{*2} M\psi_i^* \tag{2.3}$$

where ψ_i^* and λ_i^* are the i^{th} complex eigenvector and eigenfrequency, respectively. For convenience, the modal index i is dropped. Hence, λ^{*2} can now be expressed as

$$\lambda^{*^2} = \lambda^2 (1 + j\eta) \tag{2.4}$$

Approximating ψ^* by a real mode shape (ψ_R), which can be calculated from the undamped system (without CLD treatment), and pre-multiplying both sides of Equation (2.2) by ψ_R^T, one can rewrite Equation (2.4) in the following form [55]

$$\lambda^2 (1 + j\eta) = \frac{\psi_R^T \left(K_{VR} + K_P\right)\psi_R}{\psi_R^T M \psi_R} + j\frac{\psi_R^T \eta_v K_{VR} \psi_R}{\psi_R^T M \psi_R} \tag{2.5}$$

where λ^2 and $\lambda^2\eta$ can be found by equating the real and imaginary parts of Equation (2.5) as

$$\lambda^2 = \frac{\psi_R^T \left(K_{VR} + K_P\right)\psi_R}{\psi_R^T M \psi_R} \tag{2.6}$$

and

$$\lambda^2 \eta = \frac{\psi_R^T \eta_v K_{VR} \psi_R}{\psi_R^T M \psi_R} \tag{2.7}$$

Equation (2.6) reveals the undamped modal frequency based on the real part of the stiffness matrix. Eliminating λ^2 between (2.6) and (2.7), one can find the modal loss factor as

$$\eta = \eta_v \frac{\psi_R^T K_{VR} \psi_R}{\psi_R^T \left(K_{VR} + K_P\right)\psi_R} \tag{2.8}$$

In this equation $\psi_R^T K_{VR} \psi_R$ would give the modal strain energy contributed by the CLD layer and $\psi_R^T \left(K_{VR} + K_P\right)\psi_R$ is the total modal strain energy.

It should be noted that for materials with nonlinear behaviour, this approach can still be used, provided that linearization should be performed around the working condition (frequency and

temperature) or approximating the nonlinear material properties with the piecewise linearization method. In this way η_v will be found for the desired mode (frequency).

Although all of the aforementioned papers have addressed the optimal vibration control through constrained layer damping patches, and the proposed methods can somewhat find the best locations of the patches on the structure, most of them are not capable of finding the best shape of every individual patch. The present research proposes a novel integrated optimization method that can simultaneously optimize the location and shape of the patches. To this end, a fairly new structural optimization technique, called the level set method, will be used.

Chapter 3
Level set technique and its applications

Level set method (LSM) is a technique used to numerically track shapes and interfaces. One of the main advantages of this method is that its application in numerical computations involving curves and surfaces eliminates the need for parameterizing these objects, and can be done on a fixed Cartesian grid [56]. Moreover, following shape changes in a topology, such as shape split, hole development, or holes integration, is much easier by means of LSM. Therefore, LSM is a very convenient and powerful tool for modeling time-varying objects, such as the inflation of an airbag, or a drop of oil floating in water.

3.1 Moving Boundary Tracking

Consider Figure 3-1, which depicts an interface that separates two different regions. Each point on this interface can have a speed of v that shows how that point of the interface moves. For example, the light blue part can be assumed to be a piece of ice inside of some water which is freezing. Therefore, the boundary is growing, and the speed depends on the temperature drop between the two regions.

In most numerical techniques, the moving boundary is tracked by breaking it up into buoys, which are connected to each other by hypothetical ropes, as shown in Figure 3-2. Each buoy is then moved by a speed of v, while the connecting ropes keep things connected. The more number of buoys used to model the interface, the more accurate results will be achieved.

The main problem comes to the scene when the buoys want to cross over themselves or when the shape wants to break into two shapes. In this case, organizing the connecting ropes becomes very difficult (For more information, one may refer to [57]). So is there a better tool available?

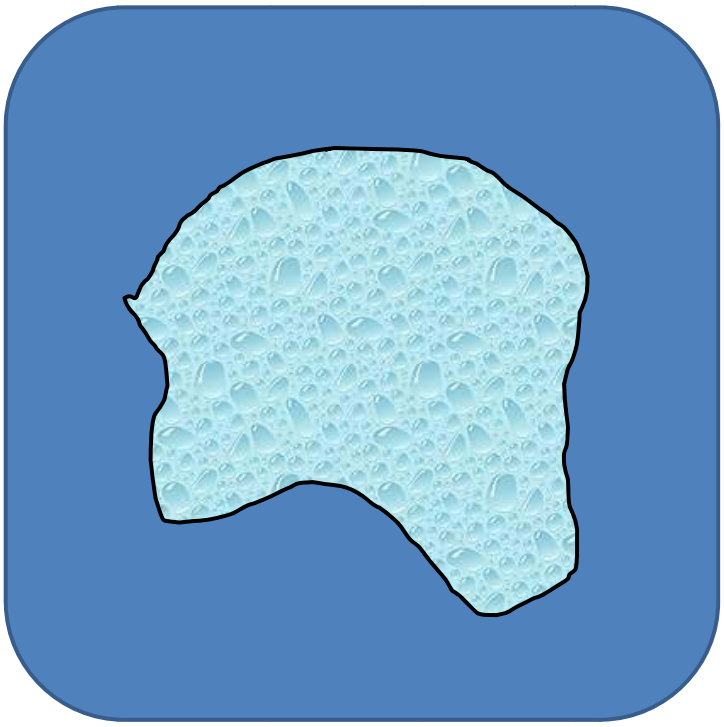

Figure 3-1: Two different regions with a moving interface

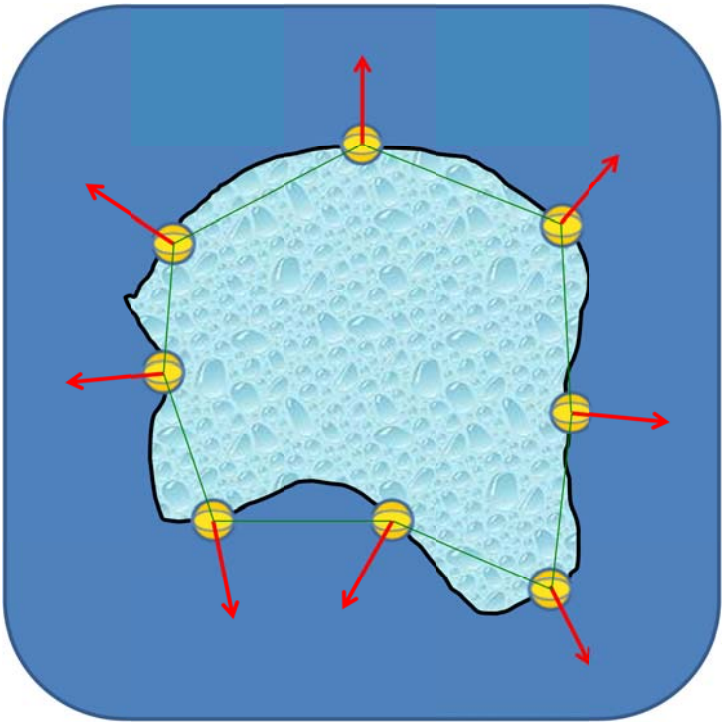

Figure 3-2: Moving interface with a speed of *v*

3.2 Level set Method

Osher and Sethin [56] proposed an approach, called level set method, which does not follow the interface itself. Now consider Figure 3-3. This method takes the red curve, i.e. the original curve, and builds it into a surface, as shown in green. This green surface has a very nice property. As shown in this figure, the green surface intersects the *xy* plane right where the original curve sits. Since this surface (function) accepts any input point in the plane and gives back its height as output, it is called the level set function. Furthermore, since all the points of the red wire have a height of zero, it is called the zero level set.

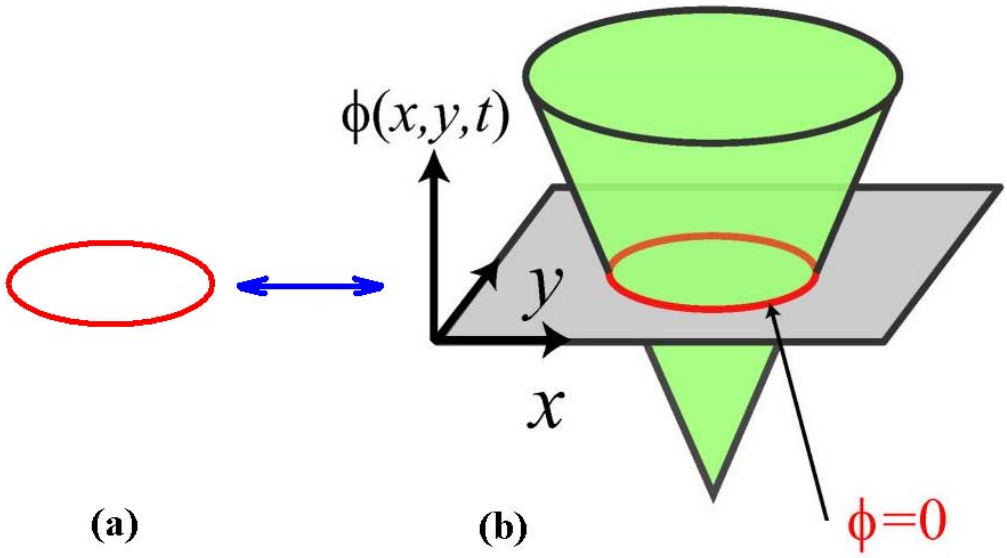

Figure 3-3: Moving interface (a) original front (b) level set function

The underlying idea is that instead of moving the original front that causes the aforementioned difficulties, the level set is being moved. In fact, the level set does everything, and the zero level set shows all the changes in the original front. The green surface, i.e. the level set function, will always remain well-behaved, while the original front (red line) can get wildly contoured. Therefore, all the complexities, such as breaking and merging, can be easily solved.

Figure 3-4 illustrates how one can describe the behavior of a moving front by means of a moving level set function. The upper part shows the zero level set, or the original front.

In summary, the level set approach reveals the motion of a moving interface by embedding the interface as the zero level set of the signed distance function. The interface's motion is essentially matched with the zero level set of the assigned level set function. Therefore, an initial value problem can be formulated in such a way that its partial differential equation resembles a Hamilton-Jacobi equation, and can describe the evolution of the level set function [58].

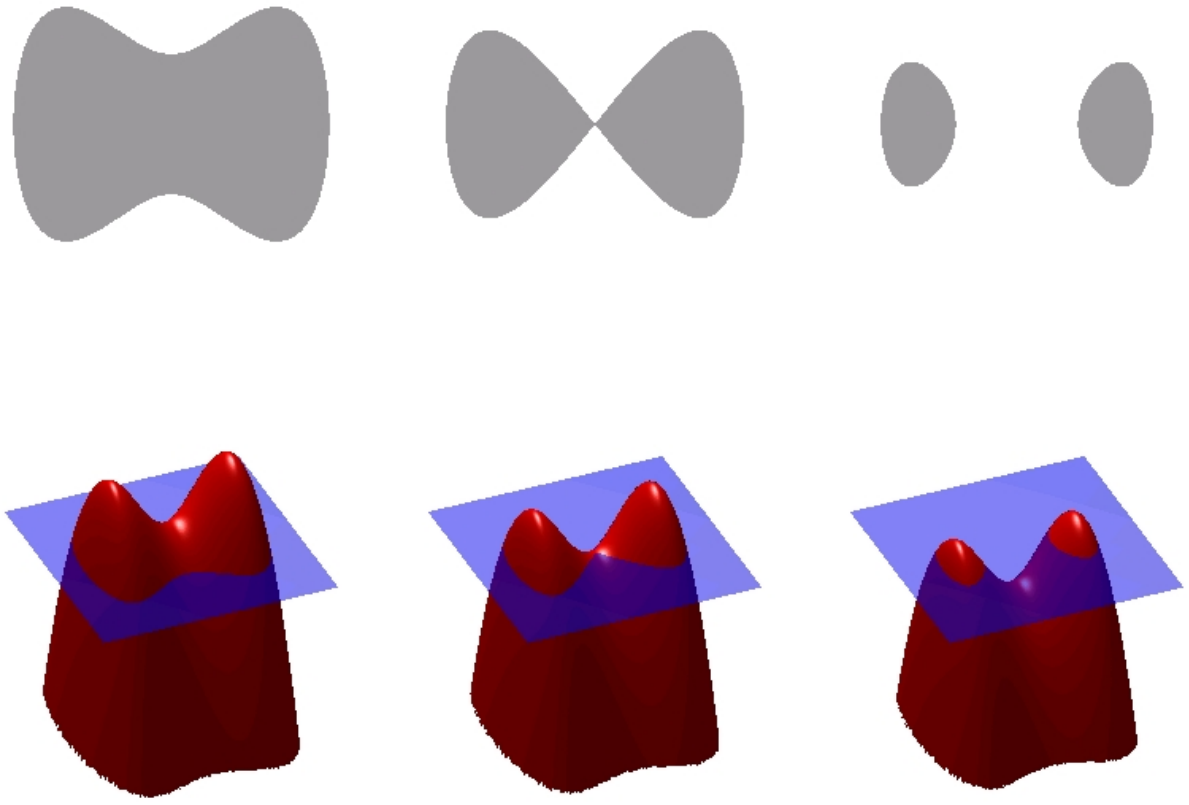

Figure 3-4: Illustration of the level set method [59]

3.3 Topology Optimization using Level set Method

Considering the aforementioned features of the level set method, several researchers have incorporated this technique into the problem of topology optimization. Malladi et al. [60] introduced a level set based algorithm for topology-independent shape modeling. Their algorithm was applicable to all models with arbitrarily complex shapes, including shapes with significant protrusions. Sethian and Weigmann then presented a combined level set and finite difference method, applicable to structural boundary design [61], to find the optimal possible design that satisfies all the imposed constraints.

3.3.1 Level set Topology Optimization Formulation

In this section, the level set topology optimization formulation for a compliance minimization problem will be explained from [62]. All other topology optimization problems can be formulated in the same way as well.

In the first step, the design domain is defined by an explicit function. Consider the cantilever beam with a hole shown in Figure 3-5.

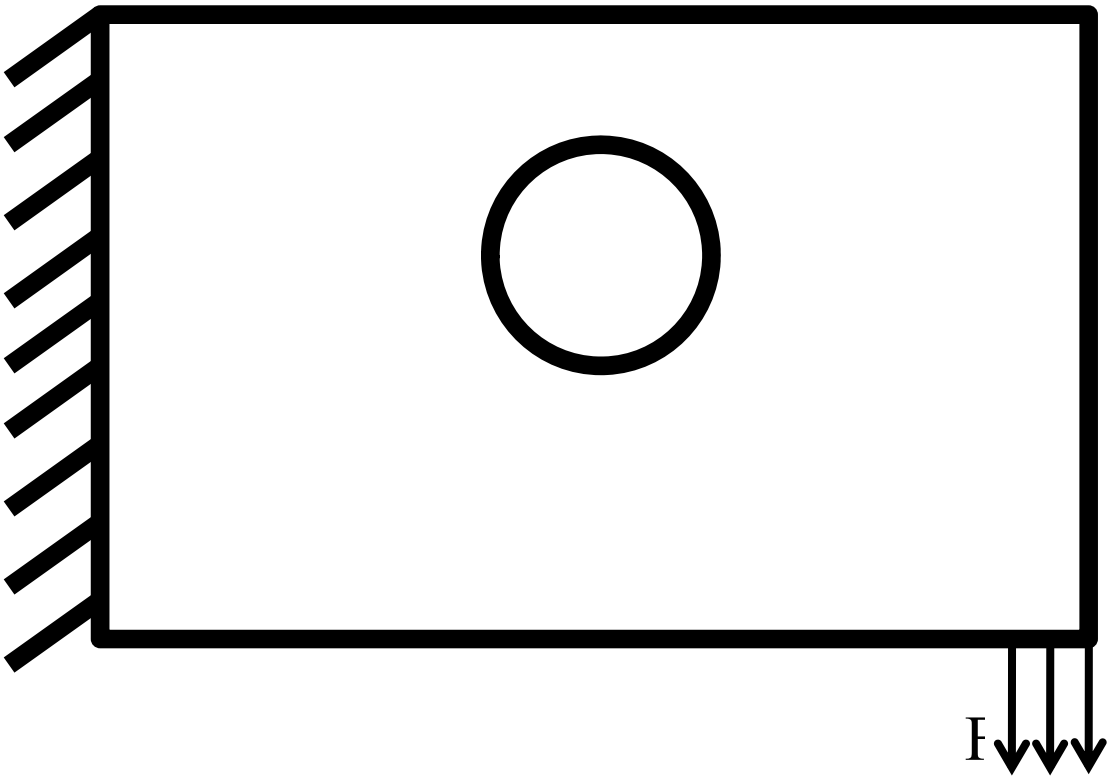

Figure 3-5: A cantilever beam under static load

Assume that there exists an explicit function $\phi(x)$ for the design domain, such that:

$$\begin{aligned} \phi(x) > 0 \quad &: \quad x \in \Omega^{+} \\ \phi(x) = 0 \quad &: \quad x \in \partial\Omega \\ \phi(x) < 0 \quad &: \quad x \in \Omega^{-} \end{aligned} \tag{3.1}$$

where x is the domain vector, Ω^{+} shows the structure material, $\partial\Omega$ expresses the structure boundaries, and Ω^{-} represents the hole in the structure, as shown in Figure 3-6.

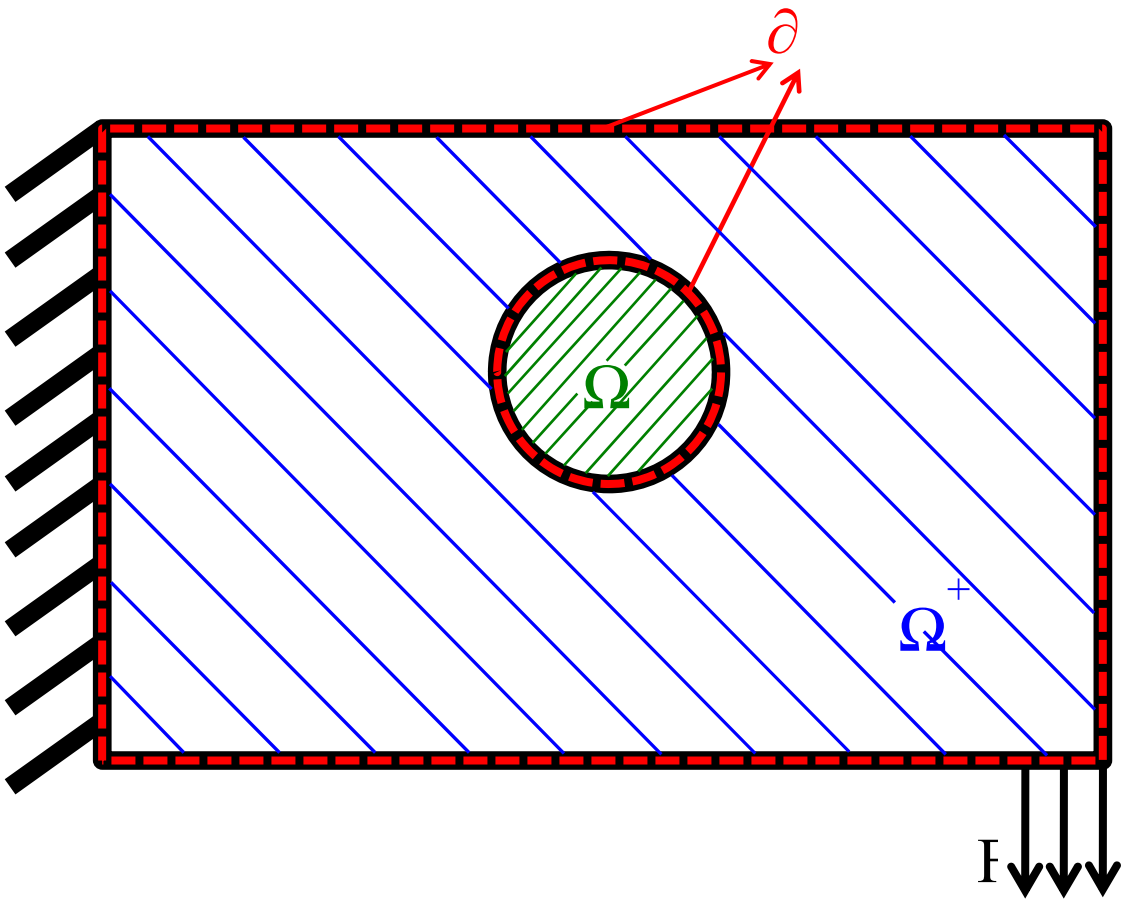

Figure 3-6: Categorization of the design domain

For a 2D compliance minimization problem, shown in Figure 3-6, the topology optimization can be expressed as:

$$\begin{aligned} &\text{minimize}: && C(\phi) = \int_{\Omega} \frac{1}{2} E(\phi)\, \varepsilon^T D \varepsilon \, \mathrm{d}\Omega \\ &\text{subjected to}: && \nabla.\left(E(\phi)\sigma\right) = f \\ & && \int_{\Omega} H(\phi)\, \mathrm{d}\Omega = V^* \end{aligned} \tag{3.2}$$

where Ω represents the design domain, and strain and stress tensors are respectively denoted by ε and σ, and D shows the elasticity matrix. V^* is the desired value of the volume in the optimally

designed structure, f is the body force and $\nabla.\left(E\left(\phi\right)\sigma\right)=f$ expresses the force equilibrium equation with ∇ as the divergence operator. In fact, the objective function, $C\left(\phi\right)$, is the strain energy of the system, which is a function of the shape of the structure and has to be minimized.

The displacement field, as well as stress and strain will all be calculated using linear elastic equations. In this formulation, $E(\phi)$ is the modulus of elasticity and is defined in the following form by the level set surface:

$$E\left(\phi\right)=E_0H\left(\phi\right)+\left(1-H\left(\phi\right)\right)E_{\min} \tag{3.3}$$

where E_0 is the elastic modulus of the material, E_{min} is the minimum relative elasticity modulus, and H is the Heaviside function, defined as:

$$H\left(\phi\right)=\begin{cases}0 & \phi\le 0\\ 1 & \phi\ge 0\end{cases} \tag{3.4}$$

In order to make sure that the structure never splits while solving the problem, the second part of Equation (3.3), i.e. $\left(1-H\left(\phi\right)\right)E_{\min}$, is defined in this way. This is actually a numerical trick, and does not have any other role in the level set approach.

In order to consider the volume constraint in the optimization problem, a Lagrangian formulation is applied. In fact, this will combine the objective and constraints, by means of a Lagrangian multiplier, λ, as expressed below:

$$J\left(\varepsilon,\phi,\lambda\right)=\int_{\Omega}\left[\frac{1}{2}E\left(\phi\right)\varepsilon^{T}D\varepsilon+\lambda\left(H\left(\phi\right)-\frac{V^{*}}{V^{\Omega}}\right)\right]\mathrm{d}\Omega \tag{3.5}$$

where the volume of the entire design domain is denoted by V^{Ω}.

Equation (3.5) is minimized when its derivative is set to zero. So the next step is to find J'. Using variational calculus [63], the variation of the Heaviside function is:

$$\delta H(\phi) = \frac{\partial H(\phi)}{\partial \phi}\delta\phi = \delta(\phi)\delta\phi = \delta\phi\big|_{\phi=0} \tag{3.6}$$

where $\delta(\phi)$ is the Dirac delta function and $\delta\phi$ represents the variation of ϕ. The other important fact to consider is that the change of shape is only influenced by the normal velocity on the material boundary, and the tangential velocity will not affect the geometry deformation. By calculating variation along normal direction, Equation (3.6) can be expressed as:

$$\delta\phi\big|_{\phi=0} = |\nabla\phi|\delta l \tag{3.7}$$

where δl is an infinitesimal variation along the normal direction $\mathbf{n} = \nabla\phi / |\nabla\phi|$. Now, the variation of J for Equation (3.5), i.e. $\delta_\phi J$, can be calculated in the following form:

$$\begin{aligned}\delta_\phi J &= \int_\Omega \left[\frac{1}{2}\frac{\partial E(\phi)}{\partial\phi}\varepsilon^T D\varepsilon + \lambda\frac{\partial H(\phi)}{\partial\phi}\right]\underbrace{\delta\phi\big|_{\phi=0}}_{|\nabla\phi|\delta l}\,\mathrm{d}\Omega \\ &= \int_\Omega \left[\frac{1}{2}(E_0 - E_{\min})\varepsilon^T D\varepsilon + \lambda\right]\delta(\phi)|\nabla\phi|\delta l\,\mathrm{d}\Omega\end{aligned} \tag{3.8}$$

From the variational principles [64], the Euler-Lagrange equation corresponding to Equation (3.8) at the extreme value point can be expressed as:

$$\left[\frac{1}{2}(E_0 - E_{\min})\varepsilon^T D\varepsilon + \lambda\right]\delta(\phi)|\nabla\phi| = 0 \tag{3.9}$$

which is impossible to solve directly for most cases. As such, one of the best approaches to tackle this problem is to solve the level set equation numerically. The corresponding level set equation is:

$$\begin{cases} \nabla.\left(E(\phi)\sigma\right) = f \\ \dfrac{\partial\phi}{\partial\tau} - \underbrace{\left[\dfrac{1}{2}\left(E_0 - E_{\min}\right)\varepsilon^T D\varepsilon + \lambda\right]\delta(\phi)}_{V_n}\left|\nabla\phi\right| = 0 \end{cases} \tag{3.10}$$

which can be solved numerically, with an initial condition of ϕ_0. In this equation, the parameter τ does not represent time. It is usually referred to as gradient descent flow and is used as pseudo-time. The solution of Equation (3.10) will converge to a local minimum (corresponding to the chosen initial value ϕ_0) for a well-posed optimization problem [62].

The final step in the formulation of the optimization problem is to find an explicit equation related to the Lagrangian multiplier, λ, based on the gradient projection method [65]. The initial condition, ϕ_0 , that is chosen in the beginning has to satisfy all the constraints of the optimization problem. These constraints should be satisfied at all times with the movement of the material boundary. For the problem at hand, there is an area constraint defined by the last part of Equation (3.2). In order to satisfy the constraint at all times, its change with time should be zero, therefore:

$$\frac{\mathrm{d}}{\mathrm{d}\tau}\left(\int_\Omega H(\phi)\,\mathrm{d}\Omega - V^*\right) = 0 \tag{3.11}$$

Since V^* is constant and its derivative is zero, this can be written as:

$$\int_\Omega \frac{\partial H(\phi)}{\partial\phi}\frac{\partial\phi}{\partial\tau}\,\mathrm{d}\Omega = 0 \tag{3.12}$$

Using Equations (3.6) and (3.10), one can rewrite Equation (3.12) in the following form:

$$\int_{\Omega}\left[\frac{1}{2}\left(E_0 - E_{\min}\right)\varepsilon^T D\varepsilon + \lambda\right]\delta(\phi)|\nabla\phi|\,\delta(\phi)\,\mathrm{d}\Omega = 0 \tag{3.13}$$

Solving Equation (3.13) for λ results in:

$$\lambda = -\frac{\int_{\Omega}\left[\frac{1}{2}\left(E_0 - E_{\min}\right)\varepsilon^T D\varepsilon\right]\delta^2(\phi)|\nabla\phi|\mathrm{d}\Omega}{\int_{\Omega}\delta^2(\phi)|\nabla\phi|\mathrm{d}\Omega} \tag{3.14}$$

What has been discussed so far demonstrates how a topology optimization problem can be formulated in the level set context as a Hamilton-Jacobi-type equation, and how it can benefit from all the features of the level set approach. Equation (3.10) should be solved numerically, and in each time step, the value of the inside of the bracket should be updated.

Formulation by means of the level set method has several advantages over conventional methods in the context of topology optimization. Firstly, level set models are topologically flexible. In fact, level set functions represent complicated surface shapes to form holes. They can also split to form multiple boundaries, and merge with other boundaries to form a single surface. Secondly, a large number of degrees of freedom can be incorporated by the models [66]. Third, shape fidelity and topology changes can simultaneously be addressed by the implicit level set methods; as such, the design boundary will be kept smooth during the entire optimization process. Fourth, since the normal component of a general velocity vector affects the shape geometry, and the tangential influences the shape parameterization, based on the discussion above Equation (3.7), the interface represented by the level set function is parametric free [67].

Fifth, in order to get a physically meaningful result for Equation (3.10), such as the level set model of the Hamilton–Jacobi equation, the theory of viscosity solutions [67,68] can be utilized.

3.3.2 Application of Level set Topology Optimization

Considering all the benefits of the level set approach, several researchers have applied this method to optimization problems. Osher and Santosa [69] applied this method to optimize the resonant frequency of a vibrating two-density inhomogeneous drum with geometrical constraints. Following this work, Maitre and Santosa [70] discussed an optimization problem over a fixed surface. They utilized the level set optimization method to find the smallest-arclength closed curve while the area enclosed by the curve is fixed.

In a few different works [66,71-73], the level set method was applied to constraint structural topology optimization problems. Ref. [72] combined the classical shape derivative and level set method for front propagation, and applied it to 2D or 3D space models with linear or nonlinear elasticity. As mentioned earlier, one of the cons against the level set method is that the final optimal shape is strongly dependent on the initial guess. In other words, this method can easily get stuck into local minima.

Wang [74] made use of a multi-phase level set method to tackle a topology optimization problem of structures with multiple materials. In his approach, m level-set functions were required in order to represent a structure with $n=2^m$ different material phases. This approach is very similar to combining colors from the three primary colors, so it is referred to as a "color" level-set. This method never faces the problem of overlap of a conventional boundary representation scheme.

Allaire and Jouve [75], as well as Haber [76], worked on the topology optimization of structures with multiple loads or frequencies by means of a multi-level set approach. It should be noted that instead of running a frequency domain analysis, static-equivalent analyses have been performed, since rigidity maximization will increase the first eigenfrequency. They presented several examples to prove that their method could be used in practical applications. One of these examples is shown in Figure 3-7. In this example, they have performed topology optimization to find the optimal design of a chair, subjected to two different loads.

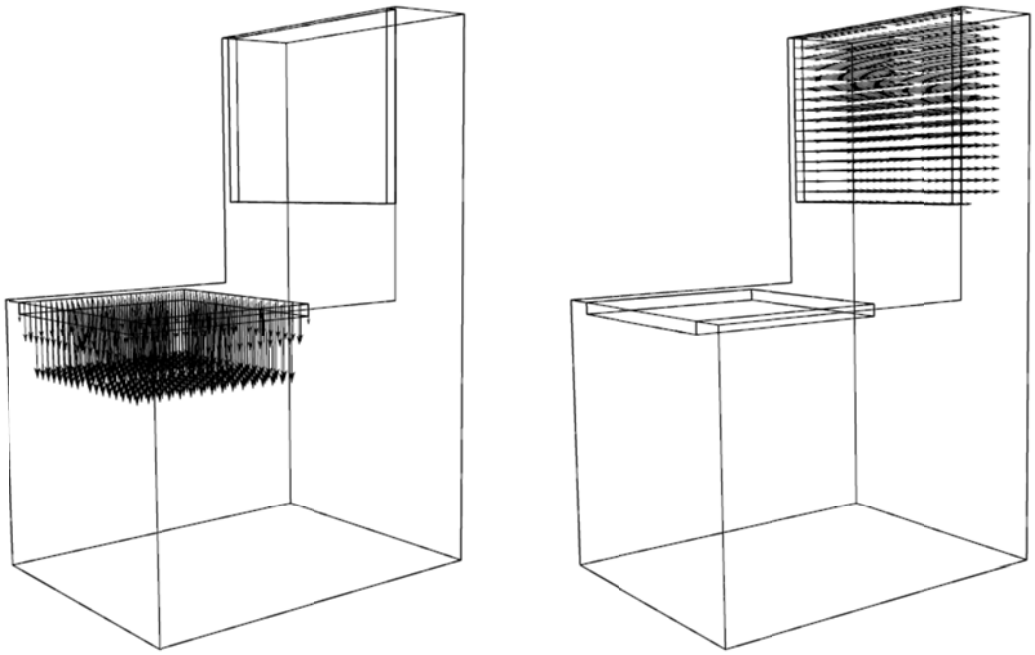

Figure 3-7: Optimal chair design: Two loading configurations [75]

Optimal design of the chair has been depicted in Figure 3-8:

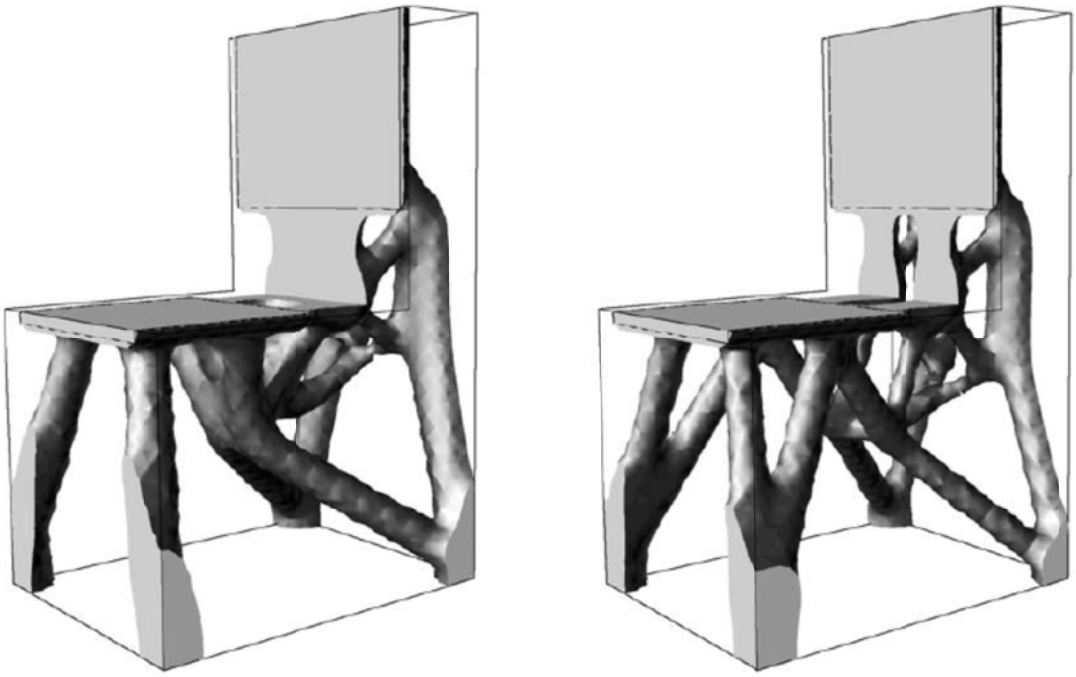

Figure 3-8: Optimal design of a chair for single (left) and multiple (right) load configurations [75]

In 2006, Xia et al. [77] proposed a semi-Lagrange method to solve the Hamilton-Jacobi partial differential equation of the level set topology optimization. The explicit upwind scheme [58] of solving level set equations severely restricts the numerical stability to the time step and requires a large number of time steps for a numerical solution. However, the proposed semi-Lagrange method allows for a much larger time step, and also requires a smaller number of time steps.

In the same line for method modification, Liu and Korvink [78] proposed an adaptive moving mesh level set method for topology optimization. Since level set surface is usually interpolated on a fixed mesh, the accuracy of the boundary position is largely dependent on the mesh density. In the proposed method, by combining the adaptive moving mesh method with a level set topology optimization method, the finite element mesh will be automatically kept with high nodal density around the structure boundaries of the material domain.

Similarly, Park and Youn [79] offered an adaptive inner-front (AIF) level set method for topology optimization of shell structures. The edge smoothing was carried out in order to suppress the numerical oscillation of solutions due to the sharp edges in the level set function in the utilization of the inner-front creation algorithm.

Recently, some attempts have been made to improve the efficiency of the level set method. Gomes and Suleman [80] proposed an extension to the conventional level set topology optimization of interfaces, and called it the spectral level set methodology. In their proposed approach, the Fourier coefficients of that function are the design variables describing the interface during the topology optimization. One of the advantages of this method is to admit an upper bound error, which is asymptotically smaller than the one for the non-adaptive spacial discretization of the level set function, in the case of a sufficiently regular interface. Furthermore, it can nucleate holes in the interior of the interface and can avoid checkerboard-like designs.

Fulmanski et al. [81] combined topological derivatives with the level set method. By doing this, they showed that utilizing topological derivatives in the framework of the level set method significantly improves the method's efficiency. Moreover, this modification makes the level set method more robust, and consequently leads to a better final solution.

Rong and Liang extended the level set optimization method to structures with bounded design domain [82]. They presented a set of new level set based optimization formulas to overcome the limitations of current level set methods for the optimal design of continuum structures with bounded design domain. Moreover, they introduced a new optimization strategy with the possibility of random topology mutations and crossover, which can lead to overcoming difficulties related to nucleating holes in the design domain using this method.

Lue et al. [83] incorporated radial basis functions into the level set topology optimization of continuum structures. In this method, the level set surface is parameterized by using radial basis functions with compact support. Therefore, the sophisticated Hamilton–Jacobi partial differential equation (PDE) is transformed into an easier size optimization of the expansion coefficients of the basis functions. They also proposed a stable numerical volume integration scheme for calculating the shape derivatives, which can effectively generate new holes in the design domain during the optimization process.

Finally, Zhuang et al. [84] introduced the element-propagating method to structural shape and topology optimization. Instead of solving the Hamilton–Jacobi partial differential equation iteratively, their method inserts and deletes basic material elements around the geometric boundary. Therefore, without solving the PDE, it realizes the dynamic updating of the material region. Their criterion for generating new holes in the material region is the strain energy density. These modifications are claimed to significantly improve the conventional level set method.

However, application of the level set method is not limited to structural topology optimization; recently, it has been brought to other fields as well. For example, Wang et al. [85,86] and XianMin and GaoFei [87] worked on the topology optimization of compliant mechanisms using the level set method. Pingen et al. [88] proposed a parametric level-set approach for the optimization of flow domains. By implementing a level set approach, they improved the versatility of the topology optimization methods for fluidic systems. Non-trivial mapping between the design variables and local material properties was achieved by means of the proposed parametric level-set approach, since it applies a material distribution approach to represent flow boundaries. They concluded that improvement would not be achieved in

convergence by utilizing a parametric level set method for fluidic systems compared to traditional methods.

In the same line, Challis and Guest [89] applied the level set method to the problem of optimization of fluids in the Stokes flow. In 2009, the level set method was applied to the topological optimization of nonlinear heat conduction problems [90]. Application of the level set method relieves the convergence difficulty in nonlinear heat-conduction problems by means of topological derivatives. Myslinski [91] utilized the level set method for optimization of contact problems. The objective was to find the best shape of the boundary of the domain occupied by the body such that the normal contact stress along the contact boundary of the body is minimized.

Finally, Park and Min [79,92] applied the level set topology optimization method in the design of a magnetic actuator and maximized its force.

3.3.3 Level set method and Damping optimization

Although researchers in many fields have shown interest in incorporating the level set method into different problems within their fields, there is a lack of research literature surrounding damping optimization. Only few studies have been carried out on simple systems to find the optimum damping set in a system. Munch et al. [93,94] tried to determine the optimal damping set needed for the stabilization of the wave equation. A linear damped wave equation was considered in two-dimensional domain Ω, with a dissipative term localized in a subset ω,

$$\begin{cases} y''_{\omega,a} - \Delta y_{\omega,a} + a(x) y'_{\omega,a} = 0 & \text{in} \quad \Omega \times (0,T) \\ y_{\omega,a} = 0 & \text{on} \quad \partial\Omega \times (0,T) \\ y_{\omega,a}(x,0) = y_0(0), \;\; y'_{\omega,a}(x,0) = y_1(0) & \text{in} \quad \Omega \end{cases} \tag{3.15}$$

where the prime sign corresponds to the partial derivative with respect to time, and the damping potential was considered to have the following form:

$$a(x) = a\chi_{\omega}(x), \qquad \forall x \in \Omega \tag{3.16}$$

In this equation, χ_{ω} represents the characteristic function of any domain ω, strictly included in Ω. In their work, the best shape of ω was found to minimize the energy of the system at a given time, *T*.

In the same line, Lassila [95] worked on the optimal damping set in a membrane. The objective was to find the optimal damping set of a two-dimensional membrane in such a way that the total energy of the membrane was minimized. The governing equations of this system are almost identical to Equation (3.15).

The next two chapters will expand on the level set technique in regards to damping optimization in structures. A comprehensive research that addresses damping optimization in complicated structures is still missing in literature. Added damping materials can affect the vibrational properties of a structure through their shapes and locations. For example in one system a circular patch may create more damping than a square patch, or in one system a patch close to the boundary may create more damping that the one located in the centre of the structure. It is very important to address both of these aspects concurrently in order to make sure that minimum amount of damping material is used while maximum vibration attenuation is achieved. In the following chapters, level set technique will be utilized to simultaneously optimize the shape and location of added damping patches while the amount of damping material remains constant.

Chapter 4

Extension of level set technique to damping optimization in plate structures

As discussed earlier, one of the efficient ways to suppress vibrations in structures is to apply CLD patches to the surface of the structure. In order to optimize the configuration of added damping materials one possibility is to cut some pre-shaped CLD patches and then try to optimally locate them on the structure. However, the shape of a patch itself plays an important role in the amount of damping in a system. So it is very advantageous to devise a method that can optimize the shape and location of CLD patches simultaneously while the amount of damping material does not change. Level set topology optimization method can handle this matter effectively as discussed in this chapter.

4.1 Problem Definition

In this section, the level set method is expanded and applied to the problem of damping optimization. Figure 4-1 illustrates a cantilever plate undergoing flexural vibrations. Vibrations suppression will be performed on the system using CLD patches. As mentioned before, for a given amount of damping material (CLD), it is desired to find their best shape and location on the structure simultaneously.

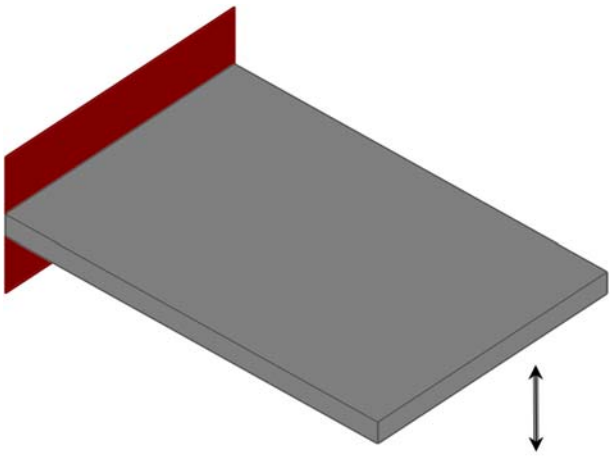

Figure 4-1: Plate undergoing flexural vibrations

Patches should be located on top of the structure so that maximum energy dissipation is achieved. Instead of considering a few pre-configured CLD patches, like Figure 4-2(a), and trying to optimally locate them on the structure, the surface of the structure will be covered with CLD patches that have an initial shape ϕ_0 and total surface area of A^* (see Figure 4-2(b)). Next, using the level set topology optimization technique, the best shape of the damping patches, $\phi_{optimum}$, will be determined for maximum vibration suppression.

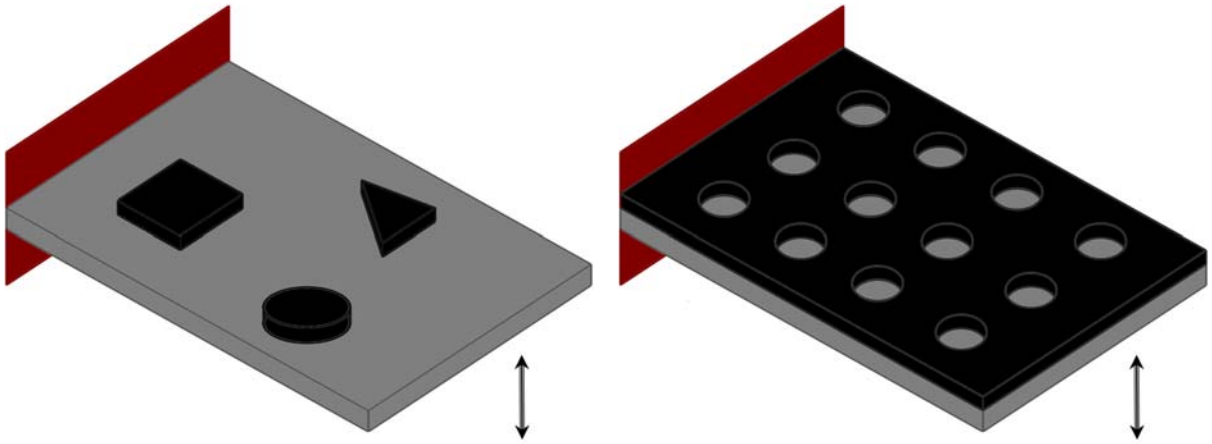

(a) (b)

Figure 4-2: CLD patches with a) Pre-configured b) initial shape of ϕ_0

4.2 Mathematical modeling

In order to formulate the damping optimization problem using the level set optimization technique, an objective function, which is a function of the shape of the damping coverage, should be defined. Without loss of generality, the damping will be considered to be inside of the structure as structural damping, as shown in Figure 4-3, so that equivalent 2D modeling can be performed.

Zheng and Tan [49] observed that the vibration response of the CLD treated beam shows more sensitivity to the location/length of the covered passive CLD patch and the shear modulus of the viscoelastic layer than other parameters, such as the thickness of the viscoelastic layer (VL) and constraining layer (CL) with its elastic modulus fixed. Therefore, the thickness of the CLD layer can be eliminated from the optimization process.

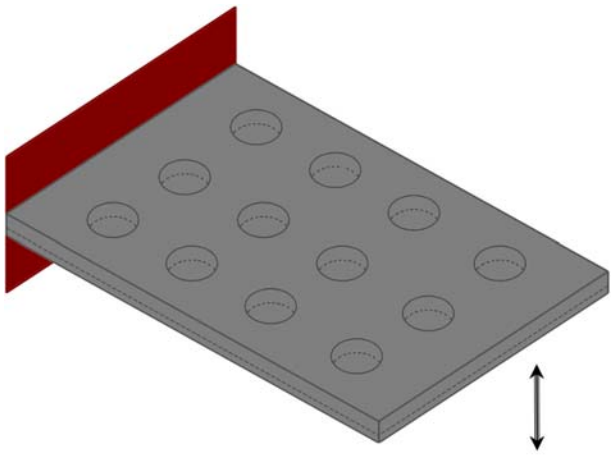

Figure 4-3: Modeling of damping as structural damping in a 2D structure

For the assumption of having the damping inside the structure, the equivalent loss factor and modal rigidity should be defined. This is done to simplify a complex problem into an equivalent

system. Finding the equivalent system was first proposed by Ross, Kerwin and Ungar and the method was named after them as RKU [27].

A fourth order differential equation is used in the RKU method for a uniform beam with the sandwich construction. This three-layer laminate system is then represented as an equivalent complex stiffness. This method assumes that the mode shapes of the structure are sinusoidal in nature, which implies a simply-supported boundary condition. Therefore, when other boundary conditions are used, the results are approximated depending on the mode shape in question [96-103].

It should be noted that when the RKU method is applied to real world complex structures, it does not precisely predict the value of damping, however it is a good damping indicator. The paramount goal is to implement a simplified method to establish a design trend that can be used in the level set optimization formulation.

In Figure 4-4, Macioce [103] compares the damping prediction of RKU and MSE methods with experimental measurements. Limitations of simplified RKU method especially when dealing with true boundary conditions (not just simply-supported) are shown. RKU over estimates the predicted the value of damping however it offers a good approximation for the damping which is sufficient for the level set optimization formulation.

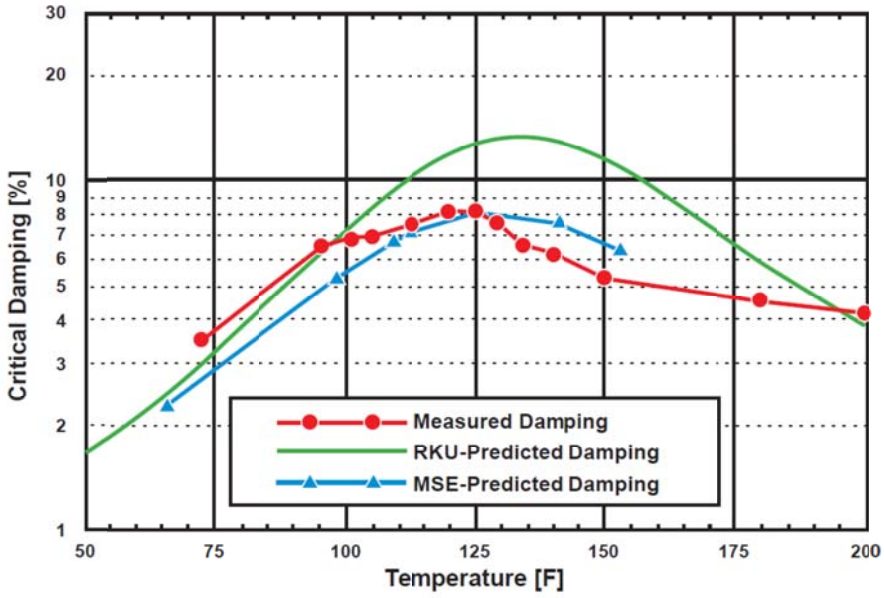

Figure 4-4: Comparison of Measured Damping vs. Predicted Damping using various modeling techniques [103]

Consider the sandwich plate shown in Figure 4-5. The viscoelastic layer is constrained between the main structure and the top constraining layer. The bending of the composite layers will produce shear strain in the viscoelastic layer and bending (extensional) strain in all three layers.

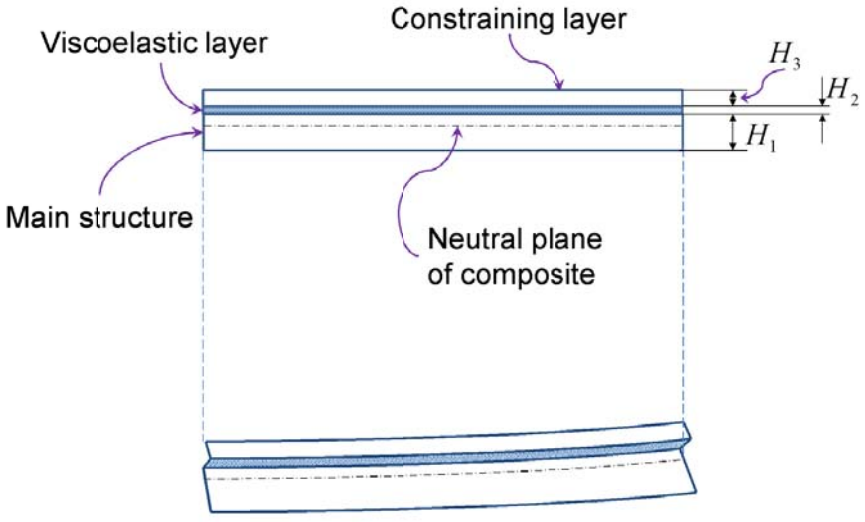

Figure 4-5: A panel with CLD layer (a) flat (b) deformed.

In most practical cases, the extensional stiffness of the viscoelastic layer is small compared to the stiffness of the other two layers; hence, the loss factor of the composite panel could be approximated using the Ross-Ungar-Kerwin method [104]

$$\eta = \frac{\beta_2^2 YX}{1+(2+Y)X+(1+Y)(1+\beta_2^2)X^2} \tag{4.1}$$

where β_2 is the loss factor of the viscoelastic layer, and Y is a stiffness parameter, defined by:

$$\frac{1}{Y} = \frac{E_1 H_1^3 + E_3 H_3^3}{12\left(H_2 + \frac{H_1+H_3}{2}\right)}\left(\frac{1}{E_1 H_1} + \frac{1}{E_3 H_3}\right) \tag{4.2}$$

where E_1, E_3, H_1 and H_3 are the moduli of elasticity and thicknesses of the two elastic layers, respectively. X in Equation (4.1) is called the shear parameter and given as:

$$X = \frac{G_2}{p^2 H_2}\left(\frac{1}{E_1 H_1} + \frac{1}{E_3 H_3}\right) \tag{4.3}$$

where G_2 is the real part of the complex shear modulus, and p is the wave number, namely the nth eigenvalue divided by the composite panel's length.

In the same manner, the equivalent modal flexural rigidity is given by [105]

$$\begin{aligned} EI = {} & \frac{1}{12}\left(E_1 H_1^3 + E_2 H_2^3 + E_2 H_2^3 - E_2 H_3^3 \frac{d-Q}{1+g_v}\right) + E_1 H_1 Q^2 + E_2 H_2\left(\frac{H_1+H_2}{2} - Q\right)^2 \\ & + E_3 H_3 (d-Q)^2 - \left[\frac{E_2 H_2\left(\frac{H_1+H_2}{2} - Q\right)}{2} + E_3 H_3 (d-Q)\right]\left(\frac{d-Q}{1+g_v}\right) \end{aligned} \tag{4.4}$$

where Q is the distance from the neutral axis of the three layer system to the neutral axis of the host system. Q and d are defined as

$$Q = \frac{E_2 H_2 \left(\frac{H_1 + H_2 - d}{2} \right) + X \left(E_2 H_2 \frac{H_1 + H_2}{2} + E_3 H_3 d \right)}{E_3 H_3 + \frac{E_2 H_2}{2} + X \left(E_1 H_1 + E_2 H_2 + E_3 H_3 \right)} \tag{4.5}$$

$$d = H_2 + \frac{H_1 + H_3}{2} \tag{4.6}$$

It should be noted again that even if the estimated loss factor and the flexural rigidity contain some errors, they will not affect the results of the original optimization problem. As an example, consider a problem of optimal viscous damper placement under a beam, with both ends simply-supported, as shown in Figure 4-6. If the viscous damping coefficient is set to either 5 NSm^{-1} or 5.1 NSm^{-1}, the optimal location for the viscous damper will be at the middle of the beam. Similarly, in the problem at hand, any minor error that occurs in finding the equivalent modal loss factor and rigidity will not affect the optimization problem.

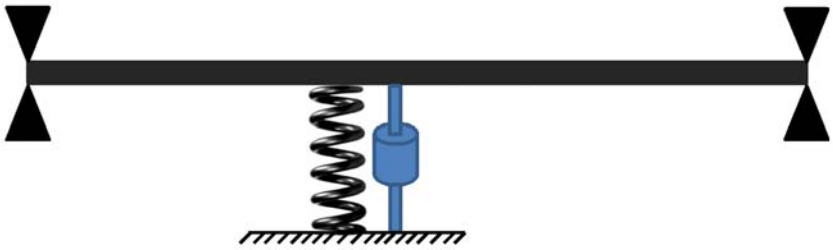

Figure 4-6: Viscous damper positioning under a beam.

Damping is defined in terms of loss factor. In order to capture the loss factor damping (or structural damping) viscoelasticity will be modeled in the frequency domain. This can be explained by means of the following equation:

$$K^* = K_{VR} + jK_2 = (1 + j\eta_v) K_{VR} \tag{4.7}$$

where K^* is the complex modulus, K_{VR} is the storage stiffness (modulus), K_2 is the loss modulus and $\eta_v = K_2 / K_{VR}$ is the loss factor. The amount of stored energy for the applied strain is defined by the storage modulus, K_{VR}, and the amount of energy dissipated is defined by the loss modulus, K_2. In the context of level set optimization, the loss factor becomes:

$$\eta_v(\phi) = \eta_0 H(\phi) \tag{4.8}$$

where η_0 is the material loss factor.

The objective of this optimization problem is to maximize the modal loss factor of one mode of vibration of the system, which is equivalent to the highest dissipated energy in that mode. Using the modal strain energy method (MSE), the modal loss factor of the first mode can be defined by Equation (2.8), which can be simplified as:

$$\eta = \eta_v(\phi)\frac{E_v}{E_{total}} \tag{4.9}$$

where E_v represents the modal strain energy contributed by the CLD layer while the total modal strain energy is denoted by E_{total}. Therefore, the topology optimization for this 2D problem can be written as:

$$\begin{aligned} &\text{minimize:} \quad C(\phi) = \int_{\Omega} -\eta_v(\phi)\frac{E_v}{E_{total}}\,\mathrm{d}\Omega \\ &\text{subjected to:} \quad \int_{\Omega} H(\phi)\,\mathrm{d}\Omega = A^* \end{aligned} \tag{4.10}$$

where Ω represents the design domain, and A^* shows the desired area of the CLD layer to be used to control excessive vibrations. The negative sign has been used to change the maximization problem to one of minimization.

It is noteworthy that higher mode shapes can also be included in the objective function. In fact the modal loss factor of each mode can be found and combined with some weighting coefficients, and then be used in the objective functions. In that case the objective function can be reformed as

$$C(\phi) = \int_{\Omega} -\sum_{m=1}^{N} \beta_m \eta_v^m(\phi) \frac{E_v^{(m)}}{E_T^{(m)}} \mathrm{d}\Omega \tag{4.11}$$

where m refers to the mode number, N is the number of desired mode shapes and β is the weighting factor of each mode. $E_v^{(m)}$ represents the modal strain energy contributed by the CLD layer in the m^{th} mode and the total modal strain energy in the m^{th} mode is denoted by $E_T^{(m)}$ while the frequency dependent material loss factor corresponding to the m^{th} mode is represented by $\eta_v^m(\phi)$. As an example, consider a system whose first and second natural frequencies are 200 Hz and 300 Hz respectively. Suppose that the material loss factor of the added CLD at 200 Hz and 300 Hz are 0.19 and 0.25, respectively. In this case the objective function to address both the first and second natural frequencies will be:

$$C(\phi) = \int_{\Omega} -\left[\beta_1 (0.19 H(\phi) \frac{E_v^{(1)}}{E_T^{(1)}} + \beta_2 (0.25 H(\phi) \frac{E_v^{(2)}}{E_T^{(2)}} \right] \mathrm{d}\Omega \tag{4.12}$$

β_1 and β_2 can be chosen according to the design requirements and the frequency band.

Since in many engineering applications the fundamental mode shape is more significant in design of the system, also for the sake of simplicity and better presentation of the work, in this section the objective function has been formulated based of the first eigenfrequency.

Lagrangian formulation is applied in order to incorporate the volume constraint into the optimization problem by means of the Lagrangian multiplier, λ, as follows:

$$J(\phi,\lambda)=\int_{\Omega}\left[-\eta_v(\phi)\frac{E_v}{E_{total}}+\lambda\left(H(\phi)-\frac{A^*}{A^{\Omega}}\right)\right]\mathrm{d}\Omega \tag{4.13}$$

where the area of the entire design domain is denoted by A^{Ω}.

When the derivative of Equation (4.13) is zero, this equation reaches its minimum. As mentioned in Chapter 3, the variation of the Heaviside function is:

$$\delta H(\phi)=\frac{\partial H(\phi)}{\partial\phi}\delta\phi=\delta(\phi)\delta\phi=\delta\phi\big|_{\phi=0} \tag{4.14}$$

where $\delta(\phi)$ is the Dirac delta function and $\delta\phi$ represents the variation of ϕ. Along the normal direction, this variational equation can be written as:

$$\delta\phi\big|_{\phi=0}=|\nabla\phi|\,\delta l \tag{4.15}$$

where δl is an infinitesimal variation along the normal direction $\mathbf{n}=\nabla\phi/|\nabla\phi|$.

The variation of J for Equation (4.13), i.e., $\delta_{\phi}J$ can be calculated in the following form

$$\begin{aligned}\delta_{\phi}J&=\int_{\Omega}\left[-\frac{\partial\eta_v(\phi)}{\partial\phi}\times\frac{E_v}{E_T}+\lambda\frac{\partial H(\phi)}{\partial\phi}\right]\underbrace{\delta\phi\big|_{\phi=0}}_{|\nabla\phi|\delta l}\mathrm{d}\Omega\\&=\int_{\Omega}\left[-\eta_0\frac{E_v}{E_{total}}+\lambda\right]\delta(\phi)|\nabla\phi|\,\delta l\mathrm{d}\Omega\end{aligned} \tag{4.16}$$

The Euler-Lagrange equation corresponding to Equation (4.16) at the extreme value point can be expressed as

$$\left[-\eta_0\frac{E_v}{E_T}+\lambda\right]\delta(\phi)|\nabla\phi|=0 \tag{4.17}$$

The Hamilton-Jacobi equation for this optimization problem can be written as:

$$\frac{\partial \phi}{\partial \tau} - \underbrace{\left[-\eta_0 \frac{E_v}{E_{total}} + \lambda \right] \delta(\phi) |\nabla \phi|}_{V_n} = 0 \tag{4.18}$$

which can be solved numerically, with an initial condition of ϕ_0 .

Finally, an explicit expression is found for Lagrangian multiplier λ according the gradient projection method [62]. The second part of Equation (4.10) defines an area constraint that should be satisfied at all time. Therefore its derivative with respect to pseudo-time should be zero, as stated below:

$$\frac{\mathrm{d}}{\mathrm{d}\tau} \left(\int_{\Omega} H(\phi) \mathrm{d}\Omega - A^* \right) = 0 \tag{4.19}$$

Since A^* is constant and its derivative is zero, Equation (4.19) can be rewritten as

$$\int_{\Omega} \frac{\partial H(\phi)}{\partial \phi} \frac{\partial \phi}{\partial \tau} \mathrm{d}\Omega = 0 \tag{4.20}$$

Substituting Equations (4.14) and (4.18) into Equation (4.20) yields

$$\int_{\Omega} \left[-\eta_0 \frac{E_v}{E_T} + \lambda \right] \delta(\phi) |\nabla \phi| . \delta(\phi) \mathrm{d}\Omega = 0 \tag{4.21}$$

The solution of Equation (4.21) gives and explicit expression for λ, in the following form:

$$\lambda = \frac{\int_{\Omega} \left(\eta_0 \frac{E_v}{E_{total}} \right) \delta^2(\phi) |\nabla \phi| \mathrm{d}\Omega}{\int_{\Omega} \delta^2(\phi) |\nabla \phi| \mathrm{d}\Omega} \tag{4.22}$$

It is noteworthy to mention that in order to ensure that Equation (4.18) converges, the step time should satisfy the Courant-Friedrichs-Lewy (CFL) condition [106], i.e.:

$$\Delta\tau \le \frac{h}{\max|V_n|} \tag{4.23}$$

In this equation, h refers to the minimum distance between grid points and $\max|V_n|$ is the maximum value of the points of the grid [58, 62]. If this condition is not satisfied, i.e. time steps are not chosen properly, for relatively large V_n, the damping patches will propagate quickly and will cover the whole surface. This will lead to an incorrect solution and convergence will not be achieved.

The following two sections will discuss the coding procedure needed to perform the level set optimization.

4.3 General Level set Topology Optimization Algorithm

Consider the topology optimization problem described by Equation (4.10). The iterative algorithm of the level set topology optimization can be written as:

1. initialize ϕ_0, which corresponds to an initial guess for Ω;
2. run a structural analysis (FEA) to evaluate V_n in Equation (4.18), this includes finding normal velocity and sensitivity analysis;
3. solve Equation (4.18) for one time step $\Delta\tau$, to find a new ϕ;
4. go to step 2;
5. iterate until convergence, i.e., $J(\varepsilon_k, \phi_k, \lambda_k) - J(\varepsilon_{k+1}, \phi_{k+1}, \lambda_{k+1}) \le \alpha$;

   where α is a convergence factor, and k shows the iteration number.

This overall optimization procedure is summarized in the flowchart shown Figure 4-7.

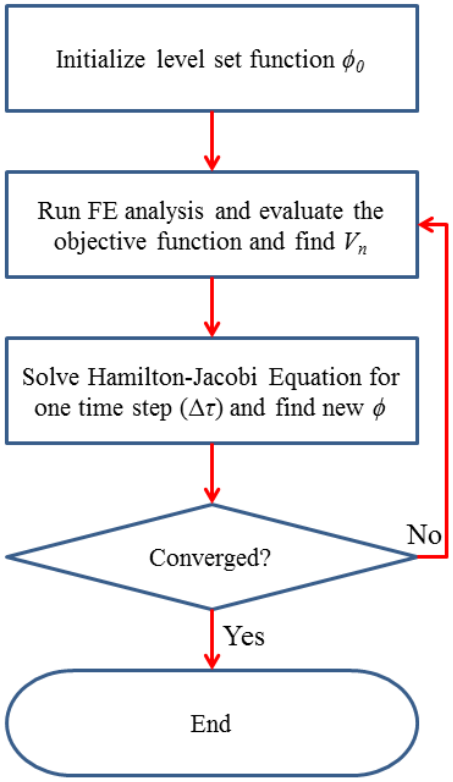

Figure 4-7: Flowchart of level set topology optimization

This algorithm and the flowchart demonstrate that an iterative process should be followed to find the optimum topology. Furthermore, most of the numerical approaches offered to solve the Hamilton-Jacobi equation are based on finite difference approaches with lots of stability difficulties.

In practice, implementing this iterative process is cumbersome. Challis [107] developed a code that combines both finite element analysis of the structure and the finite difference analysis of the Hamilton-Jacobi equation in MALTAB. Although the code is very compact, the finite element part can only handle very simple structures and is not capable of analysing complicated structures or sophisticated analysis fields. Liu et al. [62] suggested solving the Hamilton-Jacobi equation using the finite element method. This way, they formed a coupled modeling of the two different

parts of the topology optimization, i.e. structural analysis and Hamilton-Jacobi partial differential equation, in the commercial package FEMLAB. In other words, they solved both of these problems as a coupled problem in FEMLAB using the finite element method.

Although this approach is fairly simple and can easily handle practical problems, it has a significant downside that limits its practicality. In this approach, as time, τ, goes forward by a certain time step, $\Delta\tau$, at each time a structural analysis is performed to evaluate V_n. However, since the structural part is just a static analysis in this paper, it is not affected by time and thus can be performed in any time. Therefore, coupling does not influence the results, and allows to follow the entire optimization process through a coupled analysis. But what if the structural analysis is not static? What if it is dynamic, depending on time or if it is an analysis in frequency domain? A more practical method is needed to handle the proposed optimization technique.

4.4 Numerical Implementation of Level set Method in the Proposed Damping Optimization

For all the cases mentioned in the last part of Section 4.3, this method [62] cannot be applied and coupling of the non-static problems (i.e. modal or transient problems), along with time forwarding PDE, will affect the solution of the structural analysis. This will consequently lead to failure in the level set optimization.

In most research works so far, dynamic problems have been modeled by static-equivalent analysis, so that such simple coupling can be used to perform topology optimization. Furthermore, systematic work has not been completed to find a practical approach for those aforementioned cases. This is the primary reason that not much effort has been exerted to

optimize damping in the context of level set optimization, because it is not possible to model damping statically, and damping reveals its properties only in dynamic conditions.

In this work, an interactive numerical code will be developed that can handle the level set optimization of all kinds of analyses, for any type of structures (model). Unlike the code presented in [62], the structural analysis is not restricted to static analysis, and can deal with any type of analysis. Unlike [107], any type of structure, no matter how sophisticated it is, can be considered as well.

The idea is that instead of coupling the two problems (i.e. structural analysis and solving the Hamilton-Jacobi equation), two different software packages (MATLAB and COMSOL) are synchronized to interconnectedly solve the problem at hand in a desired iterative manner. Although both parts (Structural and PDE) are being solved by COMSOL, the physics are not coupled. The role of MATLAB is to manage the whole process (and check the convergence criterion), and to transfer results to/from different physics. The algorithm of performing level set topology optimization along with the corresponding physics can be expressed as

1. initialize Φ_0 in MATLAB;
2. read Φ from MATLAB in COMSOL (Number 1) and perform structural analysis to find V_n, and send V_n to MATLAB;
3. read V_n from MATLAB in COMSOL (Number 2) and solve Hamilton-Jacobi for one time step ($\Delta\tau$) to find new Φ and send it to MATLAB;
4. go to step 2;
5. iterate until convergence.

This process is shown in Figure 4-8. It is clear that there is no coupling between the two physics and each analysis is performed separately. Time forwarding (in terms of τ) is happening in physics 2, while physics 1 can independently handle any type of analysis (static, dynamic, time domain, frequency domain).

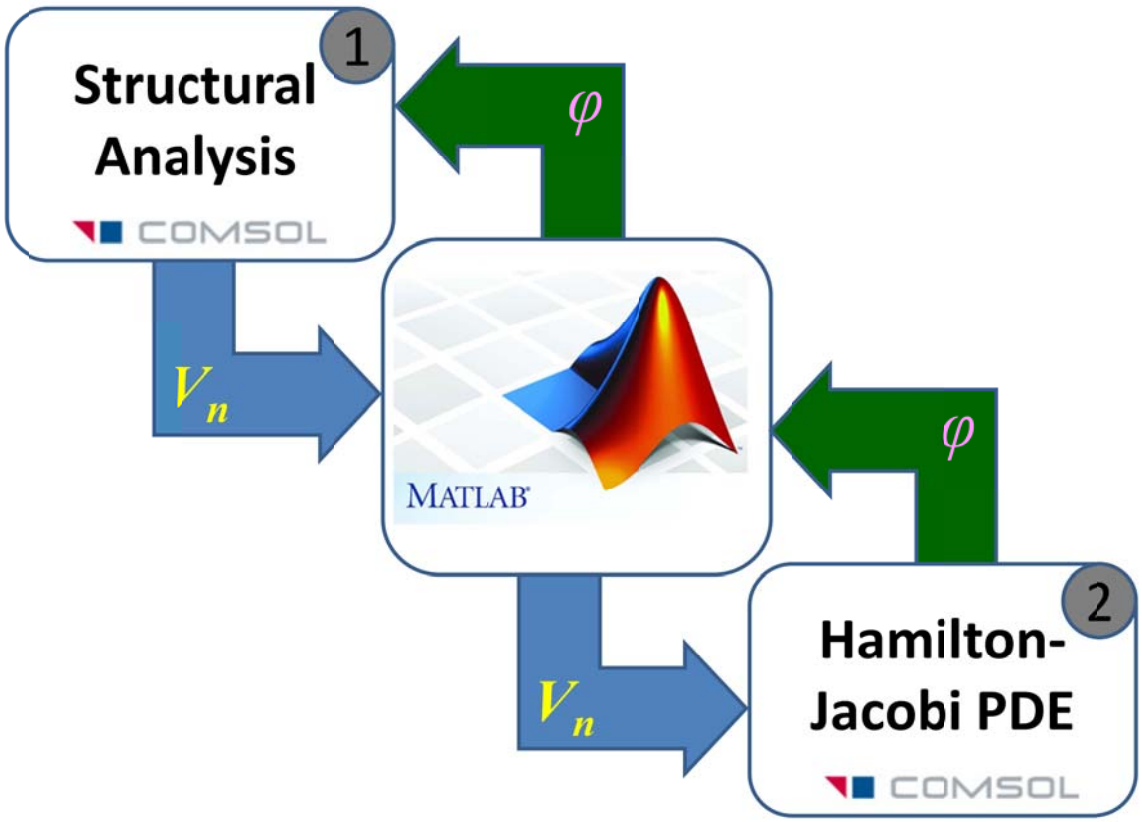

Figure 4-8: MATLAB-COMSOL interaction for level set topology optimization

It should be noted that this method is not limited to this problem and could be extended to other dynamic problems as well.

4.5 Numerical examples

In this section, to demonstrate the application of the proposed optimization technique a few examples will be discussed.

4.5.1 Case study 1: Damping Optimization in a Cantilever Plate

Consider the cantilever plate as the first example, shown in Figure 4-1. The system properties are listed in Table 4-1.

Table 4-1: Plate structure properties

Property	Value	Unit
Length	160	mm
Width	120	mm
Thickness	2	mm
Modulus of elasticity	71	GPa
Poisson ratio	0.29	-
Density	2700	Kg/m^3
CLD Material loss factor	0.79 ~ 0.99	-
CLD Specific gravity	0.53	lb/ft^2
CLD Thickness	1.5	mm

Figure 4-9 (a) and (b) illustrate the initial CLD configuration, $H(\phi_0)$, and its corresponding level set surface, ϕ_0, respectively. The gray parts represent the CLD patches. It should be noted that similar to Ref. (Liu, Korvink et al. 2005) in this example ϕ_0 has been defined using "*min*" function available in COMSOL©. A general approach for defining the initial level set function will be proposed in Chapter 5. The proposed approach is capable of producing the level set function corresponding to any initial configuration in 2D, 3D and higher dimensional domains.

The rubber material is modeled in the same way as seen in Ref. [108]; therefore, its loss factor varies from 0.79 to 0.99. In this case, in the room temperature and for the first natural frequency the material loss factor has been chosen as 0.89.

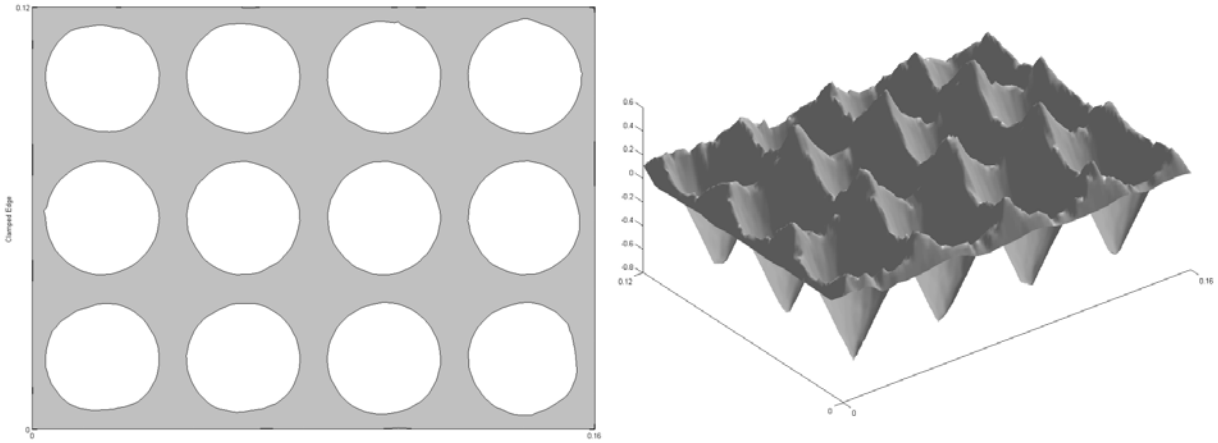

(a) (b)

Figure 4-9: (a) Initial configuration of CLD layer (area of 0.0084 m^2); (b) Corresponding level set function

The evolution of the CLD patches is shown in Figure 4-10. From these figures, it can be seen that the damping set has been pushed towards the clamped edge of the plate. The structural damping force is proportional to the rate of change of strain. For a cantilever plate type, the present case study, those regions close to the clamped edge demonstrate the highest changes of strain rate. Therefore, the results obtained from the level set optimization are in close agreement with the expected locations of the patches, since the highest level of damping force will be achieved by accumulating the damping set into the clamped edge of the plate.

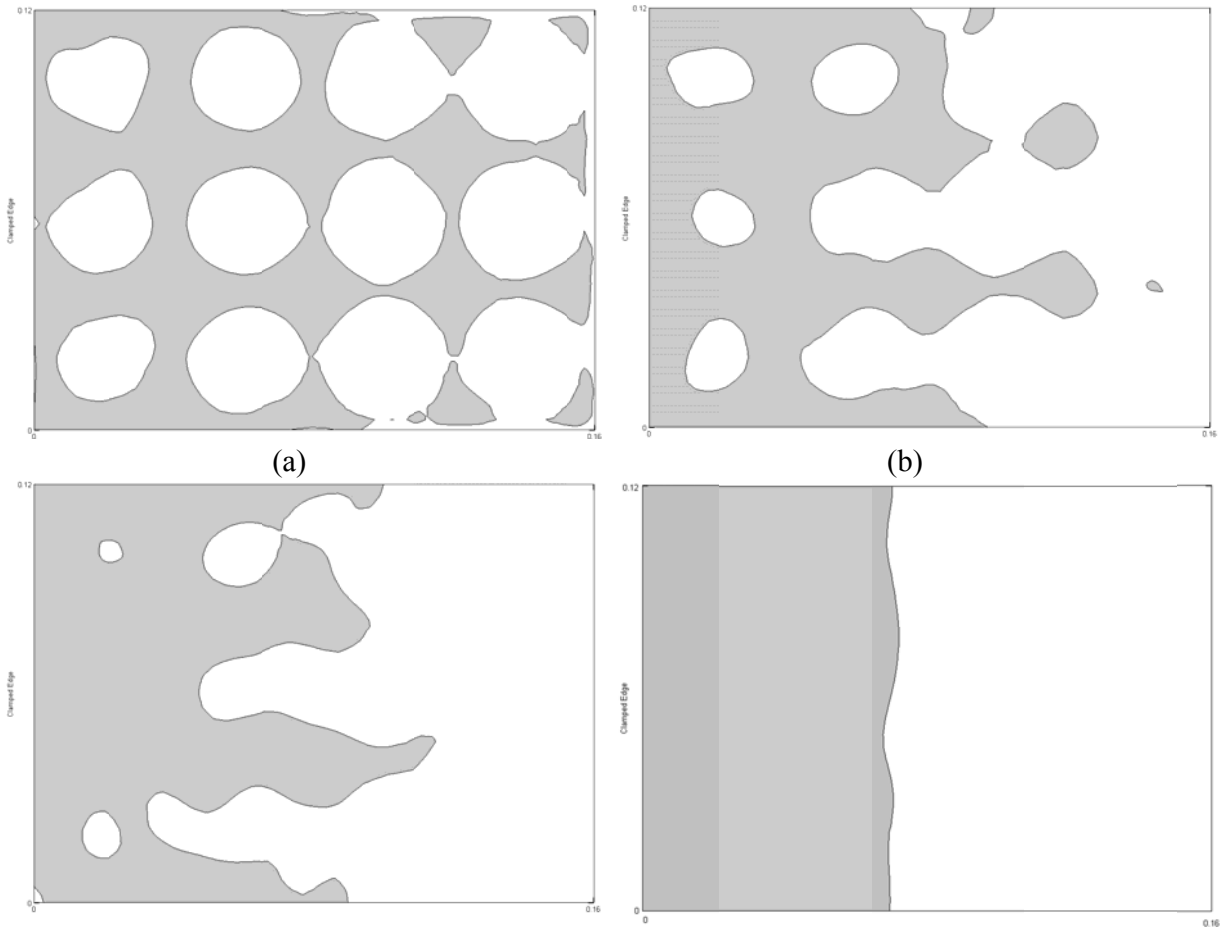

Figure 4-10: Evolution of CLD patches (System 1) (a) τ=0.1; (b) τ=0.3; (c) τ=0.5; (d) τ=4

The variations of the modal loss factor under different iterations are shown in Figure 4-11. It can be seen that the modal damping is increased with the passage of pseudo time.

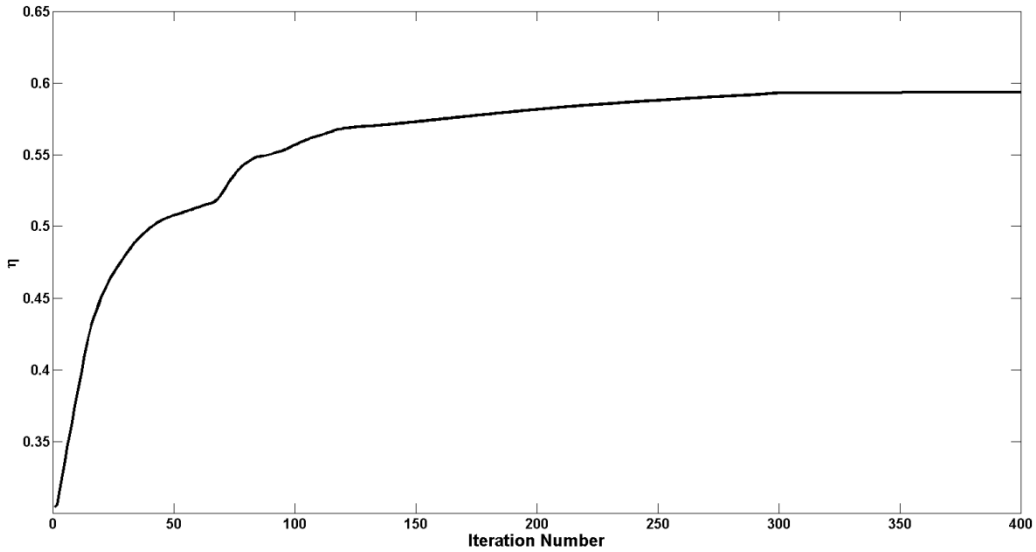

Figure 4-11: Modal loss factor in different iterations

It should be noted that the number of iterations needed for convergence, as well as the final result, depends on the initial guess. Since the energy dissipation of viscoelastic materials is proportional to the strain rate, it is desirable to locate the CLD at points of high modal curvature [109]. In order to have an appropriate initial guess, a simple modal analysis should be performed and the points with higher modal curvature will be determined. Then, the initial shape will be chosen so that more CLDs are located close to the points found in the previous step.

This example was initiated with evenly distributed damping (as shown in Figure 4-9 a), so the optimization required many iterations to converge. However, for a smarter initial guess, shown in Figure 4-12, the optimization problem will converge after 43 iterations. It should be noted that energy dissipation in CLD patches is related to the strain rate. So, if the initial configuration is chosen close to areas with high modal strain energy, fewer number of iterations will be needed and the chance of finding the global optimum will increase. For this plate in the first mode, the area close to the clamped edge encounters highest modal strain energy, therefore configuration shown in Figure 4-12 is a better choice compared to that presented in Figure 4-9.

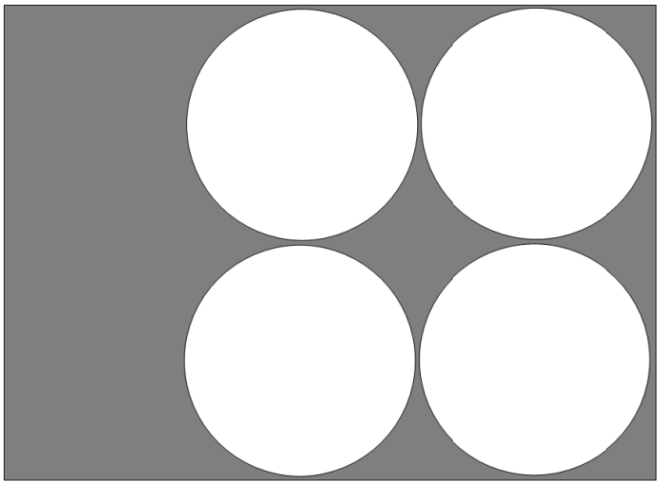

Figure 4-12: Alternative initial configuration for CLD layer (area of 0.0084 m^2)

4.5.2 Case study 2: Damping optimization of square plates with nonsymmetric cut out

Ref. [48] presents an industrial and practical example of locating damping material on top of structures. As illustrated in Figure 4-13, the structure includes square plates with a nonsymmetrical cut out

Figure 4-13: Experimental set up [48]

The test was carried out on a rectangular plate, shown in Figure 4-14(a). The plate is mounted in a relatively stiff fixture. It has zero displacement on the boundaries and does not have rotations in any direction except for the transversal direction. The material properties of different parts of the system are presented in Table 4-2. For this problem in room temperature and in the first natural frequency the loss factor has been considered to be 0.9.

Table 4-2: System properties for case study 2

Property	Value	Unit
Length	160	mm
Width	120	mm
Thickness	2	mm
Modulus of elasticity	71	GPa
Poisson ratio	0.29	-
Density	2700	Kg/m^3
Material loss factor	0.79 ~ 0.99	-
CLD Specific gravity	0.53	lb/ft^2
CLD Thickness	1.5	mm

The excitation of the fixture was done using an electromagnetic shaker of the type ‘‘Wilcoxon F4/F7’’ with a built in force gage sn 9943. The response amplitude was measured by a laser

equipment of the type ‘‘Polytec PSV 300 scanning laser vibrometer’’ including software version 8.22.

In this section, the same system is studied and the best shape and location of the damping patches will be determined using the level set method. The results will be compared with those reported in Ref. [48]. The initial configuration of the CLD patches and the corresponding level set function are shown in Figure 4-14(a) and (b), respectively. This configuration has been chosen based on the fact that CLD patches exhibit more energy dissipations close to points of high modal curvature.

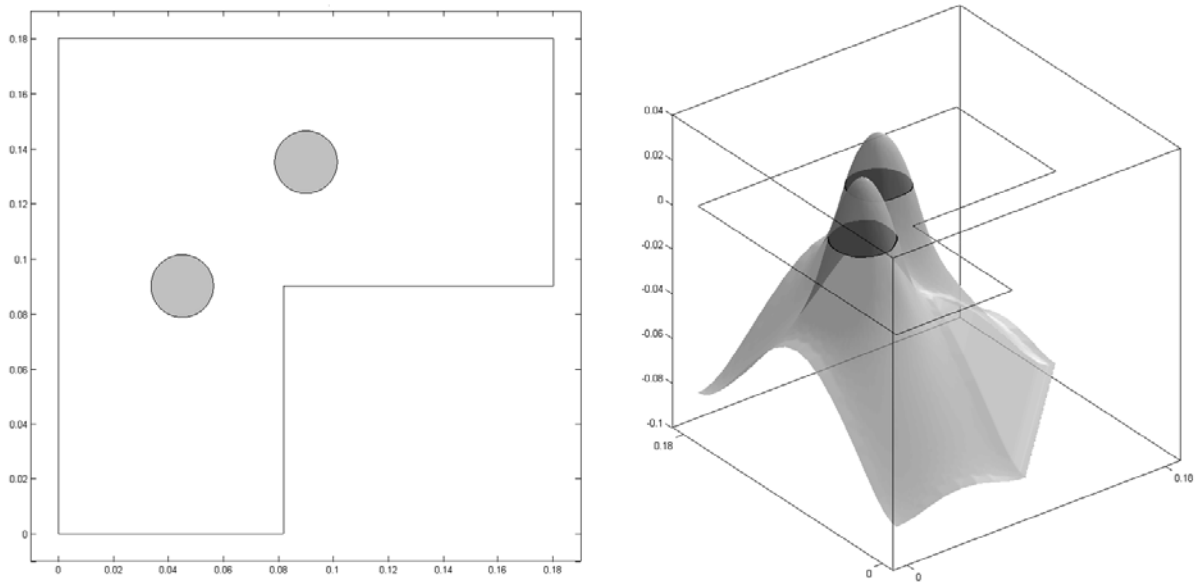

(a) (b)

Figure 4-14: (a) Initial damping configuration (b) Level set function

Figure 4-15 illustrates the evolution of the damping patches; the variations of the modal loss factor with pseudo time are shown in Figure 4-16.

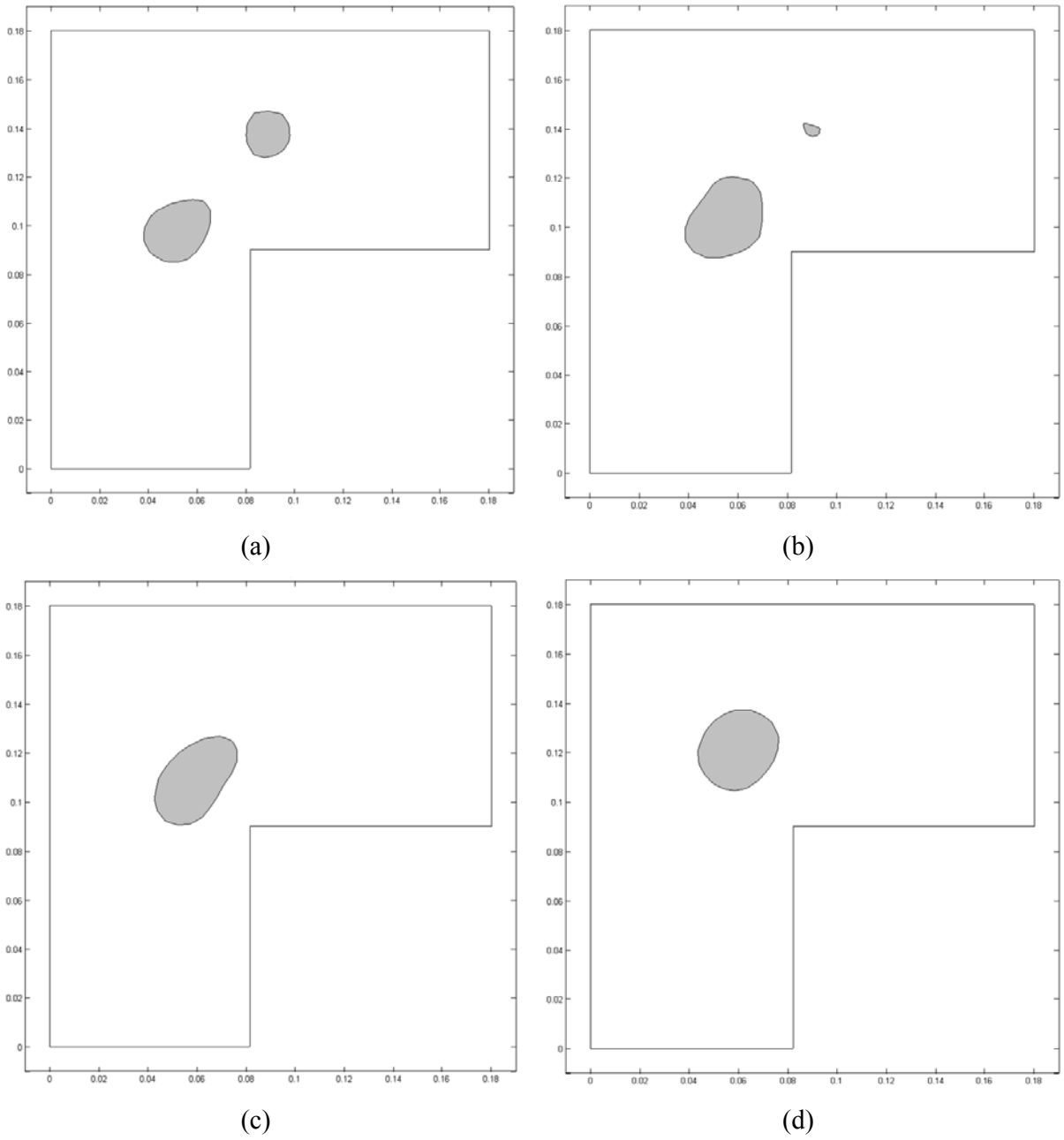

Figure 4-15: Evolution of the CLD patches (a) τ=0.02; (b) τ=0.04; (c) τ=0.12; (d) τ=0.2

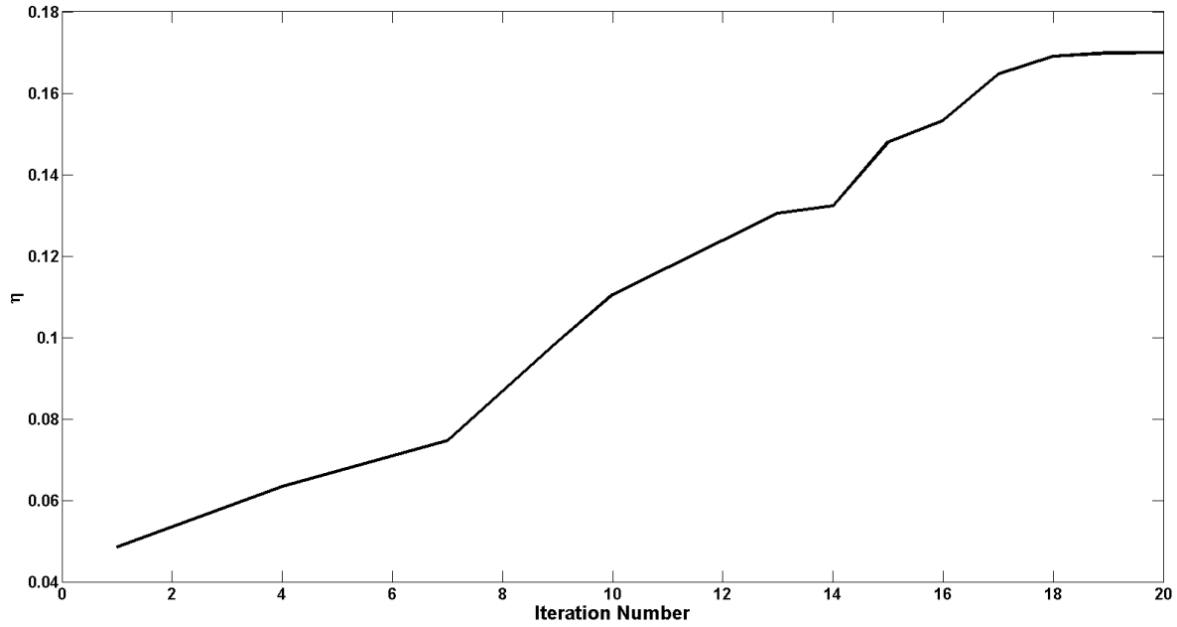

Figure 4-16: Modal loss factor under different iterations

Comparing the final results obtained with those reported in Ref. [48], as illustrated in Figure 4-17, reveals the following important observations:

(a) although the optimization start with two separate CLD patches, at the end it was found that a single patch being located in the optimum position, would work best for this system;

(b) the optimum location of the patch, found by using the level set technique is in good agreement with the experimental results presented in Ref. [48];

(c) since this method is not confined to the square shaped patches, and also is capable of providing smooth boundaries, it finds better shape of patches. For the fundamental mode, the optimum shape for the CLD patch in this system is a circle. The circular shape would give 10 percent more fundamental loss factor when compared with the square shape.

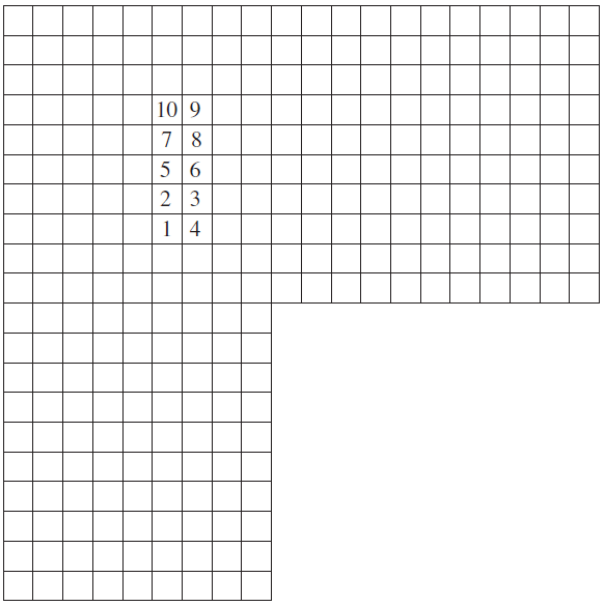

Figure 4-17: Optimum position of the CLD patch found from experimental tests [48]

It should be noted that the area of the CLD patches for both systems (i.e., the amount of applied damping material) remained the same during the optimization process. This was achieved via imposing proper constraints.

This chapter discussed the application of level set optimization technique to 2D structures. The benefits of moving boundary approach were demonstrated for 2D systems. However, in most practical cases, complex 3D structures need to be dealt with. Hence, it is required to extend the level set formulation to more general 3D domain.

Chapter 5

Extension of the proposed optimization method to 3D structures

Most engineering structures are three dimensional. For example, the vibration of an automotive dash panel with nonsymmetric shape, as shown in Figure 5-1, has to be studied in a 3D domain. In this chapter, the level set vibration control will be extended to a 3D domain and the generation of corresponding 4D functions will be presented. Two 3D structures, an automotive dash panel and a satellite dish, will be studied for optimization of added damping materials.

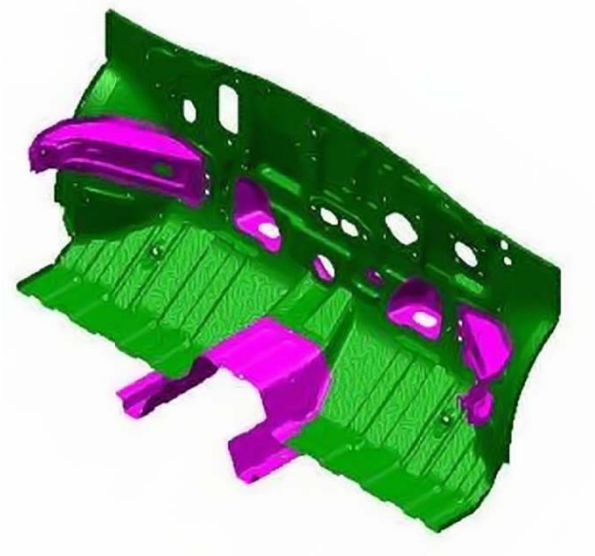

Figure 5-1: Automotive dash panel

5.1 Problem formulation and solution approach

Consider a 3D system like the dash panel shown in Figure 5-1. Vibration of such a system needs to be minimized by the application of CLD patches. The objective is to find the best shape and location for such patches. Obviously, the patches are not confined to a 2D region and can form 3D shapes; therefore, the level set optimization discussed in Chapter 3 will be expanded to the 3D domain.

In order to perform 3D level set optimization, the first requirement is to define a 4D function whose zero level set is the initial 3D configuration of the damping patches in the system. Like before, optimization will be performed on this function, and in each step, the zero level set function reveals the shape and location of the damping patches in that stage.

Infinite 4D functions can be defined to have such property, i.e. their zero level set resembles initial configuration of damping patches. Among them, signed distance function is a worthy choice. The distance from a point $\vec{X}$ to a set $\partial\Omega$ is defined as:

$$d(X) = \min_{\vec{X}_C \in \partial\Omega} \left(\left| \vec{X} - \vec{X}_C \right| \right) \tag{5.1}$$

The value of function ϕ at each point will be equal to its distance from the boundary with a sign depending on whether the point is inside or outside the region, i.e.

$$\phi(\vec{X}) = \begin{cases} -d(\vec{X}) & \vec{X} \in \Omega^+ \\ 0 & \vec{X} \in \partial\Omega \\ d(\vec{X}) & \vec{X} \in \Omega^- \end{cases} \tag{5.2}$$

In Equation (5.2), Ω^+ is outside the region, where there is no damping, while Ω^- is inside the region with damping material; $\partial\Omega$ represents the boundary of damping patches.

Figure 5-2 illustrates two examples for signed distance functions corresponding to two initial shapes. In simple words, the signed distance function gives the distance to the level set with a sign being positive inside, and negative outside.

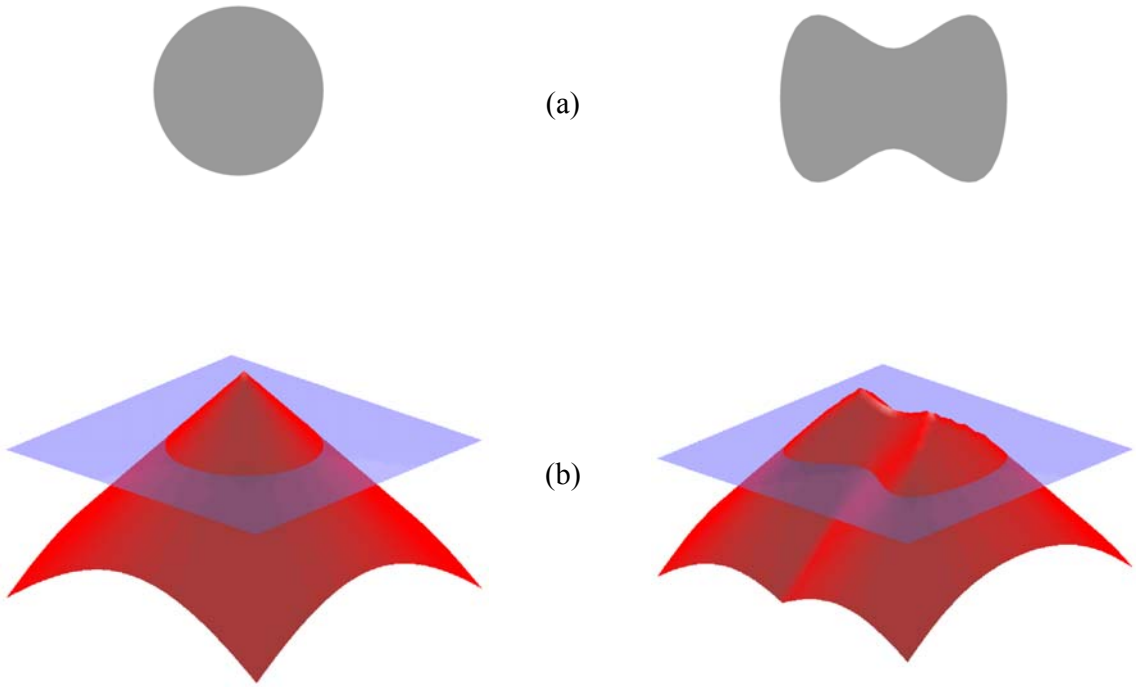

Figure 5-2: (a) Initial shape of damping patches (b) their corresponding ϕ (signed distance function). The x-y plane is shown in blue [110]

The signed distance function has several effective features, including:

- $$|\nabla \phi| = 1 \tag{5.3}$$

  It is noteworthy that during propagation, the level set function will not keep this property. That is why re-initialization methods are needed to bring the property back to ϕ. However, this is not a topic of interest in this work.

- ϕ is differentiable on $\partial\Omega$. This property is very important for continuing the front propagation because it ensures that at least the process can move forward one more step.

Now a new approach will be presented to generate such a signed distance function corresponding to the initial damping configuration. For the sake of simplicity and ease of

demonstration, suppose that the base structure is a plate. This procedure is valid for any dimensions, such as 2D, 3D, etc.

1- Model the base structure and initial damping configuration in the finite element software. It should be noted that this is only 3D modeling and does not consists of any elements or nodes. In this work, COMSOL© is used, as illustrated in Figure 5-3.

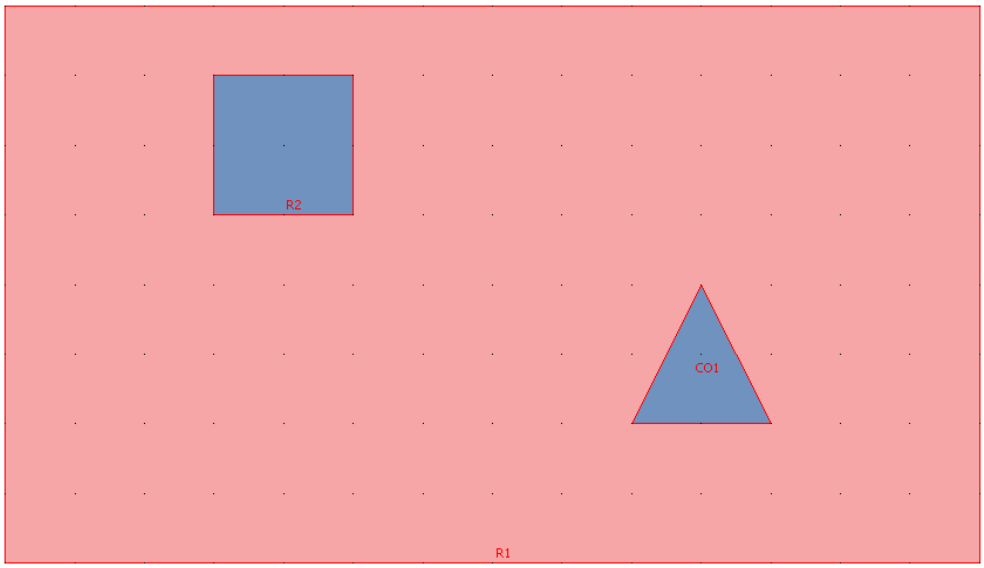

Figure 5-3: Base structure and damping configuration, modeled in COMSOL

2- Mesh the structure and added damping material. An example is shown in Figure 5-4. Note that the mesh does not have to be very fine in this stage and coarse mesh works too, because interpolation can be done in future steps. Also, this approach is independent from the element types because at this stage the locations of nodes are important rather than element properties.

3- Now, there are two sets of points available, as shown in Figure 5-5. Red points correspond to the boundary of damping patched, and blue points are located elsewhere on the structure. The list of these points and their corresponding coordinates can be easily extracted from

the software. Next, measure the distance of each point in the blue category to every point in the red group.

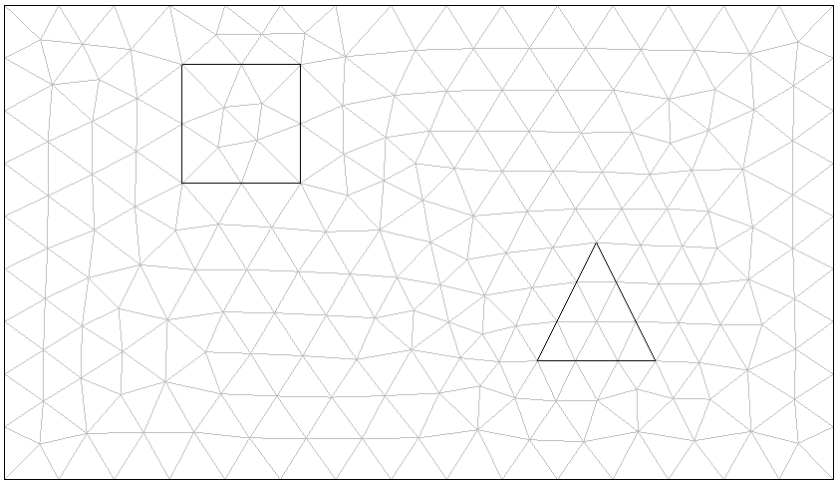

Figure 5-4: Meshed structure and damping patches

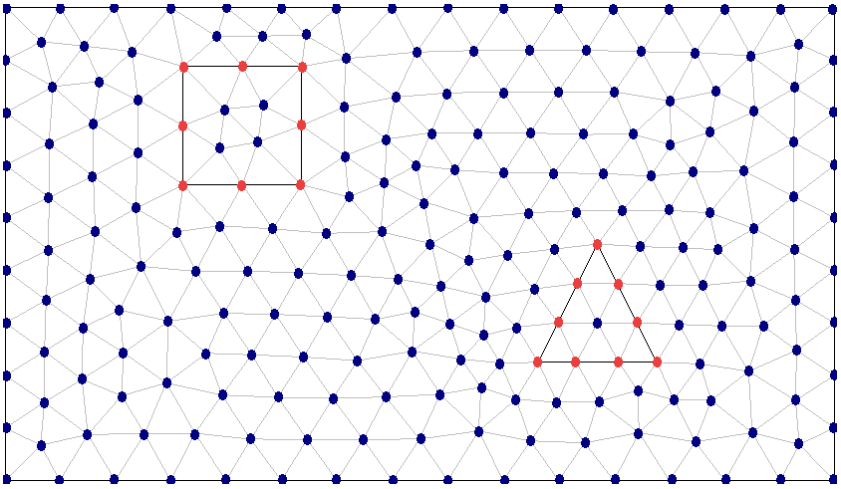

Figure 5-5: Mesh – red nodes on the border ($\partial\Omega$) and blue nodes elsewhere

If the blue set has n members and the red set has m members, then the absolute value of ϕ_i in each point will be given by Equation (5.4). Sign of ϕ_i is positive if the point is inside the boundary ($\partial\Omega$) and is negative if it is outside the boundary. In this work, this calculation is quickly performed using MATLAB©:

$$\left|\phi_i\right| = \min_{j=1..m}\left(\left|\vec{X}_i - \vec{X}_j\right|\right), \quad \vec{X}_i \notin \partial\Omega \quad , \quad \vec{X}_j \in \partial\Omega \tag{5.4}$$

In simple words, the value of ϕ at each point is the closest distance of that point from the boundary. Figure 5-6 illustrates the resulted level set function corresponding to the initial square and triangle damping configuration. In fact, if *xy* plane crosses this function at *z*=0 the initial damping shape shown in Figure 5-3 will be obtained. It should be noted that in practice, finer mesh is used in order to obtain a more uniform function.

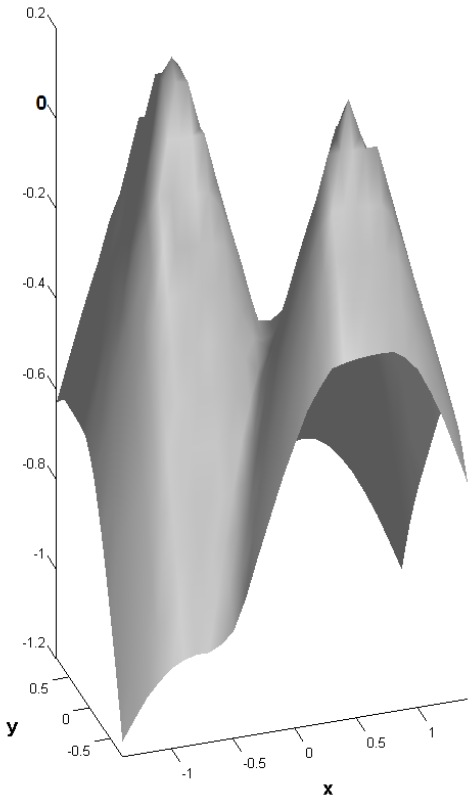

Figure 5-6: Level set function corresponding to the initial damping configuration

After generating the initial level set function, the rest of the procedure is identical to those explained in Chapter 4.

5.2 Numerical Examples

In this section two numerical examples will be discussed in detail. Satellite dishes and automotive dash panels are two of the systems in which CLD patches are commonly used to control excessive vibrations.

5.2.1 Case study 1: Vibration control in a satellite dish

Weight saving in the satellite industry has always been an important mission. Hence vibration control is inevitable. Vibrations, especially below 1 kHz, cause various problems for sensitive equipment attached to satellites [111]. One of the most commonly used methods to suppress vibrations in these structures is to apply anti-vibration mountings, or to coat the structure with viscoelastic materials [112]. In order to reduce the weight and cost penalties, the structure could be partially treated, and obviously the shape and location of such coverage will have to be determined.

In this section, a satellite dish (Figure 5-7) will be considered with a computer model (shown in Figure 5-8).

Figure 5-7: A typical satellite dish

The specifications of the satellite dish and the applied CLD patches are listed in Table 5-1. It is made of aluminum and a circle from its back is fixed to represent the support.

Table 5-1: Satellite dish specifications

Property	Value	Unit
Width	520	mm
Height	100	mm
Thickness	2	mm
Modulus of elasticity	71	GPa
Density	2700	kg/m^3
Poisson ratio	0.29	-
CLD Material loss factor	0.79 ~ 0.99	-
CLD Specific gravity	0.53	lb/ft^2
CLD Thickness	1.5	mm

Its boundary is shown in Figure 5-8(b) as a hatched circle. The satellite is welded to its support in this circle area and the rest of edges are free. A certain amount of constrained layer damping with a loss factor of 0.9 is applied to the satellite's surface in order to minimize its vibrations. The goal is to find the best shape and location of patches using the level set optimization technique.

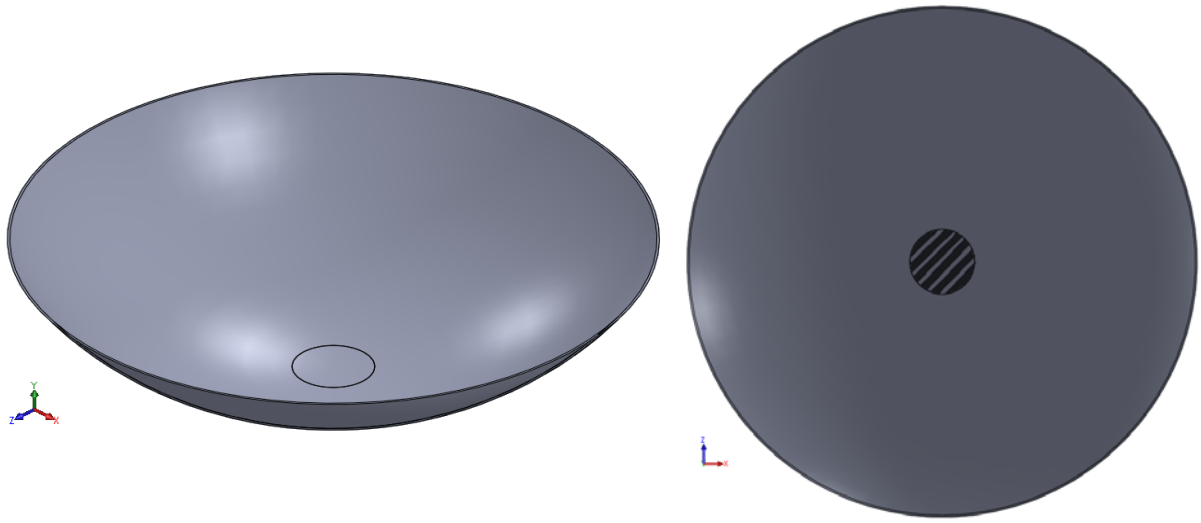

(a) (b)

Figure 5-8: Solid model generated for the satellite, (a) isometric view, (b) bottom view

Since the CLD patches' energy dissipation is related to the stain rate, it is very beneficial to perform a modal analysis on the structure before starting level set optimization. By performing the modal analysis, one can determine the locations that have highest modal strain energy at a specific mode or modes. Then the patches can be located close to those locations in order to increase the chance of finding the global minimum. Another benefit for this is reduction of optimization time due to starting the process from regions close to optimum locations.

Tetrahedral Lagrange-quadratic elements have been used in the structure finite element model. In contrast to the process mentioned for finding initial level set function, finer meshes will lead to smoother shapes however having more elements will increase the computational cost. The first four vibrational mode shapes of the satellite dish are shown in Figure 5-9. In these figures, the contour spectrum ranges from blue colour to red where blue and red illustrate minimum and maximum displacements, respectively.

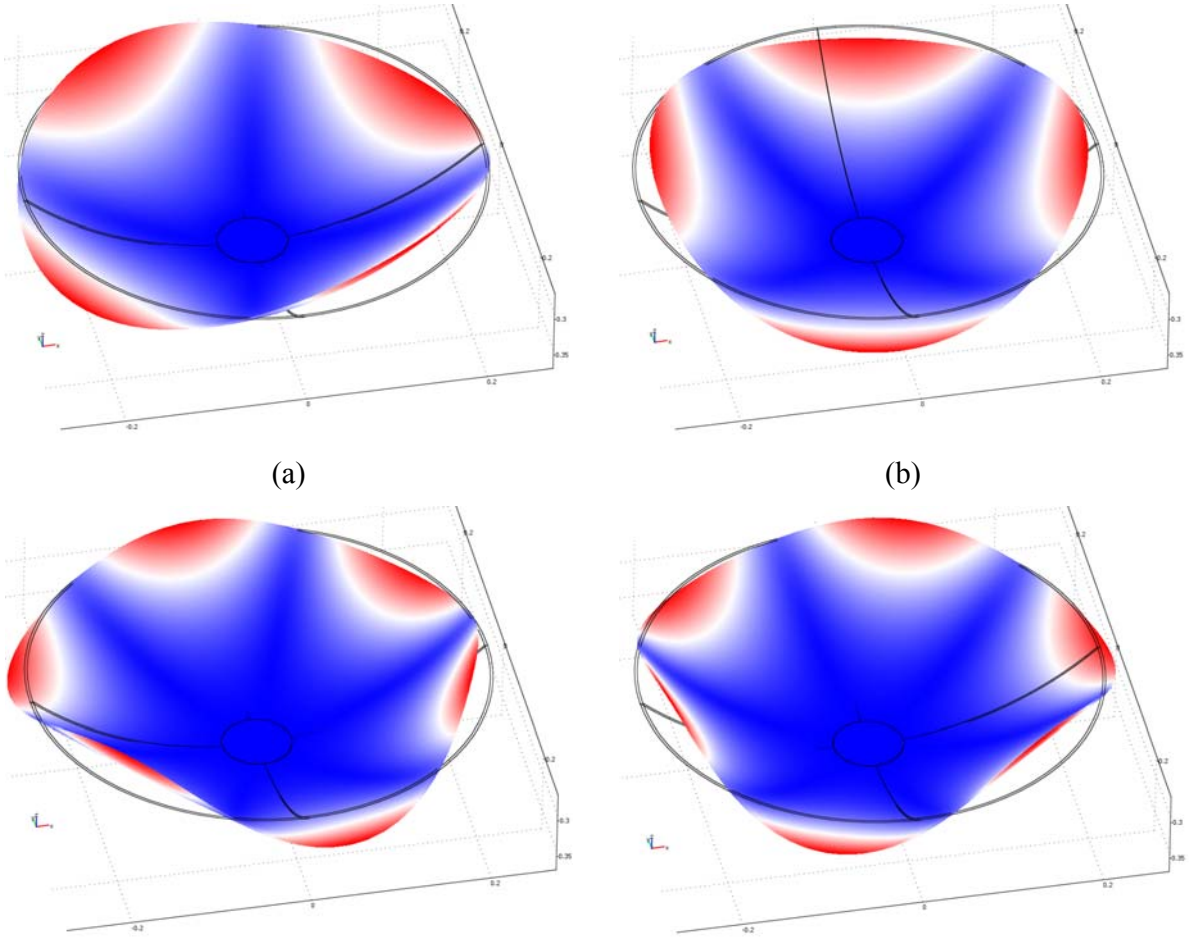

(a) (b)

(c) (d)

Figure 5-9: First four mode shapes of the satellite dish (displacement contour), a) First mode [9.49 rad/s], b) Second mode [9.50 rad/s], c)Third mode [19.55 rad/s], d) Fourth mode [19.56 rad/s]

It can be seen that modes 1 and 2 are identical but about two different axes. This also holds true for modes 3 and 4. As such, from now on, the focus will be on modes 1 and 3, since modes 2 and 4 are repeated version of modes 1 and 3, respectively. In order to have an initial estimate of the optimum locations, areas with highest modal strain energy should be determined. Figure 5-10 shows strain contour for modes 1 and 3. In these figures, contour spectrum ranges from dark blue to red colour. Maximum strain energy is illustrated by red and minimum by dark blue.

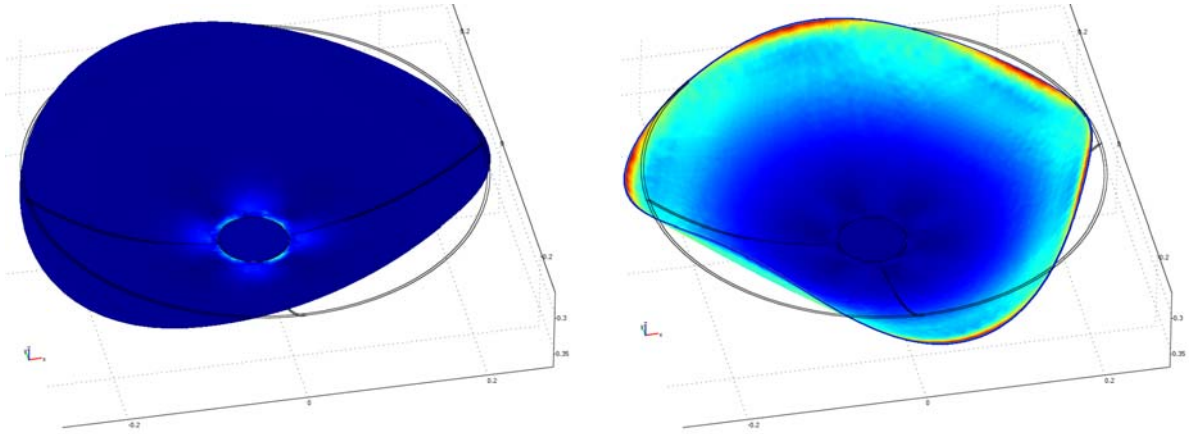

(a) (b)

Figure 5-10: Strain energy density contour, a) First mode, b) Third mode

In can be seen that in mode 1, the highest modal stain energy is observed around the centre of satellite dish where it is welded. However, in mode 3 the strain energy region is concentrated closer to the edges of the dish.

5.2.1.1 Optimization based on fundamental natural frequency

In this section, the first mode is targeted to locate the patches. Figure 5-11(a) demonstrates the initial configuration of damping patches. It should be noted that the four patches could have been placed closer to the welding area, however they were located a bit farther in order to demonstrate the evolution of boundaries towards optimum configuration.

Based on the strain contour shown in Figure 5-10(a), it is expected that damping patches move towards the bottom of the satellite, close to the fixed part. Figure 5-11 illustrates the evolution of damping patches towards optimum configuration. The optimum damping configuration matches expectations and has accumulated around locations with the highest strain rate, resulting in maximum energy dissipation.

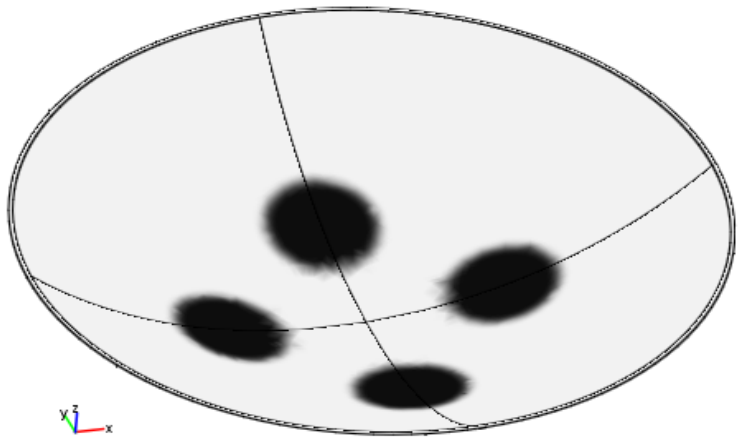

(a)

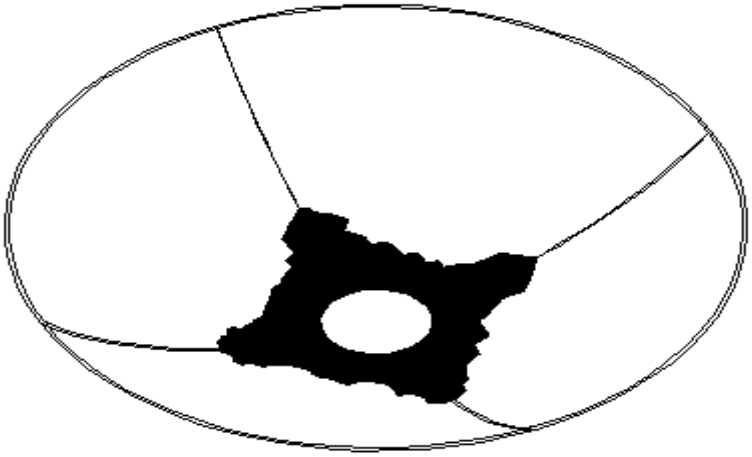

(b)

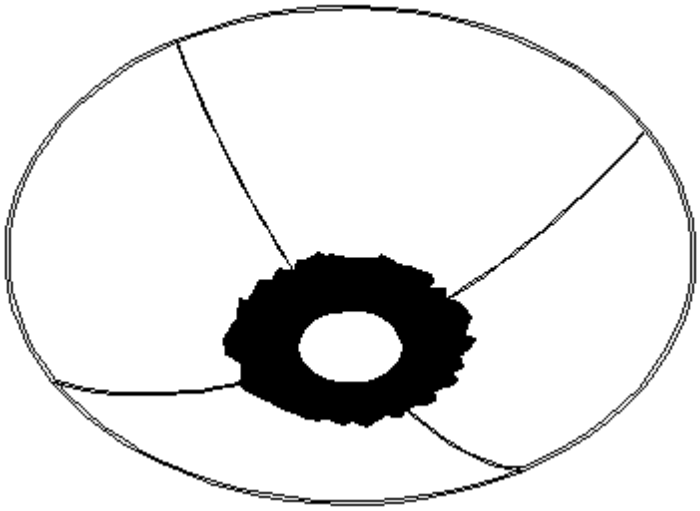

(c)

Figure 5-11: Evolution of CLD patches, a) τ=0 b) τ=0.8 c) τ=1

Modal loss factor in different iterations is demonstrated in Figure 5-12. It is increasing until the optimum damping configuration is achieved. Although the initial location of the patches were chosen based on the primary modal analysis and the strain contour, level set optimization can increase the modal loss factor by almost 6 times of that in initial configuration. In other words, although modal analysis and strain energy contour reveal some initial guess for the optimum location of damping patches, they do not provide any information regarding the optimum shape.

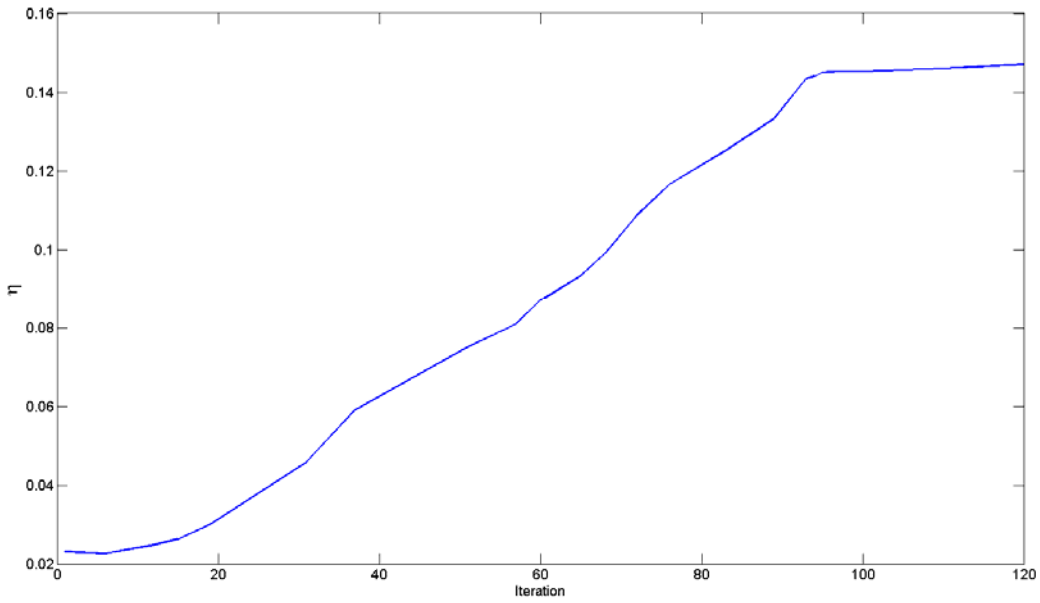

Figure 5-12: Modal loss factor in different iterations.

In order to check that the final optimum shape is not dependant on the initial symmetric locations of CLD patches, this process will be repeated using three patches. The new initial configuration is shown in Figure 5-13(a). It can be seen in Figure 5-13 that again, the damping set has moved toward the bottom of the satellite, close to the fixed part. Of course in comparison with the results in Figure 5-11 the donut shape of optimum damping configuration has remained the same but it is just smaller, because it has been formed from 3 patches not 4.

Therefore, it can be concluded that symmetric location of patches had little to do with the final optimum configuration.

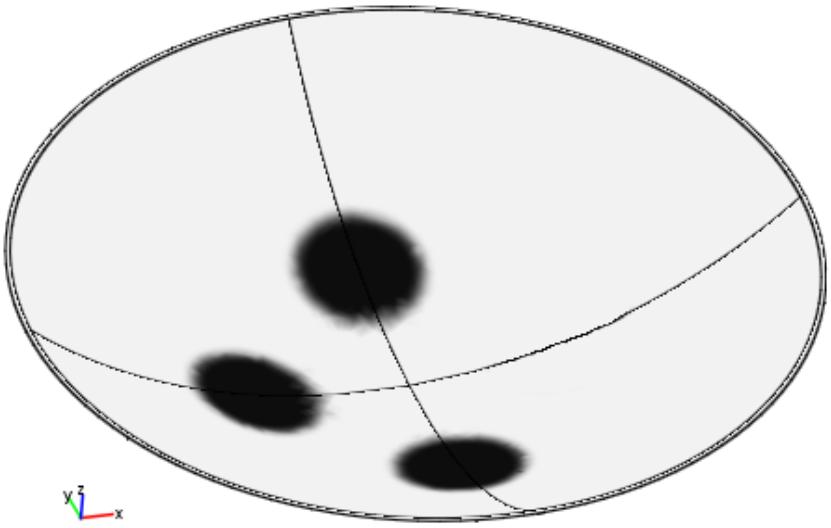

(a)

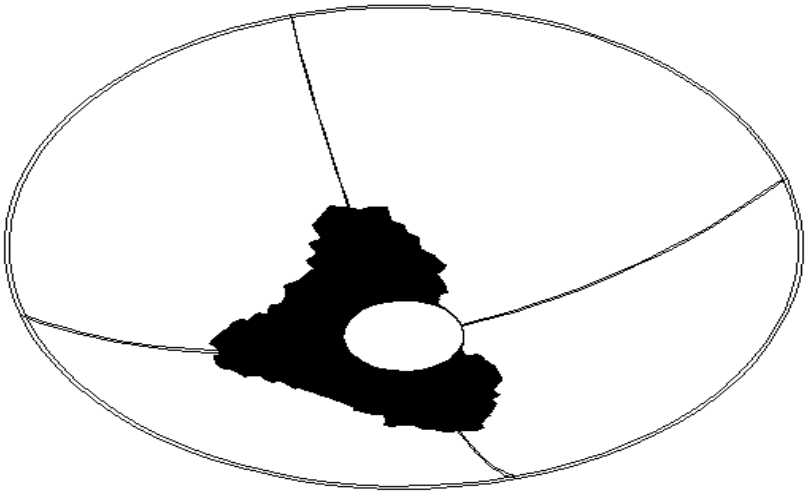

(b)

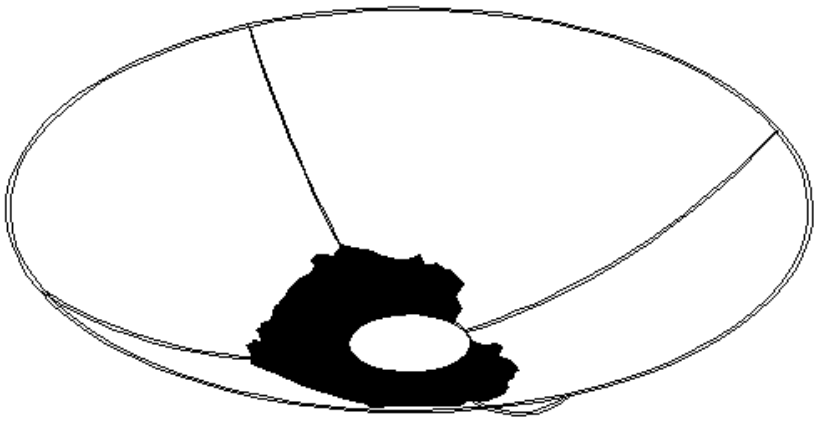

(c)

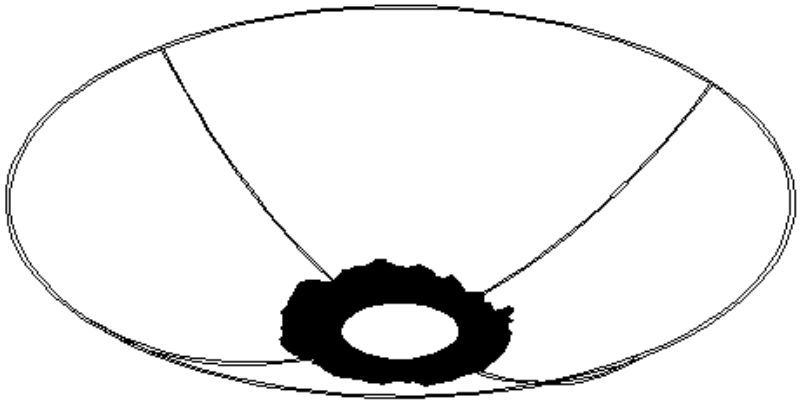

(d)

Figure 5-13: Evolution of three CLD patches, a) τ=0 b) τ=2.4 c) τ=3 d) τ=5

It can be seen that although the process was started with a few patches, the optimum configuration consists of a single patch. This is one of the most important benefits of this method that the number of pieces will be determined automatically.

5.2.1.2 Optimization based on third natural frequency

It is common to design systems based on their fundamental frequency. However, if the working frequency or excitation frequency is far from the fundamental one, those higher frequencies should be considered as well. In this section the vibrations of the same satellite system will be minimized for the third natural frequency. In other words, the best shape and location of damping

patches will be found so that the maximum energy dissipation happens around the third frequency. Like before, four initial patches will be located on the satellite dish, as shown in Figure 5-11(a). Based on Figure 5-10(b) the patches are better to be located closer to the edges for faster convergence to the optimal location. However, for the sake of comparison, the initial damping configuration is chosen identical to the one used in mode 1 analysis, and far from edges. This time, after optimization, the patches are pushed towards the tip of the satellite dish, as demonstrated in Figure 5-14.

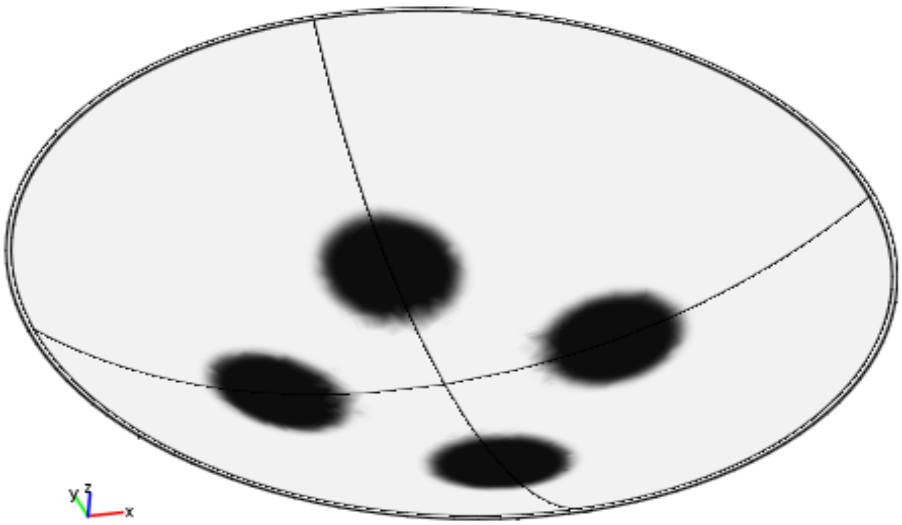

(a)

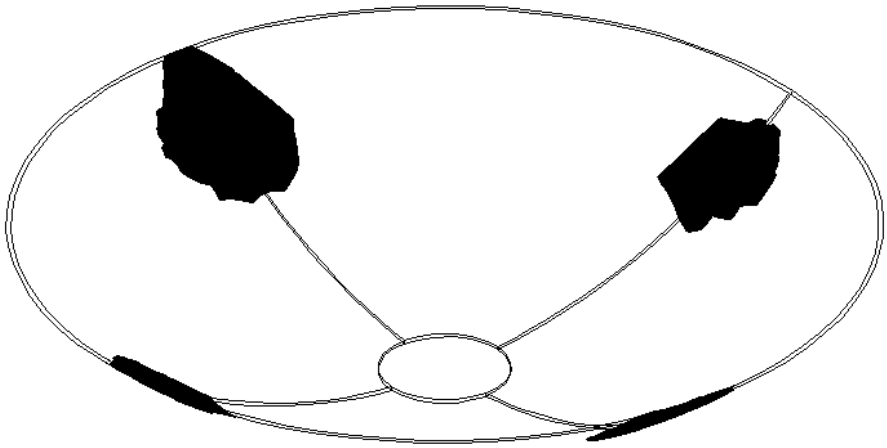

(b)

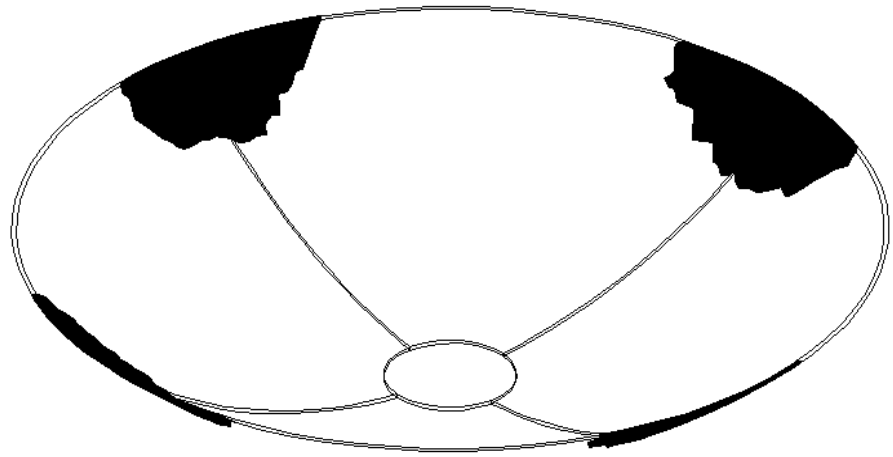

(c)

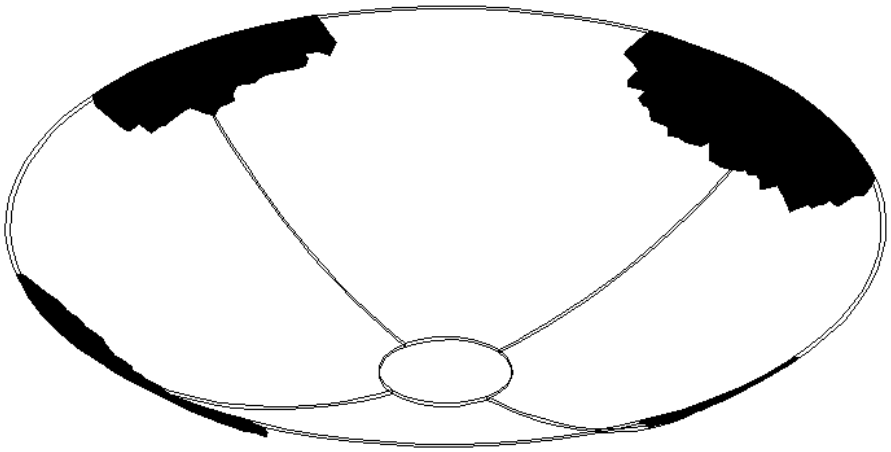

(d)

Figure 5-14: Damping evolution based on third natural frequency, a) τ=0 b) τ=0.4 c) τ=2 d) τ=4

A comparison of Figure 5-14 and Figure 5-10(b) states the reasons behind the new location for the patches. In this mode, since the highest strain change happens around the top edges of the satellite, placing damping patches at those locations will result in highest modal loss factor, and hence, maximum energy dissipation.

5.2.1.3 Optimization based on combination of the first and third natural frequencies

In some practical applications, the system works in a range of frequencies and therefore more than one mode shape have to be considered in the optimization process. In this case Equation (4.11) is used to form the objective function for the optimization. In this case study, modes 1 and 3 of the satellite dish will be combined and the best damping configuration will be found to maximize the combination of modal loss factors in both modes.

When two or more mode shapes are considered, selection of initial damping configuration is harder than single mode case. According to Figure 5-10, highest strain energy in mode 1 is close to the centre of the satellite where it is welded. However, this location provides minimum strain energy in mode 3. In the same way, high strain energy region in mode 3 corresponds to low strain energy area of mode 1. In such cases, splitting the patches and locating them in different areas will help to cover high strain energy areas in different modes. In this case study, to be consistent with previous studies, the initial configuration of CLD patches will be chosen according to Figure 5-13(a).

Figure 5-15 illustrates the optimum damping configuration for the satellite dish with a combined mode objective function. It can be seen that in contrast with the first or third mode cases, patches are neither accumulated close to the weld area nor around the edge of the dish. Instead, the patches are spread in a way that they cover high strain areas in both modes 1 and 3. This shape does not increase the loss factor of the first mode as much as the shape shown in Figure 5-11(c) and does not increase the loss factor of the third mode as much as the shape shown Figure 5-14(d). However, it maximizes the combination of loss factors of the first and third modes simultaneously.

It should also be noted that if a smaller mesh size is used and the optimization is continued with a few more iterations, smoother boundaries will be achieved for the optimum shape of the patches.

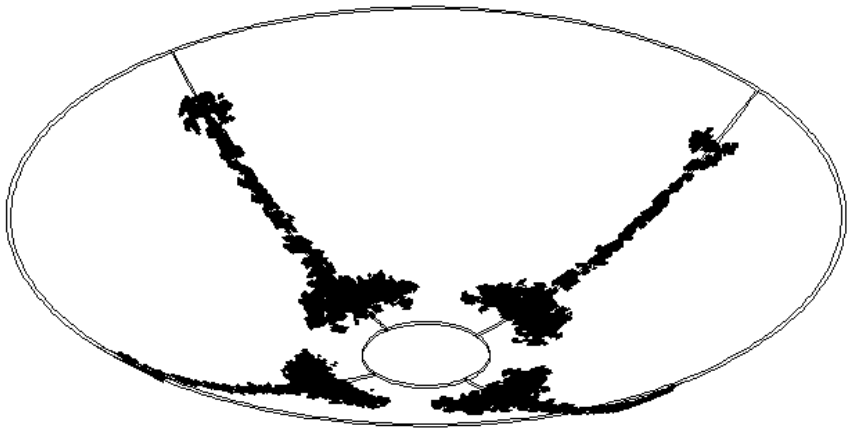

Figure 5-15: Optimum damping configuration for satellite dish when both first and third mode shapes are addressed simultaneously

5.2.2 Case study 2: Vibration control in automotive dash panel

The automotive industry has recently placed increased focus on the process of light-weighting and using lighter materials, such as magnesium, in vehicle components. However, weight reduction and the application of lightweight material can also increase unwanted noise and vibration.

One of the automotive parts that can benefit from lighter material with lower manufacturing costs is the dash panel. The dash panel is located between the engine and car interior, and thus can be an important transmitter of noise and vibration to passengers. Kurosawa et al. [113] worked on the vibration of panels with passive treatments. They focused on estimating the damped vibration of automotive body panels. Bianchini [114] worked on active vibration control

of automotive-like panels using a simple model, shown in Figure 5-16. Nagai et al. worked on the application of vibration damping steel sheets (VDSS) in automotive panels, and through experiment, confirmed that the noise reduction effect of VDSS is proportional to the logarithm of their loss factor [115].

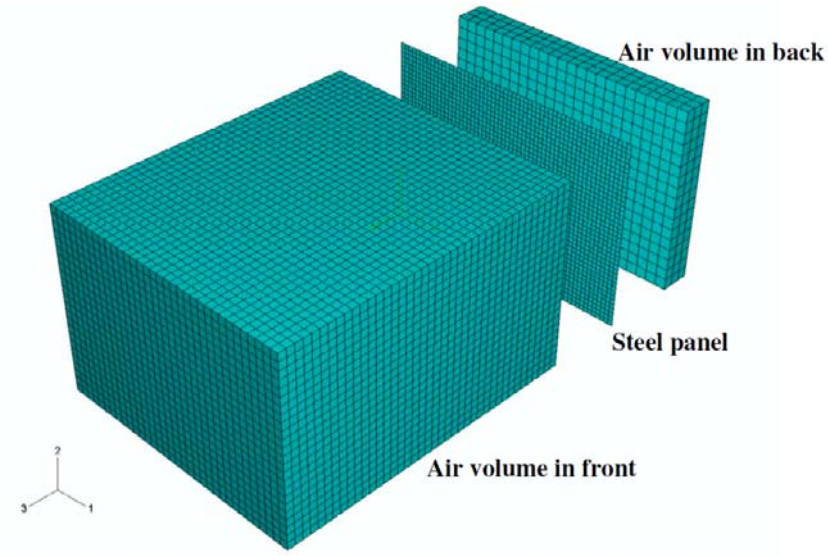

Figure 5-16: FEA model used in [114]

In this section, optimal vibration suppression will be performed on a dash panel, as shown in Figure 5-17. The best shape and location of CLD patches have to be determined to get highest modal loss factor.

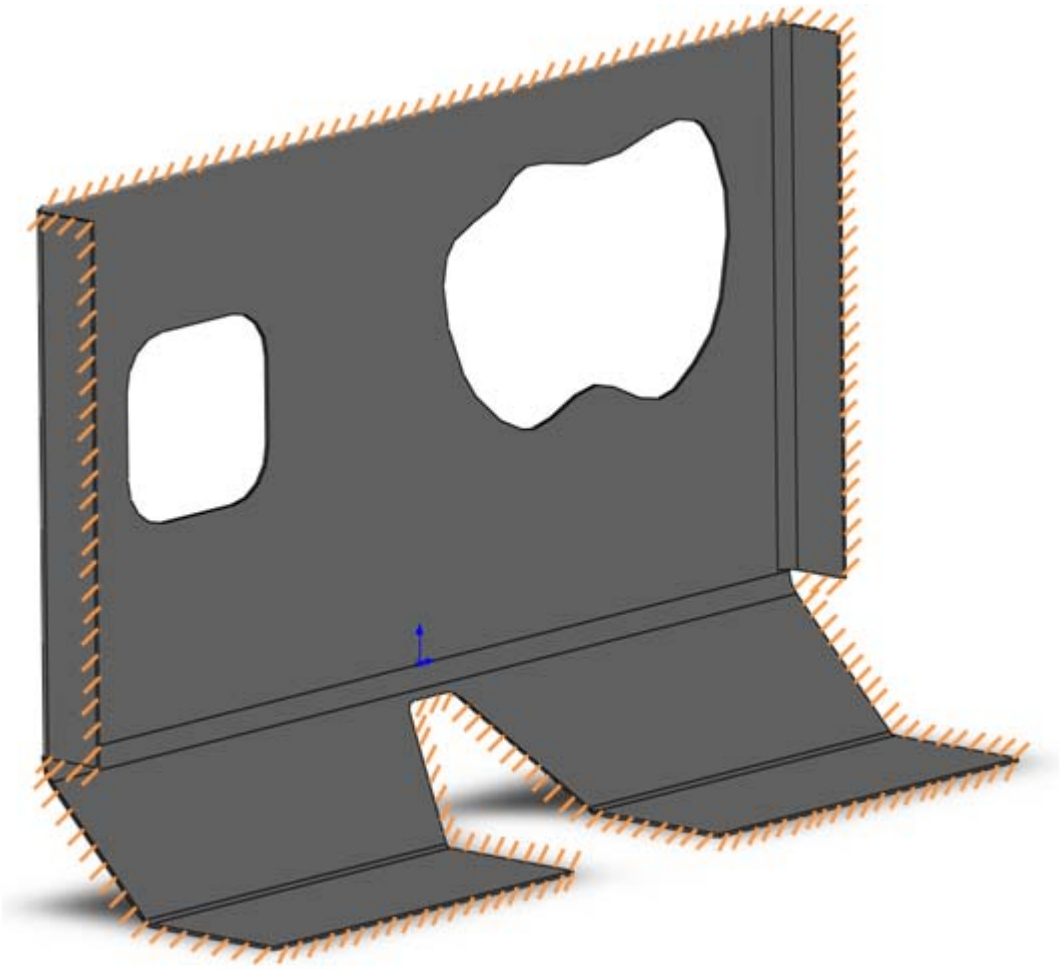

Figure 5-17: Solid model of the automotive dash panel

As explained before, in order to get an idea of where to start, it is very beneficial to perform a modal analysis first. The dash panel is made of magnesium and is fixed around its outer edges, as shown in Figure 5-17. Detailed properties of the panel and the added CLD patches are given in Table 5-2. In this case, the CLD loss factor of 0.9 is used in analysis.

Table 5-2: Material properties of automotive dash panel

Property	Value	Unit
Modulus of elasticity	71	GPa
Poisson ratio	0.29	-
Density	2700	Kg/m^3
CLD Material loss factor	0.79 ~ 0.99	-
CLD Specific gravity	0.53	lb/ft^2
CLD Thickness	1.5	mm

Tetrahedral Lagrange-quadratic elements have been used in finite element model. Figure 5-18 shows the fundamental mode shape of the dash panel, as well as its strain energy contour. In the first figure, the contour spectrum ranges from blue colour to red where blue and red illustrate minimum and maximum displacements, respectively. However, in the second figure, the contour spectrum ranges from dark blue to red colour. Maximum strain energy is illustrated by red and minimum by dark blue.

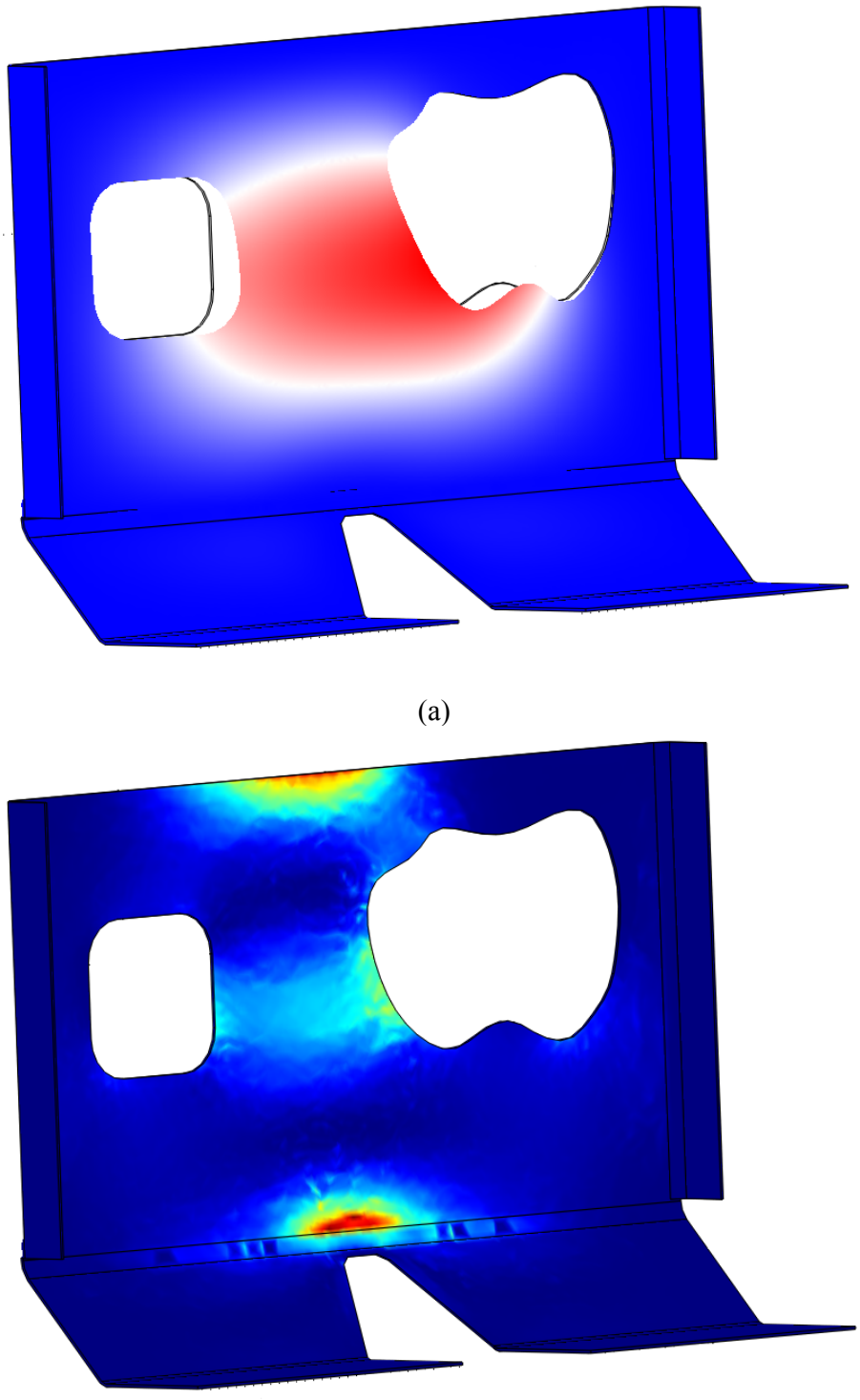

(a)

(b)

Figure 5-18: Dash panel's fundamental mode shape a) Displacement contour b) Strain energy density contour

Since the highest strain rate is happening almost around the top and bottom center of the panel, two circular CLD patches will be located close to those locations as an initial guess (see Figure 5-19(a)). The evolution of the patch toward the optimum configuration is shown in Figure 5-19, and the variation of modal loss factor in different iterations is demonstrated in Figure 5-20.

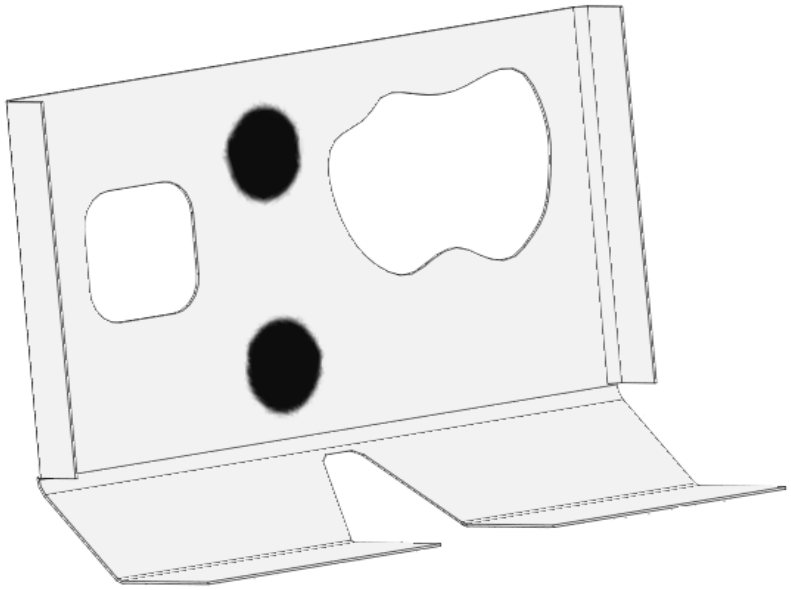

(a)

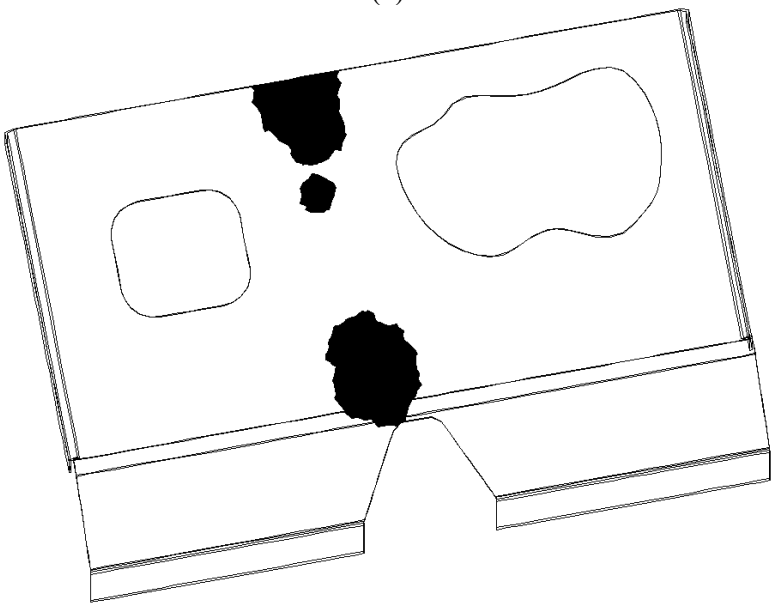

(b)

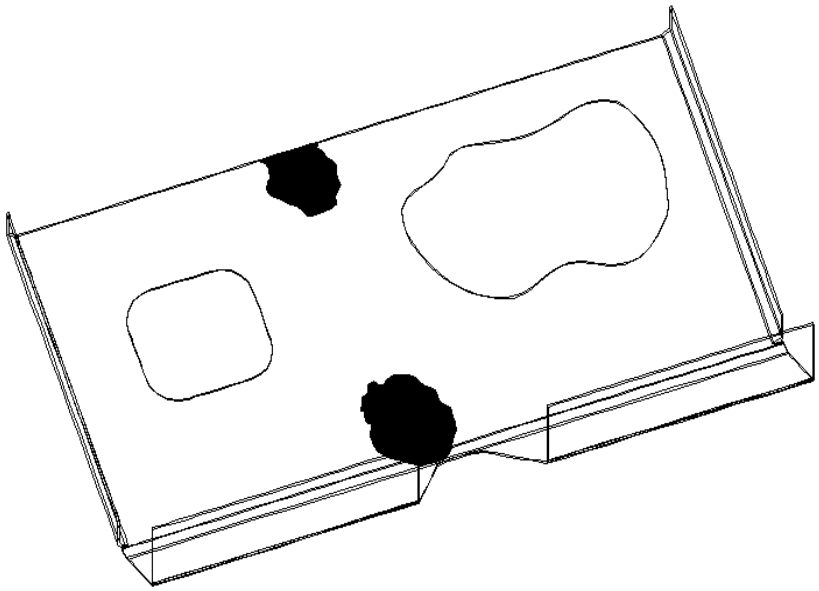

(c)

Figure 5-19: Evolution of CLD patches, a) τ=0 b) τ=0.2 c) τ=1

The modal loss factor increase during the optimization process until the optimum shape and location for the patches are achieved.

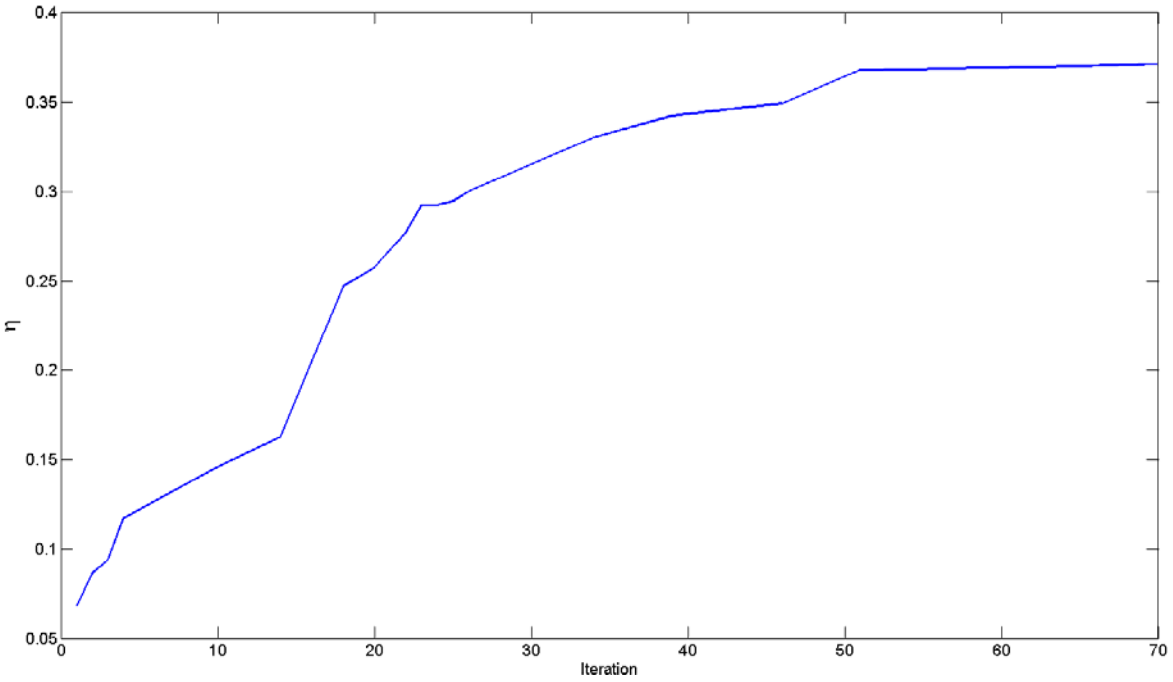

Figure 5-20: Modal loss factor for automotive dash panel in different iterations

As mentioned before, the level set optimization like other optimization methods is prone to getting stuck in local minima, and there is no guarantee that the configurations found in these case studies were the global minima. However, since the energy dissipation in CLD patches is proportional to strain energy, if the damping patches are initially located close to areas with highest modal strain energy, the chance of achieving a global optimum will increase.

Chapter 6
Experimental Studies

It is always desired to confirm theoretical work by experimental results, and vibration control is not an exception. In this chapter experimental test will be performed in order to confirm the results obtained in the previous chapters.

Tests will be performed on the rectangular plate shown in Figure 6-1. Its dimensions and material properties are listed in

Table 6-1: Dimensions and material properties of the test specimen and CLD patches

Property	Value	Unit
Length	500	mm
Width	250	mm
Thickness	0.8	mm
Modulus of elasticity	200	GPa
Poisson ratio	0.3	-
Density	7800	Kg/m^3
CLD Material loss factor	0.09 ~ 0.3	-
CLD Specific gravity	0.53	lb/ft^2
CLD Thickness	1.5	mm

The plate is fixed from top and partly on its right side. The fixed section on the right is 10 cm. CLD patches will be located on it to suppress its flexural vibrations. The best shape and location of the patches will be found theoretically and experimentally to achieve highest vibration attenuation.

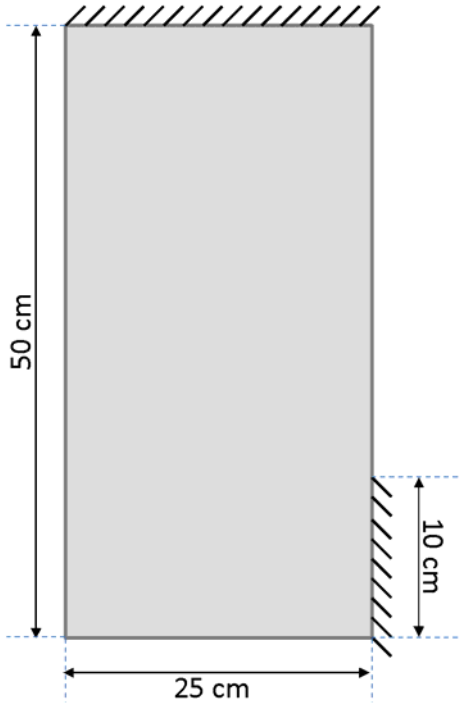

Figure 6-1: Plate with nonsymmetrical boundary conditions

6.1 Computer simulation

In this section the system will be modeled in COMSOL©. 3D tetrahedral Lagrange-quadratic elements will be used and the top edge and 10 cm from the right edge will be fixed, as seen in Figure 6-1.

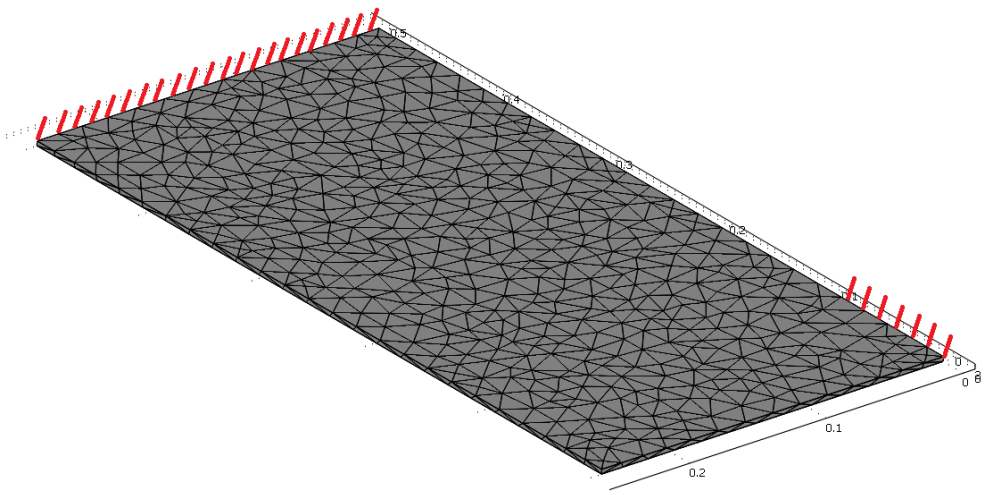

Figure 6-2: Finite element model of the plate

The first natural frequency of the system is found to be 13.62 Hz. Figure 6-3(a) illustrate the first mode shape of the system and the strain energy contour is shown in Figure 6-3(b). In the first figure the contour spectrum ranges from blue colour to red where blue and red illustrate minimum and maximum displacements respectively. However, in the second figure, the contour spectrum ranges from dark blue to red colour. Maximum strain energy is illustrated by red and minimum by dark blue. The areas with high strain energy are located close to the clamp boundaries.

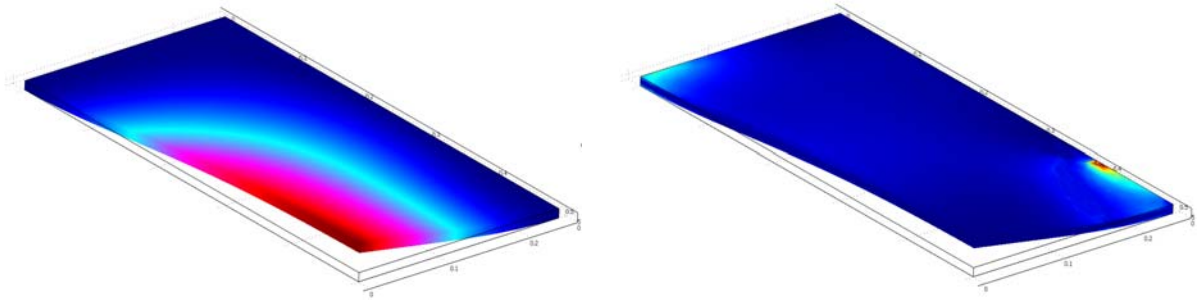

(a) (b)

Figure 6-3: First mode shape: (a) displacement contour, (b) strain energy contour

Now that the high strain energy locations are found, the optimal CLD positions can be found using the developed method. Two different configurations, each consisting of two circular patches, located on the structure with a total area of 0.25 m^2, are considered. These initial configurations are illustrated in Figure 6-4 (a) and (b). In these simulations, assuming room temperature the material loss factor was set to 0.1. The optimization needed almost 140 iterations to converge when configuration (a) was chosen as initial shape/location for CLD patches, however configuration (b) for the initial shape/location for CLD patches led to a convergence after 64. Both choices of the initial will converge to the optimum configuration, shown in Figure 6-4(c), and the patches are guided close to the boundaries. It could be seen that the distribution is not symmetric and unlike the system shown in Figure 4-10(d) where CLD patches were evenly accumulated around the constrained edge.

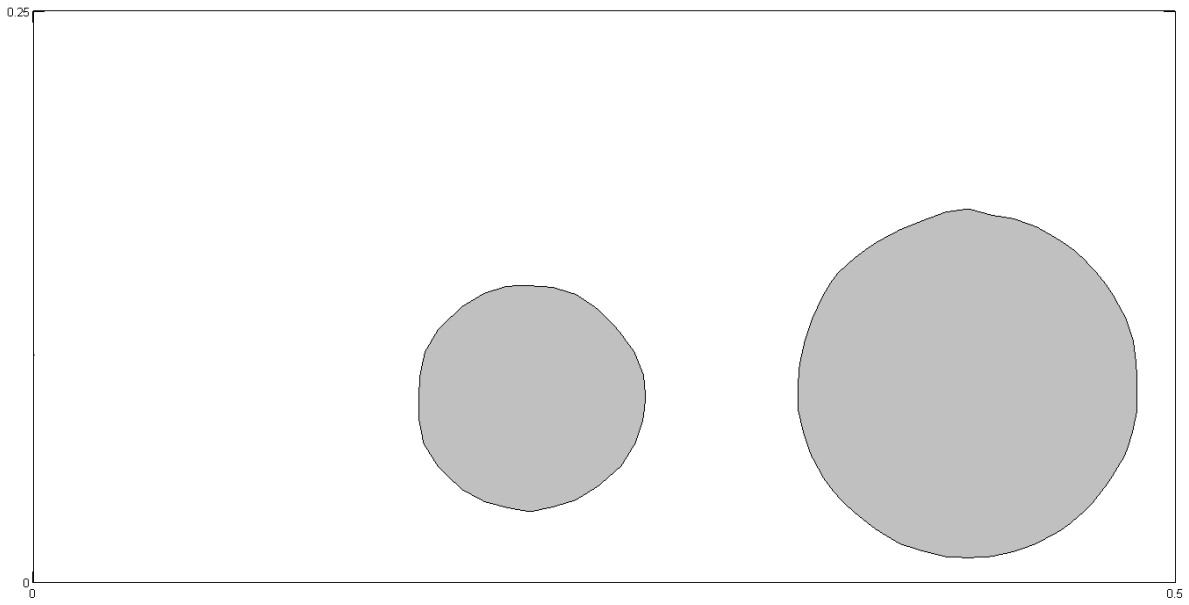

(a)

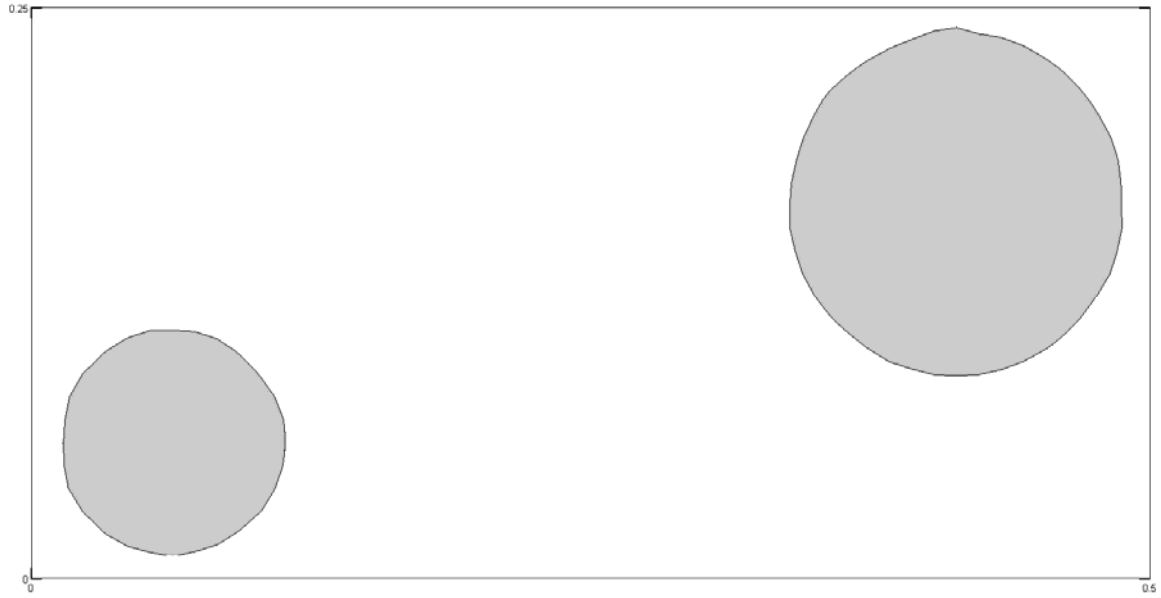

(b)

(c)

Figure 6-4: Configuration of CLD patches a) initial shape {choice 1} b) initial shape {choice 2} c) optimal shape

The change in loss factor in different iterations is shown in Figure 6-5.

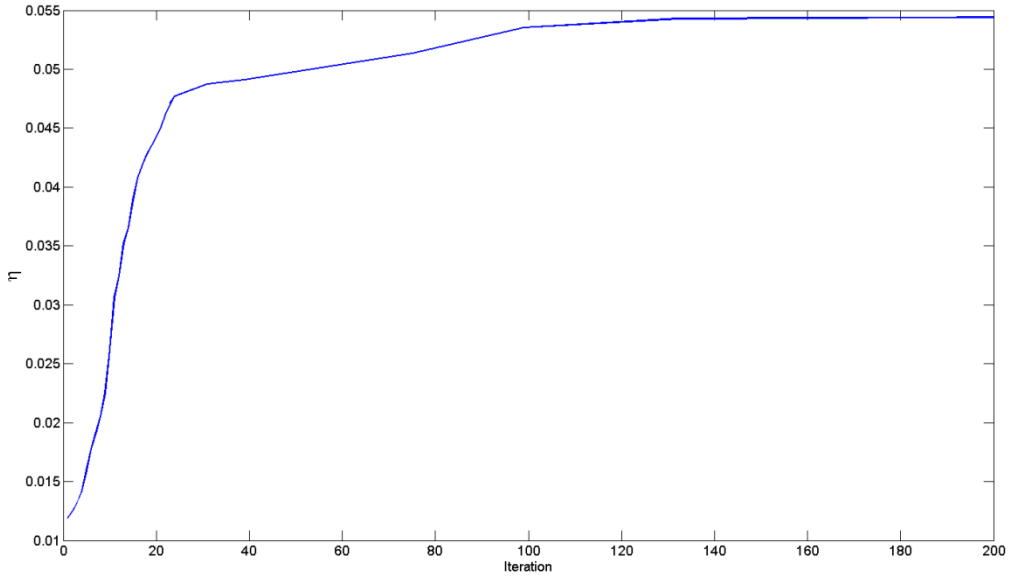

Figure 6-5: Variation of loss factor (η)

6.2 Experimental tests

Test setup shown in Figure 6-6 is used to perform experiments. It consists of the rigid frame, two non-contact displacement sensors, a rectangular plate and two supports to create non-symmetric clamp boundary condition.

Figure 6-6: Experimental test setup

Different CLD configuration, including the optimum one found in previous section, will be tested. CLD patches are from HushMat Company and their specifications are listed in Table 6-1. A typical CLD sheet is shown in Figure 6-7. These self-adhesive patches can afford excellent control of resonance-induced vibrations. Their composite loss factor does not vary too much with temperature and frequency and it falls between 0.09 and 0.3 [116].

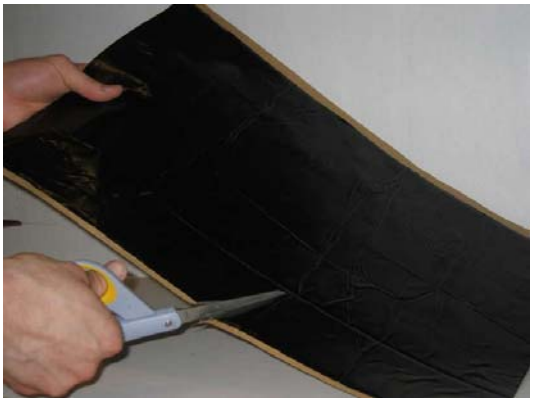

Figure 6-7: Constrained Layer Damper used for test [117]

The data acquisition system (DAQ) consists of Sensory 626 data acquisition card and a computer. This DAQ card is MATLAB-compatible, so the controller is programmed in Simulink in MATLAB. The data are collected with a sampling frequency of 1 KHz. The laser based displacement sensors are shown in Figure 6-8.

Figure 6-8: Non-contact displacement sensors

Keyence LK081 and LK031 non-contact laser sensors are utilized to read the displacements. Each laser sensor comes with its own controller. The specifications of these sensors are listed in Table 6-2. Although one sensor was sufficient, two of them were used to assure no data is lost if one of them stops working during the test. LK-031 is the top sensor since the range of displacements is smaller in this position. This sensor is located at a 30 mm horizontal distance from the plate. The bottom sensor is LK081 and is located at 80 mm away from the Plate.

Table 6-2: Specifications of non-contact laser sensors

	Top sensor	**Bottom sensor**
Sensor Head	LK-031	LK-081
Controller	LK-2001	LK-2101
Reference Distance(mm)	30	80
Measuring Range(mm)	±5	±15
Sampling Rate (μs)	512	1024
Resolution (μm)	1	3

The area of the CLD patches in all of the configurations is 0.25 m^2. All damping configurations are shown in Figure 6-9.

Configuration (a)

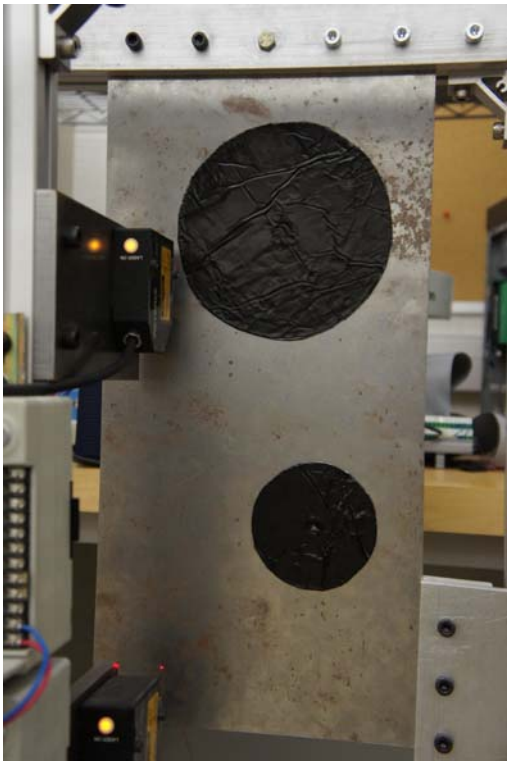

Configuration (b)

Configuration (c)

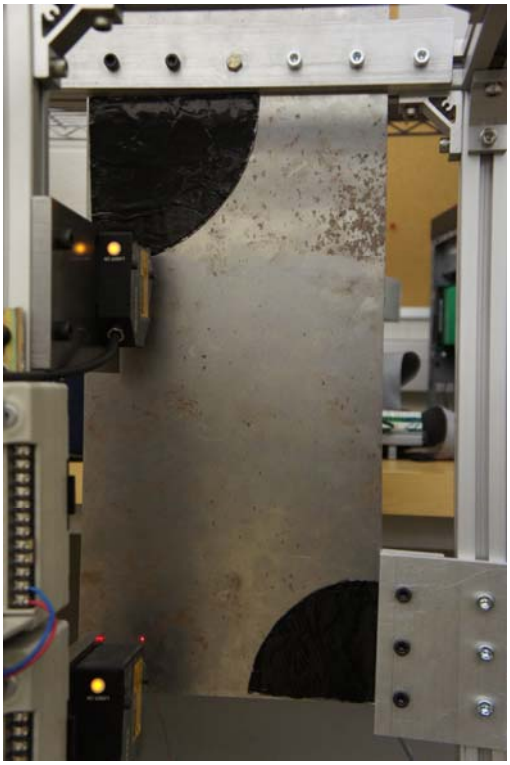

Configuration (d)

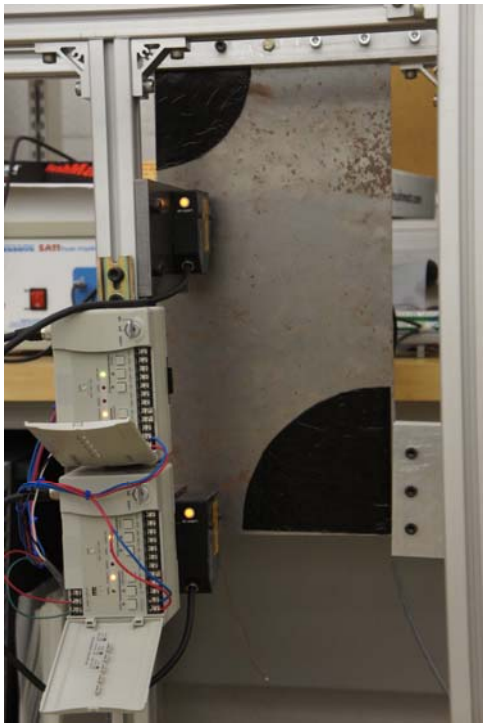

Configuration (e)

Figure 6-9: Different CLD shapes used in the experimental test

In order to excite the first natural frequency of the system, an initial displacement is applied to the bottom corner of the plate (according to Figure 6-10) and the free vibration is studied. This displacement is applied by moving the bottom corner until it reaches a stopper which shows the desired displacement. This way, the same initial displacement is applied in all the tests.

Figure 6-10: Initial displacement direction

In order to verify the finite element model, an experiment is carried out first. Before attaching the CLD patches, an impulse is applied to the bottom left corner of the plate. After performing Discrete Fourier Transform (DFT), the frequency response of the plate is found and illustrated in Figure 6-11. The first two natural frequencies of the system are captured.

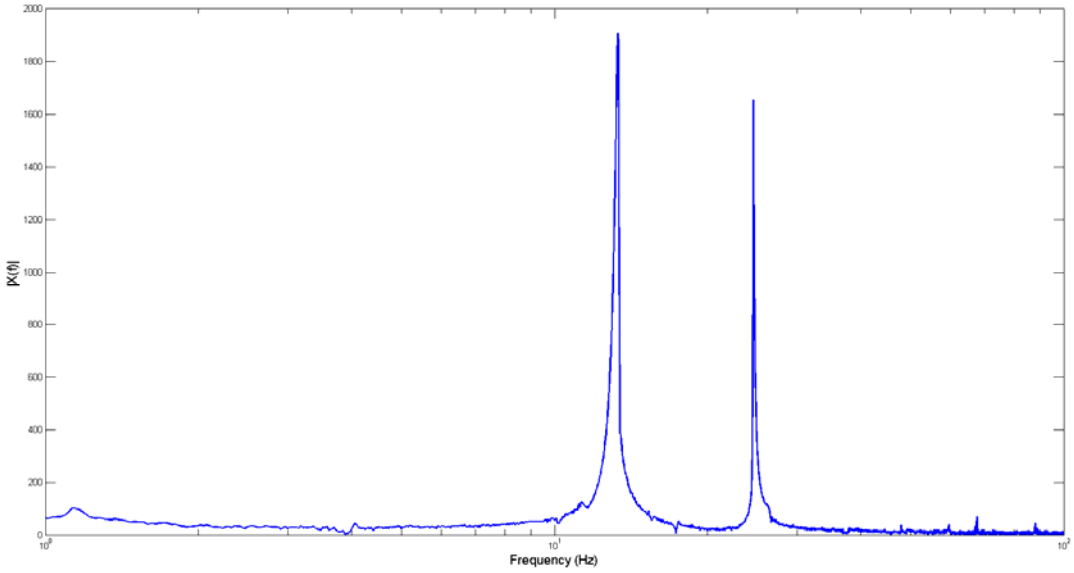

Figure 6-11: Frequency response of the plate without CLD

This experiment is repeated again when two CLD patches are attached to the plate with the configuration shown in Figure 6-9(a). The frequency response of plate with CLD is illustrated in Figure 6-12.

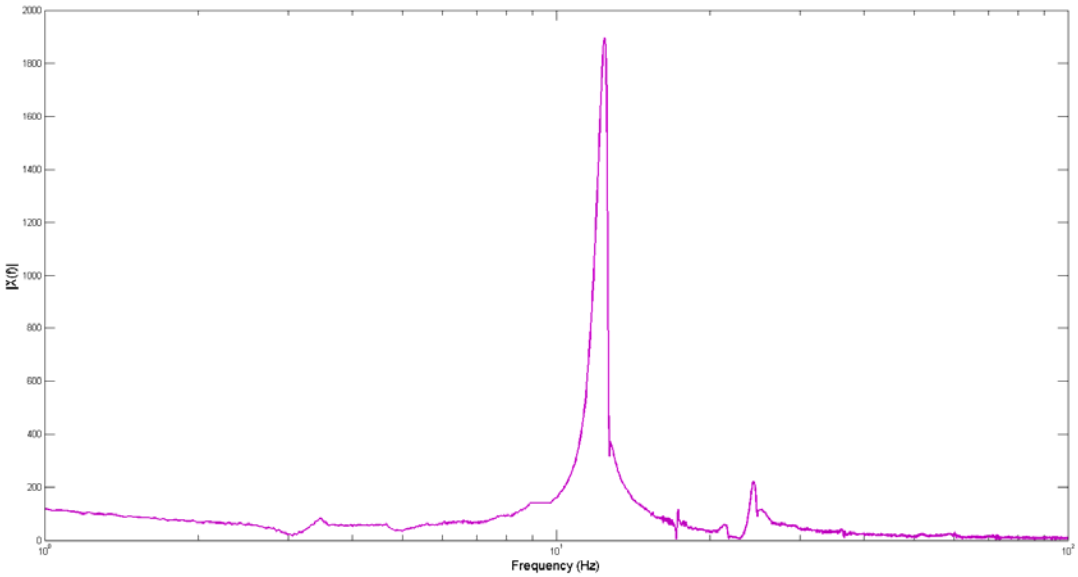

Figure 6-12: Frequency response of the plate without CLD

Table 6-3 compares the first two natural frequencies found from finite element analysis with those obtained from experiments for two different cases of the plate with and without the CLD patches.

Table 6-3: First two natural frequencies of the plate

Natural Frequency (Hz)	First	Second
Experiment (Plate without CLD)	13.31	24.57
Experiment (Plate with CLD)	12.42	24.32
Finite Element Analysis	13.62	25.01

The data presented in this table show that the simulation results are in good agreement with the experimental tests. Furthermore, it can be seen that since the weight of the added material is much less than the original plate, the CLD patches have negligible effect on the natural frequencies of the plate with CLD patches.

Displacement diagram related to each test is shown in Figure 6-13. It should be noted that the displacement in all these figures have been normalized, through dividing data by initial value of displacement) in order to have a fair comparison. Therefore each graph starts from 1.

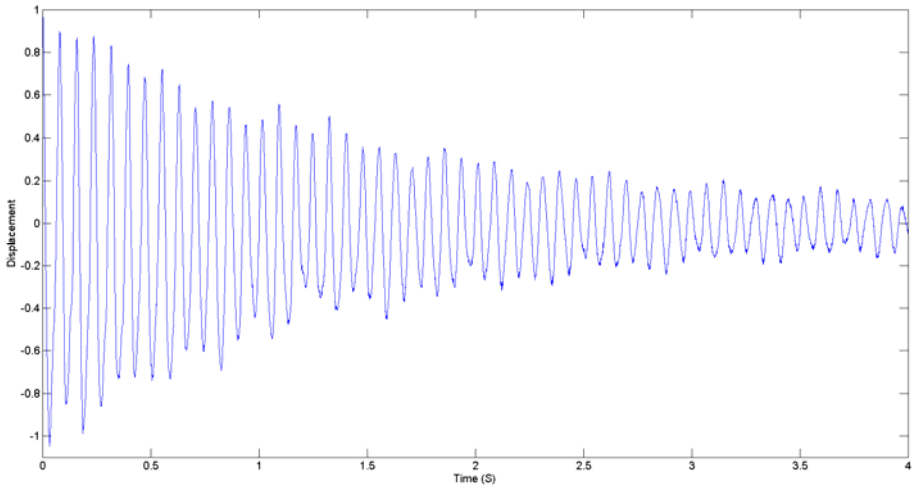

No CLD

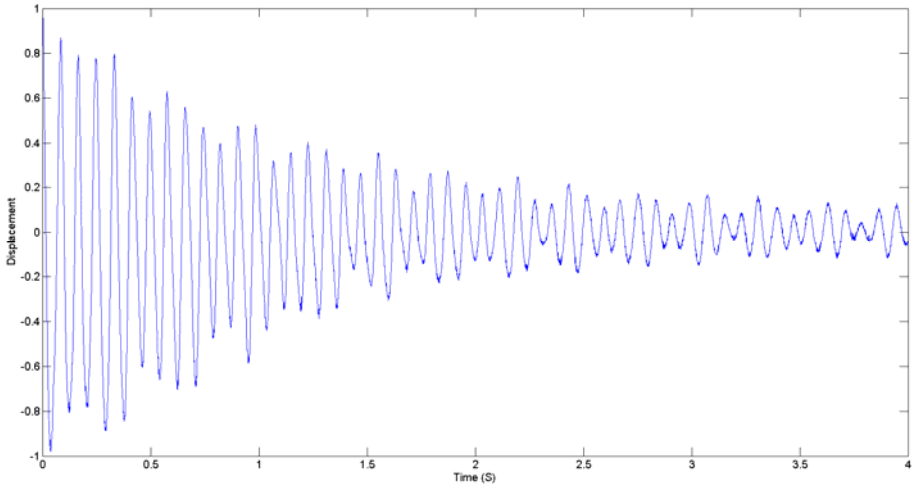

Configuration (a)

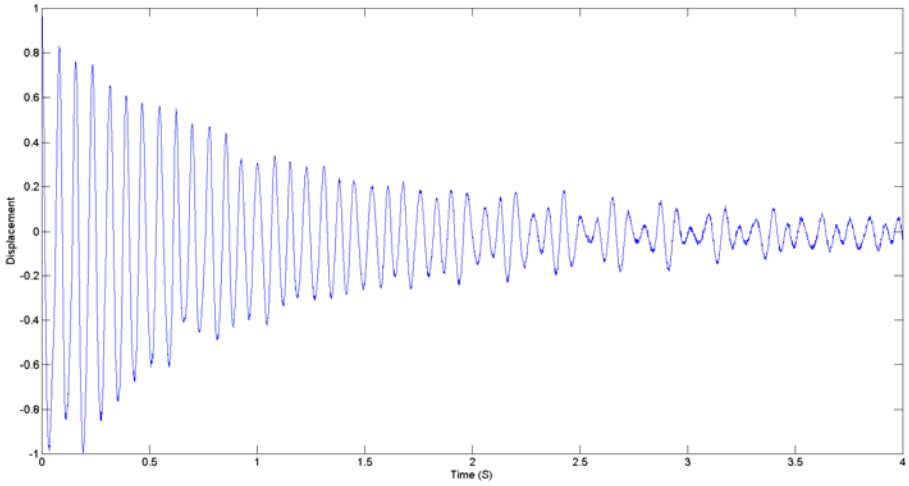

Configuration (b)

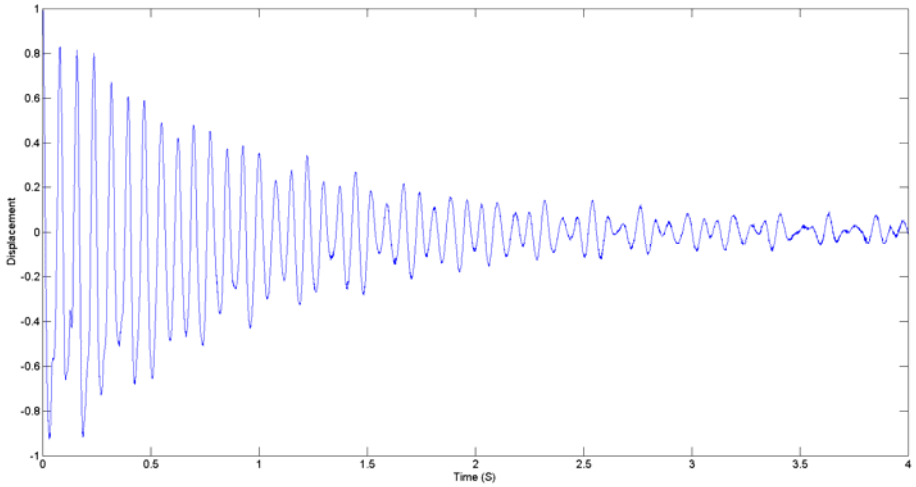

Configuration (c)

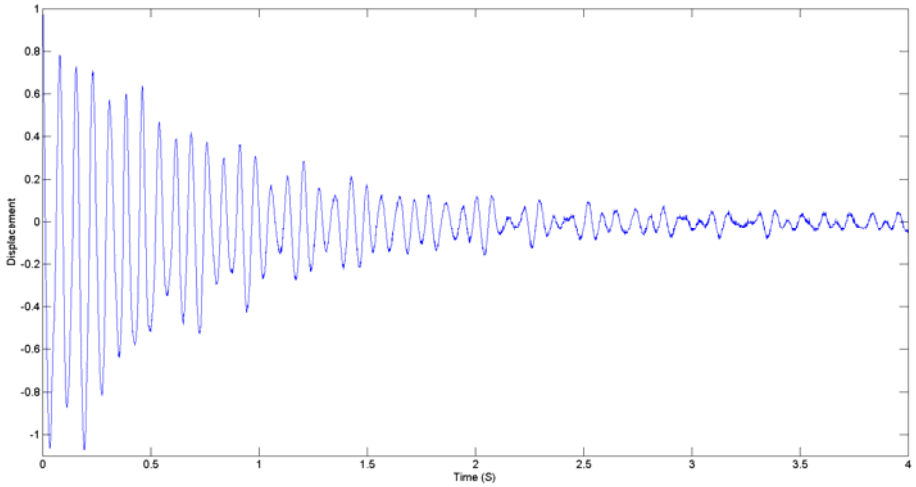

Configuration (d)

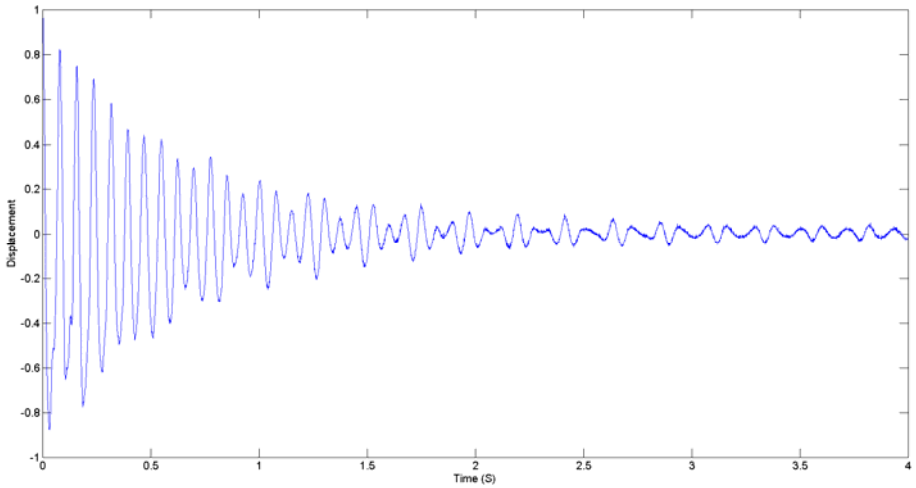

Optimum configuration

Figure 6-13: Displacement diagram for each damping configuration

In order to show the effects of damping location on the overall vibration suppression the combination of the results of all tests is depicted in Figure 6-14.

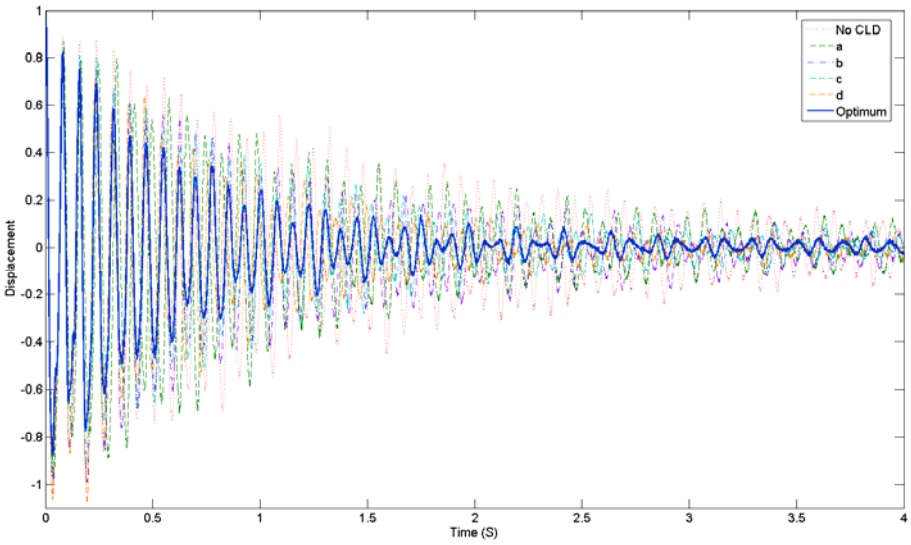

Figure 6-14: Comparative diagram of displacement tests for different damping configurations

The exponential diagram for all of the configurations is illustrated in Figure 6-15. In this figure the peak displacement of each cycle has been picked and it clearly demonstrates the decay of oscillations.

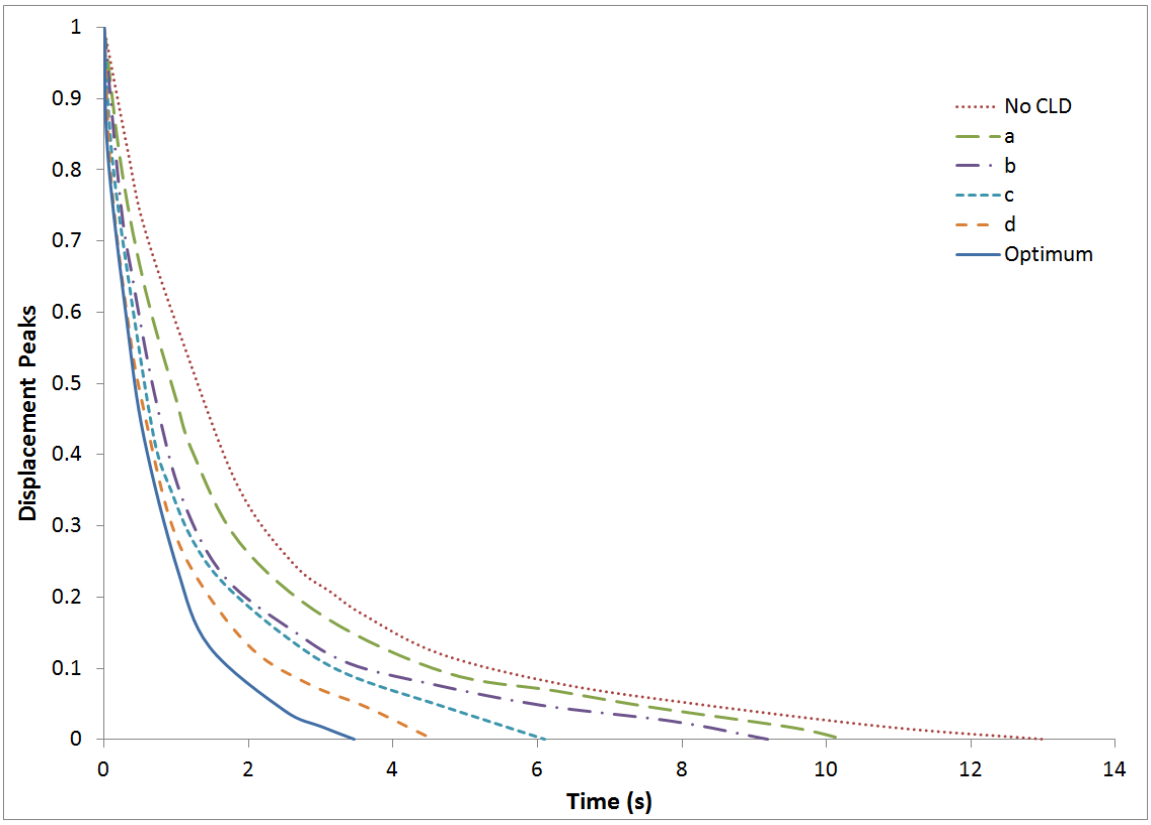

Figure 6-15: Exponential diagram (labels are based on Figure 6-9)

It could be seen that vibration is suppressed faster when optimum CLD shapes and location have been used. Quantitatively speaking, the vibrations are attenuated 73% faster when optimum configuration is applied in comparison to the case that no CLD is attached. In the same manner, configuration (d) leads to 28% quicker suppression than configuration (c).

In a time decaying diagram, like the one shown in Figure 6-16, the logarithmic decrement is defined as

$$\delta \approx \frac{1}{n} \ln \left| \frac{x_1}{x_{n+1}} \right| \tag{6.1}$$

The damping ratio is

$$\zeta = \frac{\delta}{\sqrt{(2\pi)^2 + \delta^2}} \tag{6.2}$$

and finally the loss factor could be estimated by [118]

$$\eta \approx 2\zeta \tag{6.3}$$

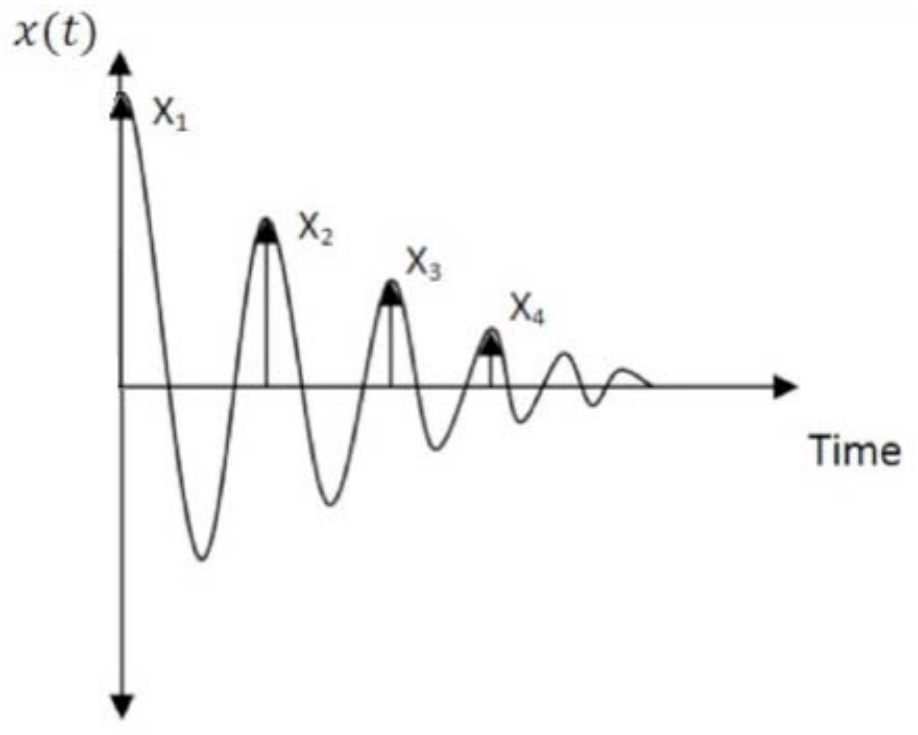

Figure 6-16: Typical decaying displacement diagram

Damping ratio related to each experiment is given in Table 6-4. It can be seen that the optimum CLD shape and location (configuration e), found via level set optimization, reveals the highest loss factor and suppresses vibrations faster.

Comparison of configurations (a) and (b) reveals the effect of location of CLD patches on loss factor. In these two configurations the shapes of CLD patches are identical while the locations of patches are different. Configuration (b) offers 20% more loss factor.

The effect of the shapes of CLD patches on loss factor can be identified by comparing configurations (c) and (d). Although in both cases patches are located close to the fixed boundaries, their shapes are different. It could be seen in Table 6-4 that configuration (d) leads to 33% more loss factor. Looking at the modal strain energy contour shown in Figure 6-3(b), one can notice that since in configuration (d) damping material are mostly accumulated around areas with high strain energy, it offers higher loss factor compared to configuration (c).

More generally, comparison of configuration (c) and (e) will show the effect of simultaneous shape and location optimization. Configuration (e) offers 60% more loss factor and 44% faster vibration attenuation than configuration (c).

The experimental results obtained in this section clearly confirm those found from simulations. The best suppression performance was coming from the optimum configuration found through level set optimization.

Table 6-4: Damping ratio

CLD configuration		Loss factor
a	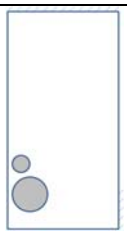	0.02
b		0.024
c		0.03
d		0.04
e		0.048

Chapter 7
Conclusion and Future Work

Among different approaches to control vibration, use of constrained layer dampers is one of the most popular ones. These polymer damping materials are light, and dissipate energy in form of heat. Their installation is easy and they do not add much manufacturing cost. Although CLD patches are relatively light, when dealing with lightweight structures it is necessary to add damping material as less as possible. To this end, one should not cover the whole surface of a structure and in turn the surface should be treated partially. Hence, the best shape and location of the CLD patches have to be determined.

7.1 Conclusions

In this research, a new technique called, level set optimization, was introduced to the field of damping optimization. Unlike most research that only focus on the optimum location of the added damping material, not only will this novel approach find the optimum location of the CLD patches it will also find their best shape simultaneously for a given surface area.

The optimization problem was first formulated for 2D structures. After choosing an initial arbitrary shape and location for the CLD patches, the best shape and their locations were found effectively using the solution of Hamilton-Jacobi partial differential equation. In another example a nonsymmetrical system from Ref. [48] was optimized using the proposed level set approach and its results were improved by more than 10%. It should be noted that in Ref. [48] the accuracy of results were examined through experimental test.

The suggested optimization method was further extended to 3D domain. A novel approach was developed to create a 4D level set function required for initiation of the optimization process. A

thorough study was performed on control of vibration in a satellite dish. Different eigen frequencies were targeted and CLD patches were optimally applied to the surface of the dish to minimize its vibration.

In another complicated example, an automotive dash panel was under study and its excessive vibration was minimized. The optimum shape and location of the patches were determined via level set technique.

In order to confirm the results obtained in this work, an experiment was carried out. Flexural vibration of a plate with nonsymmetrical boundary conditions was lower by means of CLD material. First, using level set technique the optimum shape and location of patches were determined in software.

Then experimental tests were performed on the plate. Five different damping configurations, including the optimum one, were used. Expectedly, the vibration of plate was attenuated faster when the optimum configuration was utilized for the CLD patches in comparison to all other configurations. During the experiments, the highest loss factor was achieved when damping patches were attached according to those found via level set technique. This experiment reconfirmed the accuracy of the proposed approach in finding optimum shape and location of the added material.

In general the proposed method showed a lot of capabilities in optimal vibration control in lightweight structures. On the other hand the computer code generated in this research can easily be adapted to other physical optimization problems and is not solely confined to vibration control. It can handle different physical phenomenon using finite element technique in conjunction with level set optimization approach followed by Hamilton-Jacobi PDE.

The main contributions of this research are summarized below:

- The general solution to 2D and 3D CLD applications was studied.
- The proposed level set optimization was capable of finding the best shape and location of the patches simultaneously for a given surface area (damping material).
- The level set technique was extended to concurrent shape and location optimization.
- A new numerical implementation to handle optimization problems in any complicated structure was proposed and a computer code was developed accordingly.
- Application of the proposed numerical approach made it possible to perform level set optimization in time/frequency dependent problem.
- Level set approach was extended to higher orders problems.

7.2 Future work

Like other research, there are avenues for further research in this area. When dealing with an optimization problem, one of the critical aspects that always can be improved is to reduce the possibility of getting stuck into a local minimum.

Incorporation of stochastic methods could be advantageous in escaping from local minima. A few researchers have included stochastic terms in level set technique [119-124]. Kasaiezadeh and Khajepour [125,126] have implemented active contours and stochastic fronts. By adding stochastic term to the level set PDE they confirmed that the chance escaping from local solutions would decrease compared to classical level set methods.

Another approach for moving towards the global optimum is application of multi agent techniques. In these methods the optimization starts with a few initial guesses and continues.

However, there is an interrelation between all agents. So if one of them gets stuck into a minimum the others could reach a better optimum solution. In some advanced methods [127] agents stuck in local minimums could release themselves and continue their way towards the global optimum point. For both of these suggested paths, new formulation has to been derived in the context of stochastic or multi-agent level set technique. A computer code has to be developed accordingly.

Another area for future work is to consider other types of objective functions. For examples in many cases it is important to bring the modal loss factor to a desired value for minimum amount of CLD patches.

Bibliography

[1] C. C. Fuller, S. Elliott, P.A. Nelson, Active control of vibration, Academic Press, 1997.

[2] M.O. Tokhi, S.M. Veres, O. Tokhi, Active sound and vibration control: theory and applications, Illustrated edition, Inspec/Iee, 2002.

[3] E.I. Rivin, Passive vibration isolation, American Society of Mechanical Engineers, 2003.

[4] E. Guglielmino, T. Sireteanu, C.W. Stammers, G. Ghita, M. Giuclea, Semi-active suspension control: improved vehicle ride and road friendliness, First edition, Springer, 2008.

[5] Magnesium fosters rebirth of an automotive engine, May 2007, (http://www.intlmag.org/files/mg001.pdf).

[6] D.I.G. Jones, Handbook of Viscoelastic Vibration damping, First edition, Wiley, 2001.

[7] J. Renninger, Understanding Damping Techniques for Noise and Vibration Control, (www.earsc.com/pdfs/engineering/understandingdamping.pdf).

[8] C.A. Gallimore, Passive viscoelastic constrained layer damping application for a small aircraft landing gear system, Master's thesis, Virginia Polytechnic Institute and State University, 2008.

[9] K. Misiurek, P. Sniady, Vibrations of sandwich beam due to a moving force, Composite Structures, Vol. 104, pp. 85–93, 2013.

[10] F.X. Xin , T.J. Lu, Analytical modeling of wave propagation in orthogonally rib-stiffened sandwich structures Sound radiation, Computers and Structures, Vol. 89, pp. 507–516, 2011.

[11] N. Challamel, F. Bernard, C. Casandjian, Out-of-plane behaviour of partially composite or sandwich beams by exact and finite element methods, Thin-Walled Structures, Vol. 48, pp. 561–580, 2010.

[12] S.G. Won, S.H. Bae, J.R. Cho, S.R. Bae, W.B. Jeong, Three-layered damped beam element for forced vibration analysis of symmetric sandwich structures with a viscoelastic core, Finite Elements in Analysis and Design, Vol. 68, pp. 39–51, 2013.

[13] H.D. Chalak1, A. Chakrabarti, M.A. Iqbal, A.H. Sheikh, Vibration of laminated sandwich beams having soft core, Journal of Vibration and Control, Vol. 18(10), pp. 1422–1435, 2011.

[14] V. SUDHAKAR, K. VIJAYARAJU, S. GOPALAKRISHNAN, Development of a new finite element for the analysis of sandwich beams with soft core, Journal of Sandwich Structures and Materials, Vol. 12, pp. 649–683, 2010.

[15] J.S. Grewal, R. Sedaghati, E. Esmailzadeh, Vibration analysis and design optimization of sandwich beams with constrained viscoelastic core layer, Journal of Sandwich Structures and Materials, Vol. 15(2), pp. 203–228, 2013.

[16] A.V. Lopatin, E.V. Morozov, Symmetrical vibration modes of composite sandwich plates, Journal of Sandwich Structures and Materials, Vol. 13(2), pp. 189–211, 2010.

[17] A. Arikoglu, I. Ozkol, Vibration Analysis of Composite Sandwich Plates by the Generalized Differential Quadrature Method, AIAA Journal, Vol. 50(3), pp. 620–630, 2012.

[18] F. Alijani, M. Amabili, Nonlinear vibrations of laminated and sandwich rectangular plates with free edges. Part 1: Theory and numerical simulations, Composite Structures, Vol. 105, pp. 422–436, 2013.

[19] H. R. Hamidzadeh, The effect of visco-elastic core thickness on modal loss factors of a thick three-layer cylinder, Proceedings of the Institution of Mechanical Engineers, Part K: Journal of Multi-body Dynamics, Vol. 223, pp. 1–8, 2009.

[20] L. Wu, A. Agren, U. Sundback, A study of the initial decay rate of two-dimensional vibrating structures in relation to estimates of loss factor, Journal of Sound and Vibration, Vol. 206(5), pp. 663–684, 1997.

[21] B.L. CLARKSON, R.J. POPE, Experimental determination of modal densities and loss factors of flat plates and cylinders, Journal of Sound and Vibration, Vol. 77(4), pp. 535–549, 1981.

[22] D.J. Mead, S. Markus, The forced vibration of a three-layer damped sandwich beam with arbitrary boundary conditions, Journal of Sound and Vibration, Vol. 10, pp. 163–175, 1969.

[23] C.D. Johnson, D.A. Kienholz, L.C. Rogers, Finite element prediction of damping in beams with constrained viscoelastic layers, Shock and Vibration Bulletin, pp. 71–81, 1980.

[24] M.R. Maheri, R.D. Adams, Finite-element prediction of modal response of damped layered composite panels, Composites Science and Technology, Vol. 55, pp. 13–23, 1995.

[25] S.A. Hambric, A.W. Jarrett, G.F. Lee, J.J. Fedderly, Inferring viscoelastic dynamic material properties from finite element and experimental studies of beams with constrained layer damping, Transactions of the ASME, Journal of Vibration and Acoustics, Vol. 129, pp. 158–68, 2007.

[26] P. J. Torvika, B. Runyon, Modifications to the method of modal strain energy for improved estimates of loss factors for damped structures, Shock and Vibration, Vol. 14, pp. 339–353 , 2007.

[27] D. Ross, E.E. Ungar, E.M. Kerwin, Damping of plate flexural vibrations by means of viscoelastic laminae, Colloquium on Structural Damping, American Society of Mechanical Engineers (1959).

[28] M. Gurgoze, P.C. Muller, Optimal positioning of dampers in multi-body systems, Journal of Sound and Vibration, Vol. 158, pp. 517–530, 1992.

[29] M.H. Milman, C. Chu, Optimization methods for passive damper placement and tuning, journal of guidance, Control, and Dynamics, Vol. 17, pp. 848–56, 1994.

[30] R.K. Kincaid, Solving the damper placement problem via local search heuristics, OR Spektrum, Vol. 17, pp. 149–58, 1995.

[31] D. Cvijovic, J. Klinowski, Taboo search: an approach to the multiple minima problem, Science, Vol. 267, pp. 664–664, 1995.

[32] I. Takewaki, Optimal damper placement for minimum transfer functions, Earthquake Engineering and Structural Dynamics, Vol. 26, pp. 1113–1124, 1997.

[33] I. Takewaki, S. Yoshitomi, Effects of support stiffnesses on optimal damper placement for a planar building frame, Structural Design of Tall and Special Buildings, Vol. 7, pp. 323–336, 1998.

[34] I. Takewaki, S. Yoshitomi, K. Uetani, M. Tsuji, Non-monotonic optimal damper placement via steepest direction search, Earthquake Engineering and Structural Dynamics, Vol. 28, pp. 655–670, 1999.

[35] I. Takewaki, optimal damper placement for critical excitation, Probabilistic Engineering Mechanics, Vol. 15, pp. 317–325, 2000.

[36] I. Takewaki, Optimal damper placement for planar building frames using transfer functions, Structural and Multidisciplinary Optimization, Vol. 20, pp. 280–287, 2000.

[37] F. Amini, H. Karagah, Optimal placement of semi active dampers by pole assignment method, Iranian Journal of Science and Technology, Transaction B: Engineering. Vol. 30, pp. 31–41, 2006.

[38] S.S. Joshi, Damper placement for spaceborne interferometers using h-norm optimization, American Control Conference, Vol. 6, pp. 3855–3859, 2000.

[39] A.K. Agrawal, J.N. Yang, Optimal placement of passive dampers on seismic and wind-excited buildings using combinatorial optimization, Journal of Intelligent Material Systems and Structures, Vol. 10, pp. 997–1014, 2000.

[40] O Furuya, H Hamazaki, S Fujita, Proper placement of energy absorbing devices for reduction of wind-induced vibration caused in high-rise buildings, Journal of Wind Engineering and Industrial Aerodynamics, 74-76, pp. 931–942, 1998.

[41] M.P. Singh, L.M. Moreschi, Optimal placement of dampers for passive response control, Earthquake Engineering and Structural Dynamics, Vol. 31, pp. 955–976, 2002.

[42] H.Y. Guo, L. Zhang, Optimal placement of MR dampers for structural control using identification crossover genetic algorithm, Journal of Low Frequency Noise, Vibration and Active Control, Vol. 23, pp. 167–178, 2004.

[43] J.A. Bishop, A.G. Striz, On using genetic algorithms for optimum damper placement in space trusses, Structural and Multidisciplinary Optimization, Vol. 28, pp. 136–145, 2004.

[44] H. Movaffaghi, O. Friberg, Optimal placement of dampers in structures using genetic algorithm, Engineering Computations, Vol. 23, pp. 597–606, 2006.

[45] T. Roy, D. Chakraborty, genetic algorithm based optimal design for vibration control of composite shell structures using piezoelectric sensors and actuators, International Journal of Mechanics and Materials in Design, Vol. 5, pp. 45–60, 2009.

[46] S.W. Park, Analytical modeling of viscoelastic dampers for structural and vibration control, International Journal of Solids and Structures, Vol. 38, pp. 8065–8092, 2001.

[47] M.J. Lam, D.J. Inman, W.R. Saunders, Vibration control through passive constrained layer damping and active control, Journal of Intelligent Material Systems and Structures, Vol. 8, pp. 663–677, 1997.

[48] M. Alvelid, Optimal position and shape of applied damping material, Journal of Sound and Vibration, Vol. 310, pp. 947–965, 2008.

[49] H. Zheng, C. Cai, X.M. Tan, Optimization of partial constrained layer damping treatment for vibrational energy minimization of vibrating beams, Computers & Structures, Vol. 82, pp. 2493–2507, 2004.

[50] R.A.S. Moreira, J.D. Rodrigues, Partial constrained viscoelastic damping treatment of structures: A modal strain energy approach, International Journal of Structural Stability and Dynamics, Vol. 6, pp. 397–411, 2006.

[51] S. Kodiyalam, J. Molnar, Optimization of constrained viscoelastic damping treatments for passive vibration control, Structural Dynamics and Materials Conference, 1992.

[52] J. Ro, A. Baz, Optimum placement and control of active constrained layer damping using modal strain energy approach, Journal of Vibration and Control, Vol. 8, pp. 861–76, 2002.

[53] C.D. Johnson, D.A. Klenholz, Finite element prediction of damping in structures with constrained viscoelastic layers, Structural Dynamics and Materials Conference, pp. 17–24, 1981.

[54] K.C. Chang, T.T. Soong, S. Oh, M.L. Lai, Seismic behavior of steel frame with added viscoelastic dampers, Journal of structural engineering, Vol. 121, pp. 1418–1426, 1995.

[55] M. Tsai, K. Chang, A study of the modal strain energy method for viscoelastically damped structures, Journal of the Chinese Institute of Engineers, Transactions of the Chinese Institute of Engineers, Series A, Vol. 24, pp. 311–320, 2001.

[56] S. Osher, J.A. Sethian, Fronts propagating with curvature-dependent speed: Algorithms based on Hamilton-Jacobi formulations, Journal of Computational Physics, Vol. 79, pp. 12–49 1988.

[57] J.A. Sethian, Level Set Methods and Fast Marching Methods: Evolving Interfaces in Computational Geometry, Fluid Mechanics, Computer Vision, and Materials Science, Second edition, Cambridge University Press, 1999.

[58] S Osher, R Fedkiw, Level set methods and dynamic implicit surfaces, First edition, Springer 2002.

[59] Level set method (http://en.wikipedia.org/wiki/Level_set_method).

[60] R. Malladi, J.A. Sethian, B.C. Vemuri, A fast level set based algorithm for topology-independent shape modeling, Journal of Mathematical Imaging and Vision, Vol. 6, pp. 269–289, 1996.

[61] J.A. Sethian, A. Wiegmann, Structural boundary design via level set and immersed interface methods, Journal of Computational Physics, Vol. 163, pp. 489–528, 2000.

[62] Z. Liu, J.G. Korvink, R. Huang, Structure topology optimization: fully coupled level set method via FEMLAB, Structural and Multidisciplinary Optimization, Vol. 29, pp. 407–217, 2005.

[63] L. Komzsik, Applied calculus of variations for engineers, First edition, CRC Press, 2008.

[64] C. Lanczos, The variational principles of mechanics, Fourth edition, Dover Publications 1986.

[65] H. Zhao, T. Chan, B. Merriman, S. Osher, A variational level set approach to multiphase motion, Journal of Computational Physics, Vol. 127, pp. 179–195, 1996.

[66] M.Y. Wang, X. Wang, D. Guo, A level set method for structural topology optimization, Computer Methods in Applied Mechanics and Engineering, Vol. 192, pp. 227–246, 2003.

[67] Z. Luo, L. Tong, M.Y. Wang, S. Wang, Shape and topology optimization of compliant mechanisms using a parameterization level set method, Journal of Computational Physics, Vol. 227, pp. 680–705, 2007.

[68] M.G. Crandall, Viscosity solutions of Hamilton-Jacobi equations, Transaction of the American Mathematical Society, Vol. 277, pp. 1–42, 1983.

[69] S.J. Osher, F. Santosa, Level set methods for optimization problems involving geometry and constraints I. Frequencies of a two-density inhomogeneous drum, Journal of Computational Physics, Vol. 171, pp. 272–288, 2001.

[70] E. Maitre, F. Santosa, Level set methods for optimization problems involving geometry and constraints. II: optimization over a fixed surface, Journal of Computational Physics, Vol. 227, pp. 9596-9611, 2008.

[71] M. Yulin, W. Xiaoming, A level set method for structural topology optimization and its applications, Advances in Engineering Software, Vol. 35, pp. 415–441, 2004.

[72] G. Allaire, F. Jouve, A. Toader, Structural optimization using sensitivity analysis and a level-set method, Journal of Computational Physics, Vol. 194, pp. 363–393, 2004.

[73] S.Y. Wang, K.M. Lim, B.C. Khoo, M.Y. Wang, An extended level set method for shape and topology optimization, Journal of Computational Physics, Vol. 221, pp. 395–421, 2007.

[74] M.Y. Wang, X. Wang, "Color" level sets: a multi-phase method for structural topology optimization with multiple materials, Computer Methods in Applied Mechanics and Engineering, Vol. 193, pp. 469–496, 2004.

[75] G. Allaire, F. Jouve, A level-set method for vibration and multiple loads structural optimization, Computer Methods in Applied Mechanics and Engineering, Vol. 194, pp. 3269–3290, 2005.

[76] E. Haber, A multilevel, level-set method for optimizing eigenvalues in shape design problems, Journal of Computational Physics, Vol. 198, pp. 518–534, 2004.

[77] Q. Xia, M.Y. Wang, S. Wang, S. Chen, Semi-Lagrange method for level-set-based structural topology and shape optimization, Structural and Multidisciplinary Optimization, Vol. 31, pp. 419–429, 2006.

[78] Z. Liu, J.G. Korvink, Adaptive moving mesh level set method for structure topology optimization, Engineering Optimization, Vol. 40, pp. 529–558, 2008.

[79] S. Park, S. Min, Magnetic actuator design for maximizing force using level set based topology optimization, IEEE Transactions on Magnetics, Vol. 45, pp. 2336–2339, 2009.

[80] A.A. Gomes, A. Suleman, Application of spectral level set methodology in topology optimization, Structural and Multidisciplinary Optimization, Vol. 31, pp. 430–443, 2006.

[81] P. Fulmanski, A. Laurain, J. Scheid, J. Sokolowski, Level set method with topological derivatives in shape optimization, International Journal of Computer Mathematics, Vol. 85, pp. 1491–1514, 2008.

[82] H.R. Jian, Q.L. Qing, A level set method for topology optimization of continuum structures with bounded design domains, Computer Methods in Applied Mechanics and Engineering, Vol. 197, pp. 1447–1465, 2008.

[83] Z. Luo, L. Tong, Z. Kang, A level set method for structural shape and topology optimization using radial basis functions, Computers & Structures, Vol. 87, pp. 425–434, 2009.

[84] C. Zhuang, Z. Xiong, H. Ding, Structural shape and topology optimization based on level-set modelling and the element-propagating method, Engineering Optimization, Vol. 41, pp. 537–555, 2009.

[85] Q. Xia, M.Y. Wang, Topology optimization of thermoelastic structures using level set method, Computational Mechanics, Vol. 42, pp. 837–857, 2008.

[86] J. Luo, Z. Luo, S. Chen, L. Tong, M.Y. Wang, A new level set method for systematic design of hinge-free compliant mechanisms, Computer Methods in Applied Mechanics and Engineering, Vol. 198, pp. 318–331, 2008.

[87] O. Gao-Fei, Z. XianMin, A level set method for reliability-based topology optimization of compliant mechanisms, Science in China Series E: Technological Sciences, Vol. 51, pp. 443–455, 2008.

[88] G. Pingen, M. Waidmann, A Evgrafov, K Maute, A parametric level-set approach for topology optimization of flow domains, Structural and Multidisciplinary Optimization, Vol. 41, pp. 117–131, 2010.

[89] V.J. Challis, J.K. Guest, Level set topology optimization of fluids in Stokes flow, International Journal for Numerical Methods in Engineering, Vol. 79, pp. 1284–1308, 2009.

[90] M. Kim, S. Ha, S. Cho, Level set-based topological shape optimization of nonlinear heat conduction problems using topological derivatives, Mechanics Based Design of Structures and Machines, Vol. 37, pp. 550–582, 2009.

[91] A. Myslinski, Level set method for optimization of contact problems, Engineering Analysis with Boundary Elements, Vol. 32, pp. 986–994, 2008.

[92] S. Park, S. Min, Design of magnetic actuator with nonlinear ferromagnetic materials using level-set based topology optimization, IEEE Transactions on Magnetics, Vol. 46, pp. 618–621, 2010.

[93] F. Periago, A. Munch, P. Pedregal, Optimal design of the damping set for the stabilization of the wave equation, Journal of Differential Equations, Vol. 231, pp. 331–58, 2006.

[94] A. Munch, Optimal internal dissipation of a damped wave equation using a topological approach, International Journal of Applied Mathematics and Computer Science, Vol. 19, pp. 15–37, 2009.

[95] T. Lassila, Optimal damping of a membrane and topological shape optimization, Structural and Multidisciplinary Optimization, Vol. 38, pp. 43–52, 2009.

[96] D. J. Mead, A comparison of some equations for the flexural vibration of damped sandwich beams, Journal of Sound and Vibration, Vol. 83(3), pp. 363–377, 1982.

[97] P. Bangarubabu, K. Kishore Kumar, Y. Krishna, Damping Effect of Viscoelastic Materials on Sandwich Beams, International Conference on Trends in Industrial and Mechanical Engineering (ICTIME'2012) Dubai, UAE, March 24–25, 2012.

[98] M. Edward, J.R. Kerwin, Damping of flexural waves by a constrained viscoelastic layer, The Journal of the Acoustical Society of America, Vol. 33(7), pp. 952–962, 1959.

[99] E.E. Ungar, J.R.E.M. Kervin, Loss factors of viscoelastic systems in terms of energy concepts, The Journal of the Acoustical Society of America, Vol. 34(7), pp. 1082–1089, 1962.

[100] E.E. Ungar, Loss factors of viscoelastically damped beam structures, The Journal of the Acoustical Society of America, Vol. 34(8), pp. 954–957, 1962.

[101] T.S. Plagianakos, D.A. Saravanos, Mechanics and finite elements for the damped dynamic characteristics of curvilinear laminates and composite shell structures, Journal of Sound and Vibration, Vol. 263, pp. 399–414, 2003.

[102] E.E. Ungar, J.R.E.M. Kervin, Plate Damping due to Thickness Deformations in Attached Viscoelastic Layers, The Journal of the Acoustical Society of America, Vol. 36(2), pp. 386–392, 1964.

[103] P.J. Macioce, Design for Damping,
(http://www.roush.com/Portals/1/Downloads/Articles/Appliance%20Manufacturer.pdf).

[104] M.N. Darrouj, R.G. Faulkner, Optimum design of constrained layer damping panels, Materials & Design, Vol. 10, pp. 202–208, 1989.

[105] T. Collins, K. Kochersberger, R. DeVita, Constrained layer damping treatment design for aircraft landing gear, 2009 IMAC-XXVII: Conference & Exposition on Structural Dynamics, 2009.

[106] D. Herrero, J. Martinez and P. Marti, An implementation of level set based topology optimization using GPU, 10th World Congress on Structural and Multidisciplinary Optimization, Orlando, Florida, USA, May 19 - 24, 2013.

[107] V. Challis, A discrete level-set topology optimization code written in Matlab, Structural and Multidisciplinary Optimization, Vol. 41, pp. 453–464, 2010.

[108] M. Alvelid, M. Enelund, Modelling of constrained thin rubber layer with emphasis on damping, Journal of Sound and Vibration, Vol. 300, pp. 662–675, 2007.

[109] C.M. Chia, J.A. Rongong, K. Worden, Evolution of constrained layer damping using a cellular automaton algorithm, Proceedings of the Institution of Mechanical Engineers Part C-Journal of Mechanical Engineering Science, Vol. 222, pp. 585–597, 2008.

[110] Signed distance function **(**http://en.wikipedia.org/wiki/Signed_distance_function**)**.

[111] A.C.H. Tan, T. Meurers, S.M. Veres, G. Aglietti, E. Rogers, Satellite vibration control using frequency selective feedback, Proceedings of the IEEE Conference on Decision and Control, Vol. 2, pp. 1693–1698, 2003.

[112] M. Moshrefi-Torbati, A.J. Keane, S.J. Elliott, M.J. Brennan, D.K. Anthony, E. Rogersm Active vibration control (AVC) of a satellite boom structure using optimally positioned stacked piezoelectric actuators, Journal of Sound and Vibration, Vol. 292, pp. 203–220, 2006.

[113] Y. Kurosawa, T. Yamaguchi, S. Matsumura, Damped vibration analysis of automotive panels laminated porous materials, 23rd Conference & Exposition, Structural dynamics, 2005.

[114] E. Bianchini, Active vibration control of automotive like panels, SAE Technical Paper 2008-36-0576, 2008.

[115] H. Nagai, T. Shiota, T. Taka, K. Fukui, Development of vibration damping steel sheets for inner panels of automotive vehicles, SAE Technical Paper 911083, 1991.

[116] http://static.speedwaymotors.com/pdf/Hushmat_Ultra.pdf

[117]http://mediacdn.shopatron.com/media/mfg/7718/product_image/thm/t700_x2_357fd4b058f7039f05c58c064a278803.jpg

[118] M.M. Rodriguez, Analysis of structural damping, Master's thesis, Lulea University of Technology, 2006.

[119] M. Allain, N. Bertaux, F. Galland, Nonparametric level-set segmentation based on the minimization of the stochastic complexity, Advanced Concepts for Intelligent Vision Systems, Lecture Notes in Computer Science Vol. 5259, pp. 506–517, 2008.

[120] C. Avenel, E. Memin, P. Perez, Tracking level set representation driven by a stochastic dynamics, Curves and Surfaces 2011, LNCS 6920, pp. 130–141, 2012.

[121] O. Juan, R. Keriven, G. Postelnicu, Stochastic motion and the level set method in computer vision: stochastic active contours, International Journal of Computer Vision, Vol. 69, pp. 7–25, 2006.

[122] F. Khalifa, A. Elnakib, G.M. Beache, G. Gimel'farb, M. El-Ghar, R. Ouseph, G. Sokhadze, S. Manning, P. McClure, A. El-Baz, 3D kidney segmentation from ct images using a level set approach guided by a novel stochastic speed function, Medical Image Computing and Computer-Assisted Intervention, 14(3) pp. 587–594, 2011.

[123] N.L. Yan, K.L. Hwee, A.M. Yip, A stochastic level set method for subspace mumford-shah based image segmentation, Proceedings of the International Conference On Image Processing Computer Vision and Pattern Recognition, CSREA , United States, Vol. 2, pp. 511–516, 2011.

[124] N.L. Yan, K.L. Hwee, A.M. Yip, A multiresolution stochastic level set method for Mumford-Shah image segmentation, IEEE Transactions on Image Processing, Vol. 17, pp. 2289–2300, 2008.

[125] A. Kasaiezadeh, A. Khajepour, Multi-agent stochastic level set method in image segmentation, Computer Vision and Image Understanding, Vol. 117 (9), pp. 1147–1162, 2013.

[126] A. Kasaiezadeh, A. Khajepour, Active contours with stochastic fronts and mechanical topology optimization, Journal of Mechanical Design, Vol. 135(4), 2013.

[127] A. Kasaiezadeh, A. Khajepour, S.L. Waslander, Spiral bacterial foraging optimization method, 2010 American Control Conference, Baltimore, MD, USA, June 30-July 02, pp. 4845–4850, 2010.